

Nuclear export of single native mRNA molecules  
observed via light sheet fluorescence microscopy  
and  
transcriptional regulation of *BR2.1* during heat-shock

Dissertation zur Erlangung des Doktorgrades (Dr. rer. nat.)  
der Mathematisch-Naturwissenschaftlichen Fakultät  
der Rheinischen Friedrich-Wilhelms-Universität Bonn

vorgelegt von

**Tim Patrick Kaminski**  
aus Haan/Rhld.

Bonn, Mai 2014



Angefertigt mit Genehmigung der Mathematisch-Naturwissenschaftlichen Fakultät  
der Rheinischen Friedrich-Wilhelms-Universität Bonn.

In der Dissertation eingebunden:

Zusammenfassung

Lebenslauf

1. Gutachter: Prof. Dr. Ulrich Kubitscheck
2. Gutachter: Prof. Dr. Rudolf Merkel

Tag der Promotion: 05.08.2014

Erscheinungsjahr: 2014

# Contents

<b>List of Figures</b>	<b>iv</b>
<b>List of Tables</b>	<b>vii</b>
<b>1 Introduction</b>	<b>1</b>
1.1 Introduction: Transcription . . . . .	3
1.1.1 The Transcription Cycle . . . . .	3
1.2 Aim: Transcriptional regulation of <i>BR2.1</i> . . . . .	11
1.3 Nucleocytoplasmic Trafficking . . . . .	12
1.3.1 The Nuclear Pore Complex . . . . .	13
1.3.2 The mRNA-Export Pathway . . . . .	14
1.4 Aim and Measurement Principles . . . . .	17
1.5 Statistical Analysis . . . . .	19
1.5.1 Dwell Time Modeling Using Gamma Distribution . . . . .	20
1.5.2 Parametric-Bootstrapping Based Hypothesis testing . . . . .	21
1.5.3 Non-Parametric-Bootstrapping . . . . .	24
1.6 <i>Chironomus tentans</i> . . . . .	25
1.6.1 The BR Genes of <i>Chironomus tentans</i> . . . . .	29
1.6.2 Transcription of the <i>BR2.1</i> and its Regulation . . . . .	30
<b>2 Materials and Methods</b>	<b>33</b>
2.1 Buffers . . . . .	33
2.2 Materials . . . . .	35
2.3 Antibodies . . . . .	36
2.4 Immunostaining of <i>C. tentans</i> Larval Salivary Glands . . . . .	36
2.5 Fluorescence <i>in situ</i> Hybridization . . . . .	36
2.6 Dissection of <i>C. tentans</i> Larval Salivary Glands . . . . .	37
2.7 Dissection of <i>C. tentans</i> Larval Mid Gut . . . . .	38
2.8 Microinjection of <i>C. tentans</i> Larval Salivary Glands . . . . .	39

2.9	Collection of <i>C. tentans</i> Hemolymph . . . . .	40
2.10	DNA Extraction . . . . .	40
2.11	Potassium Permanganate Foot-Printing . . . . .	42
2.12	DNA Fragment Length Analysis . . . . .	44
2.13	Kinetic Data Fitting . . . . .	45
2.14	Model Selection . . . . .	46
2.15	Goodness-of-Fit Test by Parametric Bootstrapping . . . . .	47
2.16	Non-Parametric Bootstrapping . . . . .	47
2.17	mRNP-Particle Export Analysis . . . . .	47
2.18	Overlay of Export Trajectories and NPC-Structure . . . . .	48
2.19	Light Sheet Microscope . . . . .	49
2.20	Single Molecule Imaging in <i>C. tentans</i> Salivary Glands by Light Sheet Microscopy . . . . .	50
<b>3</b>	<b>Results I: Single Molecule Observation of mRNP-Particle Export</b>	<b>51</b>
3.1	Light Sheet Characterization . . . . .	51
3.2	Establishing Whole Mount Fluorescence <i>in situ</i> Hybridization . . . . .	53
3.3	Testing of Different Incubation Media . . . . .	54
3.4	Single Molecule Observation of mRNP-Particle Export . . . . .	57
3.4.1	Image and Kinetic Data Analysis . . . . .	58
3.4.2	Export Kinetics of Native mRNP-Particles . . . . .	60
3.4.3	Nuclear Probing Kinetics of Native mRNP-Particles . . . . .	65
3.4.4	Cytoplasmic Probing Kinetics of Native mRNP-Particles . . . . .	68
3.4.5	Trajectory Analysis . . . . .	70
3.4.6	Dbp5-Kinetics at the Nuclear Envelope . . . . .	71
<b>4</b>	<b>Results II: Transcriptional Regulation of BR-Genes</b>	<b>76</b>
4.1	Transcriptional Block of BR2.1 Genes During Heat-Shock . . . . .	78
4.2	RNA Polymerase II Localization and Transcriptional Status . . . . .	80
4.2.1	RNA Polymerase II Footprinting . . . . .	81
4.3	RNA Polymerase II CTD Phosphorylation . . . . .	85
4.4	Recovery of BR2 Transcriptional Activity After Heat-Shock Release . . . . .	86
<b>5</b>	<b>Discussion I: Imaging Export of Single Native mRNP-Particles</b>	<b>88</b>
5.1	Imaging the mRNA-Export . . . . .	88
5.2	Incubation Media . . . . .	89

5.3	mRNA Labeling . . . . .	90
5.4	Export and Probing Kinetics of mRNP-Particles . . . . .	92
5.4.1	Dwell Time Analysis . . . . .	92
5.4.2	mRNP-Particle Export And Probing Kinetics . . . . .	94
5.5	Dbp5 Turnover Kinetics at the NPC . . . . .	98
<b>6</b>	<b>Discussion II: Heat-Shock-Induced Transcription Block</b>	<b>100</b>
<b>7</b>	<b>Outlook</b>	<b>103</b>
7.1	How to Proceed in Imaging mRNP-Particle Export? . . . . .	103
7.2	Further Investigation of the Reversible Transcription Block During Stable Elongation . . . . .	104
	<b>Works cited</b>	<b>105</b>
	<b>Works not-cited</b>	<b>115</b>
	<b>List of Abbreviations and Notations</b>	<b>118</b>
	<b>Appendix</b>	<b>120</b>
	<b>Summary</b>	<b>124</b>
	<b>Zusammenfassung</b>	<b>126</b>



# List of Figures

1.1	Stages of protein biosynthesis . . . . .	2
1.2	Transcription initiation and early elongation . . . . .	5
1.3	Model of elongation arrest dependent Rpb1 ubiquitination . . . . .	10
1.4	NPC scheme . . . . .	13
1.5	Dbp5 reaction scheme. . . . .	16
1.6	Image analysis procedure . . . . .	18
1.7	Examples of gamma distributions with varying S and k . . . . .	21
1.8	Parametric bootstrapping scheme . . . . .	22
1.9	Q-Q plot of $\chi^2$ * quantiles against theoretical expected . . . . .	23
1.10	Increasing accuracy of critical value estimation with increasing number of bootstrap cycles by parametric bootstrapping . . . . .	23
1.11	Non-parametric bootstrapping scheme . . . . .	24
1.12	Adult and larval stage of <i>C. tentans</i> . . . . .	25
1.13	Salivary gland of <i>C. tentans</i> . . . . .	26
1.14	Sketch of <i>C. tentans</i> salivary gland cell geometry . . . . .	27
1.15	Propidiumiodidstaining of <i>C. tentans</i> salivary glands . . . . .	28
1.16	Scale drawing of BR2.1 intron-exon structure . . . . .	30
2.1	Potassium permanganate foot-printing of RNA-Polymerase II . . . . .	42
2.2	Kymograph analysis . . . . .	48
2.3	Schematic drawing of the Light Sheet Microscope setup . . . . .	50
3.1	Chromatic shift and geometry of the light sheet . . . . .	52
3.2	Chromatic shift of double labeled nuclear envelope . . . . .	53
3.3	Whole mount fluorescence in situ hybridization of <i>C. tentans</i> salivary glands . .	54
3.4	Representative images of the BR2.1-mRNA distribution after incubation in dif- ferent media . . . . .	56
3.5	Labeling of nascent mRNP-particles and the Nuclear envelope . . . . .	57
3.6	Characterization scheme of mRNP NE interaction . . . . .	59



3.7	Model selection for mRNP export based on the $AIC_c$ . . . . .	62
3.8	Fitting of the cumulative NE-interaction time distribution of all export events . . . . .	63
3.9	Goodness-of-fit test of the mRNP-particle export kinetics approximation . . . . .	63
3.10	Variance Estimation of the of $\tau_{1exp}$ and $\tau_{2exp}$ . . . . .	64
3.11	Model selection for the nuclear probing kinetics by $AIC_c$ . . . . .	65
3.12	Fitting of the cumulative nuclear probing kinetics. . . . .	66
3.13	Goodness-of-fit test of the nuclear probing kinetics approximation . . . . .	67
3.14	Estimation of the Variance of $\tau_{1nprobing}$ and $\tau_{2nprobing}$ . . . . .	67
3.15	Fitting of the cumulative cytoplasmic probing kinetics. . . . .	68
3.16	Goodness-of-fit test of the cytoplasmic probing kinetics approximation . . . . .	69
3.17	Estimation of the Variance of $\tau_{cprobing}$ . . . . .	69
3.18	Trajectory analysis of export events $\geq 300$ ms . . . . .	70
3.19	Fitting of the cumulative Dbp5 NE interaction time distribution imaged with 50 Hz. . . . .	71
3.20	Goodness-of-fit test of the Dbp5 NPC binding kinetics approximation . . . . .	72
3.21	Variance estimation of $\tau_{Dbp5_{50Hz}}$ . . . . .	72
3.22	Model selection for Dbp5 NE interaction kinetics imaged with 200Hz . . . . .	73
3.23	Fitting of the cumulative Dbp5 NE interaction time distribution imaged at 200 Hz. . . . .	74
3.24	Goodness-of-fit test of the Dbp5 NPC binding kinetics approximation . . . . .	74
3.25	Estimation of the Variance of $\tau_{1Dbp5_{200Hz}}$ and $\tau_{2Dbp5_{200Hz}}$ . . . . .	75
4.1	BR2.1-mRNA distribution after heat-shock . . . . .	77
4.2	Stable transcription block of BR2.1 induced by heat-shock . . . . .	78
4.3	Quantification of BR2.1 transcriptional activity of heat-shocked salivary glands and control glands . . . . .	79
4.4	Transcription block of the BR2.1 gene could is sustained for extended time periods under heat-shock . . . . .	80
4.5	RNAPII localization in heat-shocked salivary glands . . . . .	81
4.6	Potassium permanganate footprinting of midgut tissue . . . . .	82
4.7	Potassium permanganate footprinting of heat-shocked salivary glands . . . . .	84
4.8	Phosphorylation status of RNAPII after heat-shock . . . . .	85
4.9	Transcriptional activity recovery after heat-shock release . . . . .	87
7.1	Interaction types of mRNP-particles with the NE . . . . .	122

7.2 Quantification of the transcriptional activity and transcript concentration at the BR2-puff before and after heat shock. . . . . 123



# List of Tables

1.1	Exon and intron lengths of the BR-genes . . . . .	29
2.1	Used materials . . . . .	35
2.2	Used antibodies . . . . .	36
3.1	Overview of the different incubation media tested . . . . .	55
5.1	Comparison of the mRNP-particle export kinetics . . . . .	95
7.2	Fitted time constants and ratios for nuclear export, nucleoplasmic probing, cytoplasmic probing and the Dbp5 NE interaction. . . . .	120
7.3	Theoretical $\sigma_S$ for given number of observations $n$ and number of rate limiting steps $S$ . . . . .	121

# 1 Introduction

Two different biological questions were investigated in this thesis. The initial aim was to measure the messenger ribonucleoprotein (mRNP)-particle export kinetics. During investigating mRNP-particle export a control experiment pointed to a new transcription regulation mechanism which could change the general model of transcription regulation. Both processes, mRNP-particle export and transcriptional regulation are crucial steps of gene expression (Fig. 1.1).

The following sections of the introduction are given in chronological order, equivalent to the chronological processes during gene expression. At first, a general introduction of transcription, mRNP-particle export and the applied statistical methods, will be given. *Chironomus tentans* was used as a model organism in both investigations. Since the investigation of mRNP-particle export and transcription regulation are two separate topics, the results and discussion chapters are subdivided. To image the mRNP-particle export, a light sheet fluorescence microscope was used. A short overview of the instrument is given at section 2.19 (p. 49) and the advancements achieved during this thesis are described in chapter 3.1 (p. 51).

Gene expression can be separated into transcription and translation. Transcription means the synthesis of an ribonucleic acid (RNA) polynucleotide along a deoxyribonucleic acid (DNA) matrix. Translation is the synthesis of a polypeptide along a RNA matrix. While in prokaryotes translation begins while the synthesis of the RNA-polynucleotide is not finished, in eukaryotes these two processes are spatially and therefore also temporarily separated. Transcription of genomic DNA is restricted to the nucleus which contains the genomic DNA. Translation takes place in the cytoplasm. The spatial separation is achieved by the nuclear envelope and allows mRNA processing. Exchange of molecules between nucleoplasm and cytoplasm is possible through nuclear pore complexes (NPCs).

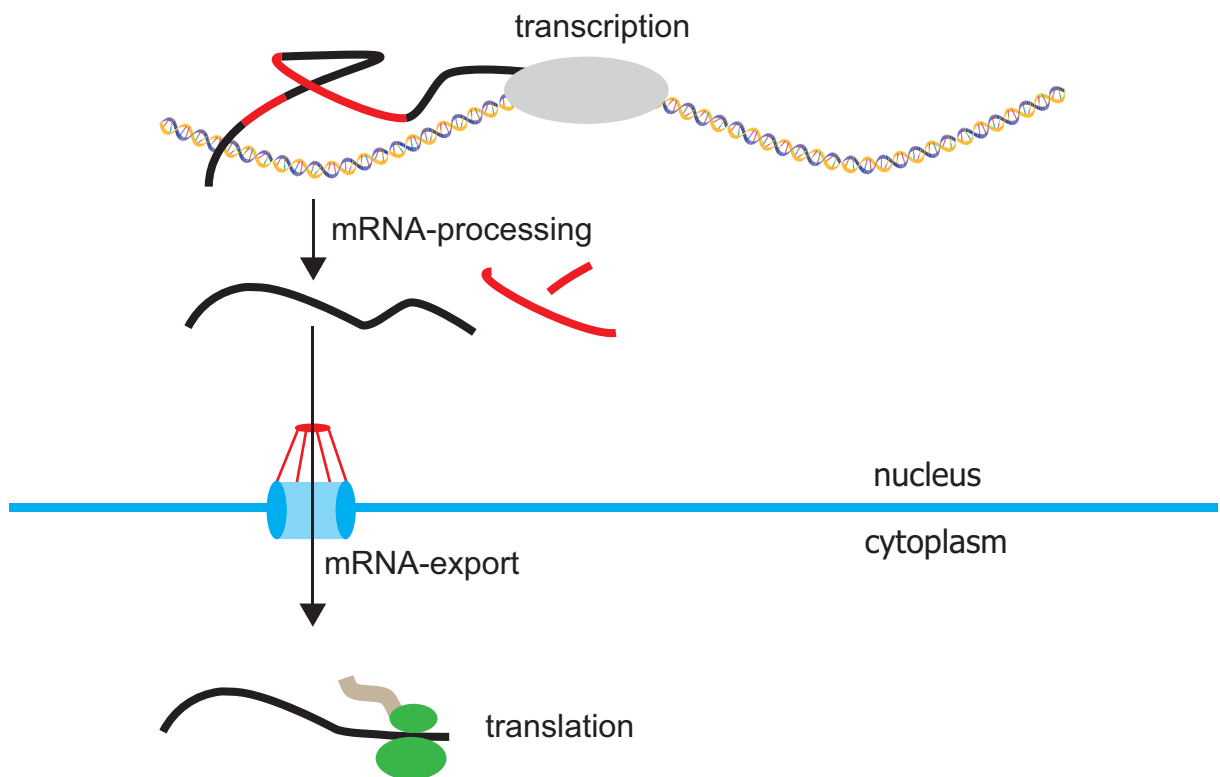


**Figure 1.1:** *Stages of protein biosynthesis.* Packaging of the mRNA into an mRNP-particle and mRNA-processing is a cotranscriptional process. Fully processed mRNP-particles are exported into the cytoplasm where the mRNA is translated by ribosomes into a polypeptide chain.

## 1.1 Introduction: Transcription

All organisms use DNA for long term information storage. Information read back starts at transcribing DNA into RNA. Regulation of genetic information usage begins at the level of transcription. Still far away from being understood, we start to get an impression of the complex regulatory network controlling transcription. This complex network is able to regulate the transcription of thousands of different genes, individually. This is even more astonishing, because transcription of all nuclear genes is mainly accomplished by only three different DNA-dependent RNA polymerases in animals (RNAPI-III) and a single one in prokaryotes.<sup>[23]</sup> The recently discovered RNAP IV and V are plant specific.<sup>[45]</sup> All protein-coding and most small nuclear RNA (snRNA) genes are transcribed by RNAPII. Since the work in this thesis investigated transcriptional regulation of a protein coding gene, the introduction only covers RNAPII.

Transcription and its regulation involve numerous proteins.<sup>[124]</sup> The interaction network of these proteins is poorly understood, which gives rise to different models and presumptions of transcriptional regulation. In the following, a very basic scheme of the transcription cycle and its basic regulatory modes will be presented.

*Svejstrup* describes a general model of the regulatory network of RNAPII, explaining how such a high number of accessory factors can interact with a single RNAPII.<sup>[121]</sup> Assuming binding and dissociation of the accessory factors to the elongation complex as several partially competitive equilibrium reactions, would enables RNAPII to interact with a high number of factors. If the action of a specific factor is needed, the equilibrium is shifted towards this factor, which enables it to take action on the elongation complex.

In the following, several interaction partners of RNAPII will be introduced. For the understanding and discussion of the data presented here it is not necessary to know the names of the interaction partners but to know their impact to the transcription process.

### 1.1.1 The Transcription Cycle

RNAPII consists of twelve RNA polymerase b subunits (Rpb 1-12) with a total mass of 514 kDa.<sup>[23]</sup> Examination of eukaryotic RNA polymerases by different methods led to two parallel nomenclatures: RNA polymerase I,II,III or RNA polymerase A,B,C. Today RNAP I-III is most commonly used. Rpb1 is the largest subunit, which harbors the active center for the RNA polynucleotide synthesis along a DNA template. Its C-terminal domain (CTD) contains a heptapeptide repeat with the consensus sequence  $Y_1S_2P_3T_4S_5P_6S_7$ .<sup>[139]</sup> Post-translational modifications of this heptapeptide repeats are essential to control the different stages of transcription and the

transition between the stages. The main stages of transcription are initiation, elongation and termination. The basic framework for accessory factor association is set by post-translational modifications of the CTD.<sup>[16,100,139]</sup> Transcription initiation of RNAPII depends on several proteins e.g. general transcription factors (TFII) and general co-factors. A controlled formation of the pre-initiation complex (PIC) at the promoter is essential for site-specific transcription initiation. The PIC positions RNAPII at the transcription start site and supports the formation of a transcription bubble by melting the DNA and placing it into the active center of RNAPII. It can be assembled sequentially or using the holoenzyme pathway.<sup>[124]</sup> During sequential assembly the creation of a PIC is initiated by TFIID via recognition of certain promoter elements (DNA-motifs) e.g. a TATA box. This is followed by stepwise binding of TFIIA and TFIIB which stabilize TFIID. After stabilization RNAPII/TFIIF is recruited, with subsequent entry of TFIIE and TFIIH into the PIC (Fig. 1.2 a). The PIC formation is adenosine triphosphate (ATP)-independent. During the holoenzyme pathway a TFIID/TFIIA complex binds to the core promoter followed by the recruitment of the pre-assembled RNAPII holoenzyme. Different compositions of the RNAPII holoenzyme were reported (reviewed in *Thomas et al.*<sup>[124]</sup>).

PIC assembly offers the first chance to regulate gene expression. It is inhibited by DNA compaction into chromatin. Upon stimulation, gene specific activators recruit co-activators to the DNA. Co-activators can build a scaffold for PIC assembly.<sup>[134]</sup> Furthermore, they can assist by clearing the promoter region from histones. The removal of histones from the promoter is sufficient for the initiation of transcription for many genes. Other genes can still be repressed, while the promoter is free of nucleosomes. Nucleosomes do not have to be removed from the DNA necessarily to clear the promoter. ATP-dependent nucleosome-remodeling complexes use ATP-hydrolysis to move histones to another piece of DNA or onto histone binding proteins. This often enables more rapid access to the promoter than removal of histones by post-translational modifications like acetylation.<sup>[21,134]</sup>

After PIC formation the DNA is ATP-dependently melted and a so called open complex is formed. Subsequently, the first 2-3 nucleotides are synthesized. During this stage RNAPII is still associated with the PIC and abortive initiation can occur which results in release of the short mRNA piece. At this stage the CTD is phosphorylated at serine-5. It is thought that serine-5 phosphorylation supports promoter escape by destabilizing interactions of RNAPII and promoter-bound factors. Furthermore, serine-5 phosphorylation is essential to recruit the capping complex which modifies the mRNA-5'-end by the methylation cap.<sup>[93]</sup> Early elongation is slow and not very progressive. The early elongation complex is prone for pausing, arresting and premature termination.

Elongation complexes are termed paused if the forward movement has stopped but they are



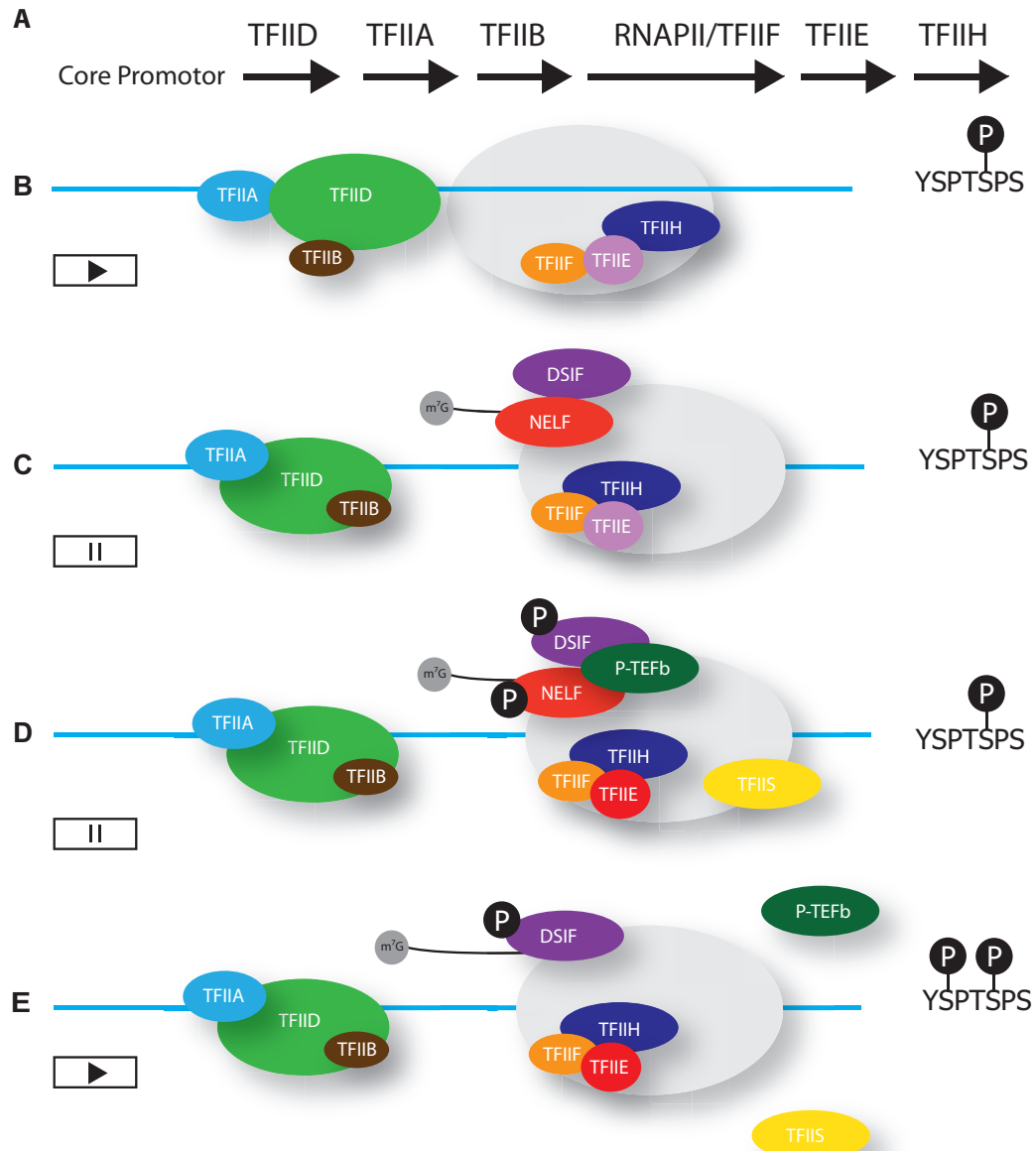


**Figure 1.2: Transcription initiation and early elongation.** (A) TFIID initiates the PIC formation by recognition of core promoter elements and binding to them. TFIIA&B stabilize this binding and TFIIB recruits RNAPII in association with TFIIF to the growing PIC. TFIIB&F are involved in transcription start site selection. TFIIIE&H are essential for DNA melting and establishing a transcription competent PIC. (B) After synthesis of the first nucleotides, RNAPII escapes from the promoter. CTD serine-5 phosphorylation is thought to promote the dissociation of the elongation complex from the promoter bound initiation factors. (C) After promoter escape the nascent transcript is extended and accessible from the outside. In a sequence-independent manner DSIF and NELF recognize the nascent transcript and are recruited to the early elongation complex where they induce pausing. (D) P-TEFb and TFIIIS release the early elongation complex from the pause. P-TEFb phosphorylates NELF, DSIF and RNAPII-CTD at serine-2. (E) P-TEFb and phosphorylated NELF dissociate from the elongation complex while phosphorylated DSIF stays associated. This figure is based on figures of Thomas et al., Chiba et al. and Nechaev et al.<sup>[19,94,124]</sup>

still transcriptionally competent and the RNA-3'-end remains at the active site. After backtracking of RNAPII, the RNA 3'-end is dislocated from the active site and RNAPII cannot continue transcription without assistance of cofactors. Arrested early elongation complexes can be reactivated by TFIIIS.

The release from pausing can be the rate-limiting step of the transcription cycle.<sup>[110]</sup> The promoter proximal pausing is characterized by elongation complexes, which temporarily halt transcription and need appropriate signals to enter productive elongation. The action of unphosphorylated DSIF and NELF introduce pausing of RNAPII. P-TEFb phosphorylates DSIF, NELF and the CTD at serine-2. This terminates the pause. After phosphorylation NELF dissociates while DSIF stays associated to the elongation complex.<sup>[93]</sup>

Promoter proximal pausing is thought to be a checkpoint for correct transcription complex assembly.<sup>[93]</sup> Furthermore, it is able to decrease the delay between regulatory signals and transcription start or shut-down.<sup>[8,63,94]</sup> While a rapid initiation is reasonable for stress-induced genes like heat shock genes, it does not explain widespread of promoter proximal pausing throughout the genome.<sup>[43,55]</sup> *Boettinger et al.* suggested that promoter proximal pausing helps to coordinate the expression across populations of cells.<sup>[8,144]</sup> This hypothesis is based on the high incidence of promoter proximal pausing among genes which are isochronically activated in cell populations. Promoter proximal pausing reduces the number of rate limiting steps to yield productive elongation. Modeling shows that promoter proximal pausing can not only reduce the delay until transcription initiation, but also reduces the deviation of the waiting time distribution from stimulus to first transcription, significantly.<sup>[8]</sup>

Some of the best examined genes showing promoter proximal pausing are the heat shock genes of *Drosophila*, especially the *Hsp70* loci. Upon heat shock the heat shock factor (HSF) recruits additional co-activators to the *Hsp70* promoter. This step is essential, but not sufficient to recruit P-TEFb. By P-TEFb recruitment RNAPII is released more efficiently from promoter proximal pausing and starts productive elongation.

After leaving the proximal pause site, RNAPII enters productive elongation and is thought to proceed through the remainder of the gene.<sup>[110]</sup> During productive elongation, RNAPII is very stably associated to the DNA and the transcript. This stable association is necessary to successfully transcribe large genes. Transcription of the largest human gene (*dystrophin*) takes 16 h.<sup>[122]</sup> Productive elongation is a discontinuous process.<sup>[29,145]</sup> During productive elongation RNAPII can pause, backtrack or be arrested. Different obstacles like topological constraints, nucleosomes, DNA lesions or certain sequences can cause these intermissions during productive elongation. Even in close to optimal purified *in vitro* environments, RNAPII pauses, backtracks and arrests.<sup>[145]</sup> Since RNAPII is associated tightly to the DNA, it is important that

RNAPII does not arrest persistently. A persistently arrested RNAPII would block the transcription of the gene. Depending on the affected gene this could be lethal to the cell. Therefore, accessory factors ensure that RNAPII stays processive. Arrested RNAPII is reactivated or removed from the DNA if it is irreversibly arrested.<sup>[38,121]</sup> Furthermore, several mechanisms exist that remove obstacles to ensure further transcription. Pausing or a just slowed down transcription however, affect downstream processes like splicing and vice versa.<sup>[60,82]</sup>

Single exons can be skipped by not using a splice site. This process is called alternative splicing. Alternative splicing is a mechanism by which a single gene can code for numerous proteins. Many splice variants are expressed cell- or tissue-specificly. Alternative splicing is intensively used by the majority of eukaryotes. Sixty percent of the human genes show alternative splicing.<sup>[53]</sup>

Alternative splicing can be regulated via manipulation of the transcription elongation rate.<sup>[60]</sup> Decreasing the elongation rate or pausing enhances the chance of splice site recognition. A high elongation rate can cause an "override" of a splice site and the exon would be spliced out with the subsequent intron. It is assumed that the downstream elongation rate of RNAPII during productive elongation is regulated by the promoter structure and recruitment of transcription activators and co-activators.<sup>[24,59]</sup> This illustrates that RNAPII is a target of regulatory processes during productive elongation.

Pausing of RNAPII during stable elongation is a highly unstable state. From the pausing state RNAPII can switch back to active transcription or it may enter a transcriptional arrest.<sup>[38]</sup> Transcriptional arrest is characterized by a loss of contact between the transcript 3'-OH tail and active site of RNAPII.<sup>[121]</sup> RNAPII backtracks before being arrested. The first step of backtracking is an isomerization of RNAPII into a state that is unfavorable for NTP binding.<sup>[96]</sup> In a second step, RNAPII moves back by one nucleotide. This disrupts the interaction of the active site and the extendable RNA 3'-OH-end. The backtracked RNA enters the so called funnel of RNAPII. Backtracking by one nucleotide frays the 3' nucleotide of the RNA against a gating tyrosine located at the funnel entry. Further backtracking seems to be hampered since the base stacking of the RNA is disturbed by this tyrosine.<sup>[18]</sup> Backtracking is usually limited by the funnel geometry to 7 bp to 9 bp.<sup>[137]</sup> Arrested RNAPII can be recovered spontaneously, by TFIIS-stimulated RNA-cleavage or alternative mechanisms. TFIIS can enter the funnel from the outside and supports the cleavage of the RNA to regain an extendable 3'-OH at the active site. Alternative mechanisms do not necessarily include RNA cleavage. For example the Ccr4-Not-mediated recovery of RNAPII does not involve RNA cleavage. Ccr4-Not assists by realigning the RNA-3'-OH end and the active site of RNAPII.<sup>[61]</sup>

The collision between a paused and a trailing RNAPII, literally pushes paused RNAPII

through a pause site. For several eukaryotic genes, a burst-like transcription has been shown.<sup>[102]</sup> This results in a distance of only a few hundred nucleotides between the individual polymerases.<sup>[15,20]</sup> If the pause lasts more than a few seconds, the trailing polymerase will clash inescapably with the leading polymerase. This full elastic rear-end collision can drive the leading polymerase through the pause site. The trailing polymerase backtracks after collision and is thought to run into the leading polymerases until its elongation continues. RNAPII collisions does not cause a detaching from the DNA.<sup>[108]</sup>

Persistently arrested elongation complexes are subject to ubiquitination. The encoded message of ubiquitination is more diverse than only directing the elongation complex to proteasomal degradation. Target of RNAPII ubiquitination is its subunit Rpb1. Ubiquitination of Rpb1 is a multistep process which can result in the continuation of transcription or, as a last resort, in the degradation of the elongation complex.<sup>[139]</sup> The degradation of the elongation complex ensures clearance of the gene by the cost of loosing the nascent transcript and Rpb1 by proteasomal degradation.<sup>[81]</sup> Ubiquitination is limited to CTD serine-2-phosphorylated RNAPII, which ensures that only elongation complexes engaged in productive elongation are targeted.<sup>[117,139]</sup>

Ubiquitin is linked to the amino-terminal-end or a lysine side chain of the target protein via its carboxyterminal group. Additional ubiquitins can be added to the first ubiquitin via one of its seven lysine residues, yielding a polyubiquitin chain attached to the target protein.<sup>[141]</sup> The different topologies of ubiquitination encode different messages. First, mono- and poly-ubiquitination are distinguished. Polyubiquitin-chains are differentiated by the lysine which is used to link the single ubiquitins. While Lys-48 linked chains direct the target to proteasomal degradation by the 26S proteasome, Lys-63 can encodes different messages.<sup>[126]</sup>

A model for the ubiquitination of arrested elongation complexes by *Wilson et al.* shows that it is not a one-way process with a predetermined outcome (Fig. 1.3).<sup>[139]</sup> Ubiquitin attached to only two out of 93 surface located lysine residues of Rpb1, specifically (Lys-330 and Lys-695).<sup>[117]</sup> Single point mutation of either of these lysines show significant changes in RNAPII ubiquitination but are not lethal. In contrast, mutating both ubiquitination sites is lethal, showing the redundancy and importance of proteasomal degradation of persistently arrested RNAPII. Taken together, these results indicate that ubiquitination of Rpb1 is more than a simple mechanism for degradation of RNAPII. It underlines the hypothesis that loosing an elongation complex by proteasomal degradation is disadvantageous. But the ability to clear the gene of a persistently arrested elongation complex by the cost of loosing the elongation complex is vital.

A regulatory use of persistent or long term RNAPII arrest during productive elongation is not known.

Termination of transcription is needed to prevent RNAPII from interfering with transcription of downstream genes and to recycle RNAPII to ensure that there is a pool of available RNAPII.<sup>[62]</sup> Position of the termination site can vary from a few base-pairs to several kilo base-pairs downstream of the 3'-end of the transcript site (<sup>[103]</sup> and references therein). Termination of RNAPII activity at protein coding genes is coupled to transcript pre-mRNA 3'-processing and depends on an intact poly-adenylation signal. The pre-mRNA 3'-end processing complex is built up of more than 14 polypeptides with a size of ~1 MDa. The poly-adenylation site consists of the highly conserved hexamer AAUAAA (poly-A-signal), 10 bp to 30 bp upstream of the cleavage site and a more diffuse GU-rich sequence downstream of the cleavage site. Transcription of the poly-A-signal and binding of the cleavage and polyadenylation specificity factor (CPSF) induces pausing of RNAPII. The downstream GU-rich sequence is recognized by the cleavage stimulatory factor (CstF). By CstF binding to the GU-rich signal, CPSF detaches from the RNAPII body and joins CstF at the CTD of Rpb1. This leads to CPSF-mediated endonucleolytic cleavage and 3'-end processing of the transcript. The remaining 5'-end RNA, which is still linked to RNAPII is bound by Xrn-2 a 5'-3' exonuclease which closes up to RNAPII. Pausing of RNAPII is thought to give Xrn2 the chance to catch up with RNAPII and the 3'-end processing complex time to assemble and cleave the transcript. The collision of Xrn2 and RNAPII is thought to promote termination.<sup>[62,136]</sup>

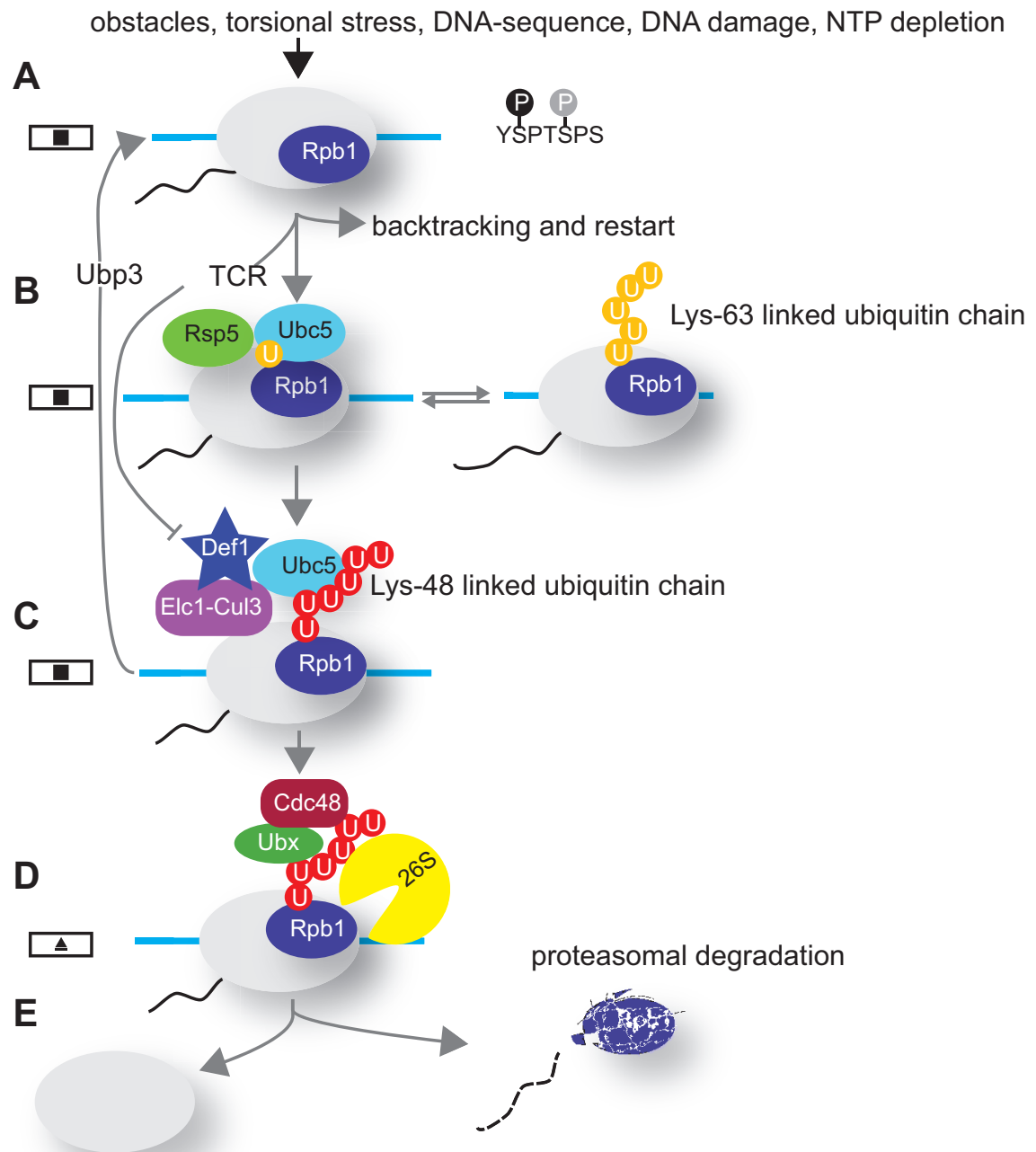


**Figure 1.3: Model of elongation arrest dependent *Rpb1* ubiquitination.** After arrest (A) *Rsp5* and *Ubc5* attach a single ubiquitin to RNAPII subunit *Rpb1* (B). This can be extended to a Lys-63 linked polyubiquitin chain. The Lys-63 linked polyubiquitin chain does not direct *Rpb1* to proteasomal degradation. (C) Mono-ubiquitinated *Rpb1* is recognized by *Def1*, *Elc1-Cul3* and *Ubc5*. This adds a Lys-48 linked polyubiquitin chain. The Lys-48 linked polyubiquitin chain can be removed by the action of *Ubp3*. (D) If not removed, the ATPase *Cdc48-Ubx5* and the 26S proteasome bind to the Lys-48 linked polyubiquitin chain, which leads to the proteasomal degradation (E) of *Rpb1* and disassembly of the elongation complex. This figure is modified from Wilson et al.<sup>[139]</sup>

## 1.2 Aim: Transcriptional regulation of *BR2.1*

Investigation of the heat-shocked-induced down-regulation of *BR2.1* transcription was initially performed due to the observation that *BR2.1* mRNA is left at the *BR-2*-puff after heat-shock. This fact was unexpected, even when considering already known mechanisms for the regulation of transcription. Transcriptional regulation is a key step in gene expression control. A new transcriptional regulation mechanism could change the views and models of the control of gene expression regulation significantly. Due to impact of a new transcription regulation mechanism this observation had to be confirmed by several independent experiments, first. Later experiments might then provide additional insight.

## 1.3 Nucleocytoplasmic Trafficking

Nucleus and cytoplasm are separated by the nuclear envelope. The nuclear envelope consists of two lipid bi-layers. The lumen between the bi-layers is called perinuclear space and is contiguous with the lumen of the endoplasmic reticulum. Nuclear pore complexes span the nuclear envelope (NE) and through it almost all nucleocytoplasmic material is exchanged. Particles with a molecular mass below ~20 kDa to 40 kDa are able to diffuse through the NPC freely.<sup>[128]</sup> For particles with a higher mass the NPC forms a permeability barrier. They need the assistance of transport factors to cross it.

Several nucleocytoplasmic transport mechanisms for various cargoes are known.<sup>[123]</sup> All known nucleocytoplasmic transport routes are uni-directional for im- or export and share the same principle of how the directionality is achieved. On one side of the NPC, the cargo is bound either directly by a transport factor or by adapter proteins which recruit transport factors. It is then able to diffuse through the NPC. On the other side of the NPC, the cargo transport factor complex is efficiently dissolved and recycled. Without the transport factor the cargo is now trapped on the other side of the NPC. The transport itself is an equilibrium reaction between the transport factor-bound cargo at both sides of the NPC. By actively imbalancing the concentration of transport factor bound cargo in one compartment this reaction gains a directional net flux.<sup>[57]</sup> A localization sequence motif of the cargo defines whether a cargo is imported into the nucleus or is exported out of it. Cargoes carrying both, a nuclear localization sequence (NLS) and a nuclear export sequence (NES), can shuttle between nucleus and cytoplasm. The efficiency of the cargo transport factor association and dissociation defines the efficiency of the directional transport. The translocation through the NPC occurs via Brownian motion. The transport direction follows the gradient of transport factor bound cargo.

The final result is an uneven distribution of the cargo in nucleus and cytoplasm. Therefore, this transport process requires energy. The energy is provided as chemical energy and is used to introduce a concentration imbalance of the factor cargo complexes at the two compartments. This source-sink principle is a common transport mechanism in organisms and for example is used for the long distance phloem transport in plants.<sup>[71]</sup> *Michael Elbaums* lab showed in several publications how the reaction kinetics of the single equilibrium reactions can set up the directional transport through the NPC.<sup>[57,58]</sup>



### 1.3.1 The Nuclear Pore Complex

The NPC consists of the central framework, the cytoplasmic filaments and the nuclear basket (Fig. 1.4). It shows an octagonally cylindrical symmetry about its nucleocytoplasmic axis and a planar pseudo-symmetry through the nuclear envelope.<sup>[48]</sup> Considering its high mass it consists of a surprisingly low number of different proteins (~30) called nucleoporins. Nucleoporins are commonly named Nup followed by their molecular mass. Nups are subdivided into membrane-anchored Nups, barrier Nups or scaffold Nups. Each Nups is present 8-, 16-, 32-, or 48-times in each NPC. While all eukaryotes share this basic sketch, the dimensions and the total molecular mass of the NPC among them varies broadly (~66 MDa *Saccharomyces cerevisiae*, 112 MDa *Xenopus laevis*). The protein composition of the NPC is well studied and reviewed in detail by Grossman *et al.*<sup>[39]</sup>

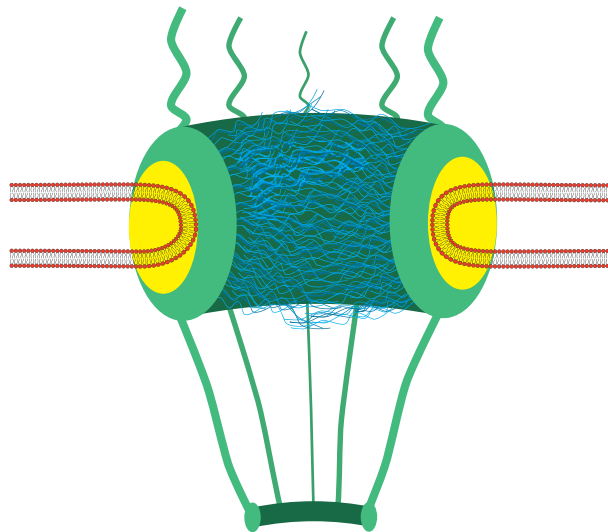


**Figure 1.4: NPC-geometry.** The NPC is anchored via the pore membrane (POM) proteins (yellow) to the nuclear membrane. The Nups of the central framework adapt to the POM-proteins. The Nups of the central provide adaption point for the cytoplasmic and nucleoplasmic filament. The nuclear filaments are interconnected at their opposite end to the central framework and form the so called nuclear basket.

Filamentous Nups are anchored at the inner surface of the central framework.<sup>[39]</sup> These Nups contain phenylalanine-glycine repeats and are therefore called FG-Nups. FG-Nups contain large 'intrinsically disordered domains'.<sup>[87]</sup> The FG-repeats are essential for the formation the permeability barrier.<sup>[34]</sup> Its integrity is essential for viability.<sup>[119]</sup> The structural organization of the FG-Nups and the mechanism by which they form the permeability barrier is a highly debated topic.<sup>[143]</sup> Particles with a diameter below 5 nm are able to pass the NPC freely.<sup>[89]</sup> Larger molecules need transport factors to cross the permeability barrier.<sup>[39]</sup> The specific low affinity interaction of the transport factors and the FG-Nups allow them and the transport factor

cargo complexes to cross this permeability barrier. By adding a high number of transport factors to it even bulky and very artificial cargoes as quantum dots can cross the NPC.<sup>[77]</sup>

The nuclear basket consists of eight spokes which are inter-connected at their nucleoplasmic end. The nuclear basket is essential for quality control of the mRNA before export.<sup>[36]</sup>

The eight cytoplasmic filaments contains proteins, which provide essential interaction domains for the mRNA export.<sup>[47,69]</sup> The asymmetric layout of the NPC forms the scaffold for the asymmetric reaction scheme of mRNA-export.

### 1.3.2 The mRNA-Export Pathway

The separation of transcription and translation allows processing of the mRNA, e.g. splicing. Eukaryotic genes contain introns and exons. Exons are the sequence parts, which are used for translation. For a long time, introns were seen as genetic junk. By now, it is recognized that they are important, e.g., for regulatory processes. But not all exons coded in a single gene are present in the fully processed mRNA. By a mechanism termed alternative splicing, the exon composition of the fully processed mRNA can be varied. Which exons are spliced out is often a highly regulated process. Alternative splicing enables a cell to code numerous protein variants by a single gene and therefore increases the diversity of eukaryotic gene expression tremendously.

Next to the proteins required for splicing, numerous proteins bind to the mRNA during maturation. Only a minority of them is essential for mRNA-export. The processing of the mRNA begins co-transcriptionally. After the transcript reaches a length of 20-30 nucleotides, the 5' end is modified with a 7-methylguanosine cap, which is bound by the cap binding complex.<sup>[14,112]</sup> The 7-methylguanosine cap is important to protect the nascent mRNA against degradation and only to a minor extend for mRNA export. Nevertheless, uncapped mRNA is exported less efficiently compared to capped mRNA.<sup>[17]</sup>

Splicing of the nascent mRNA starts co-transcriptionally, too. The exon junction complex is recruited to the splice site presumably by components of the spliceosome.<sup>[10,68]</sup>

Next to splicing, capping of the mRNA is important for the recruitment of the transcription-export (TREX) complex. The TREX complex consists of the THO complex. Aly acts as adaptor for the Nxf1-Nxt1 heterodimer. By interacting with the FG-nucleoporins Nxf1-Nxt1 acts as transport factor for mRNA and is indispensable.<sup>[14,41]</sup>

The nascent transcript is packaged cotranscriptionally by six core heterogeneous nuclear ribonucleoproteins (hnRNP) (A1, A2, B1, B2, C1 and C2) in a bead-on-a-string like structure resembling the structure of DNA nucleosomes.<sup>[6,52]</sup> The hnRNP family contains more than 20 different proteins. All of them contain one or more RNA binding domains. They are

involved in mRNA packaging, RNA biogenesis and regulatory processes. Hrp36 is the *C. tentans* homologue of hnRNP A1. Hrp36 and other hnRNPs accompany the mRNA from transcription to and through the NPC to the ribosome.<sup>[26,51,131,147]</sup>

The complex of the mRNA and its associated messenger ribonucleoproteins is called mRNP-complex or mRNP-particle. After dissociation from the chromatin the mRNP-particle is already export competent. But before the mRNP-particle can enter the central framework it passes a quality control located at the nuclear basket. In yeast, mRNP-particles which are not fully processed, are retained by Mlp1. By knocking out Mlp1 or preventing its binding to the nuclear basket, not completely processed mRNAs can traverse the NPC.<sup>[36]</sup> Therefore, successful splicing is not a prerequisite for an mRNA to be export competent. As a result of inhibiting splicing, a high concentration of unspliced mRNA is located at the cytoplasm.<sup>[76]</sup> The high number of unspliced mRNA approaching the NPC seem to overstress this quality control step which, indicates that not fully spliced mRNAs are actively retained from entering the NPC, too.

Dbp5 is an RNA helicase, which is located at the cytoplasmic side of the NPC and is essential for mRNP-particle export. Actual models propose that Dbp5 removes export factors from the mRNA at the cytoplasmic side of the NPC. Thereby it prevents the backsliding of mRNP-particles into the nucleus once they exited the NPC at the cytoplasmic side and induces a net flux of mRNP-particles out of the nucleus. Based on this model of mRNA-export Dbp5 and its helicase activity are of great interest. The different published models of the Dbp5 reaction scheme during mRNA-export differ slightly.<sup>[9,47,69,90,125,135]</sup> All share the common idea that the essential factors for the Dbp5 cycle are located at the cytoplasmic side of the NPC (Fig. 1.5). Inhibiting Dbp5 causes the accumulation of mRNA in the nucleus.<sup>[47]</sup> Furthermore, perturbation of Gle1 localization at the NPC causes nuclear mRNA accumulation, too.<sup>[95]</sup> FRAP measurements showed that the accumulation of Dbp5 at the NPC is highly dynamic. Dbp5 mutants lacking RNA-binding compete with functional Dbp5 for Gle1 binding and has a dominant negative effect on mRNA-export.<sup>[47]</sup> According to the actual models of mRNA export we would expect an equal distribution of mRNA if Dbp5 activity is inhibited. Based on the data collected from experiments inhibiting Dbp5 or the spatial organization of its cycle, Dbp5 rather facilitates the exit of mRNPs out of the nucleus than preventing the backsliding of single mRNPs into the nucleus.

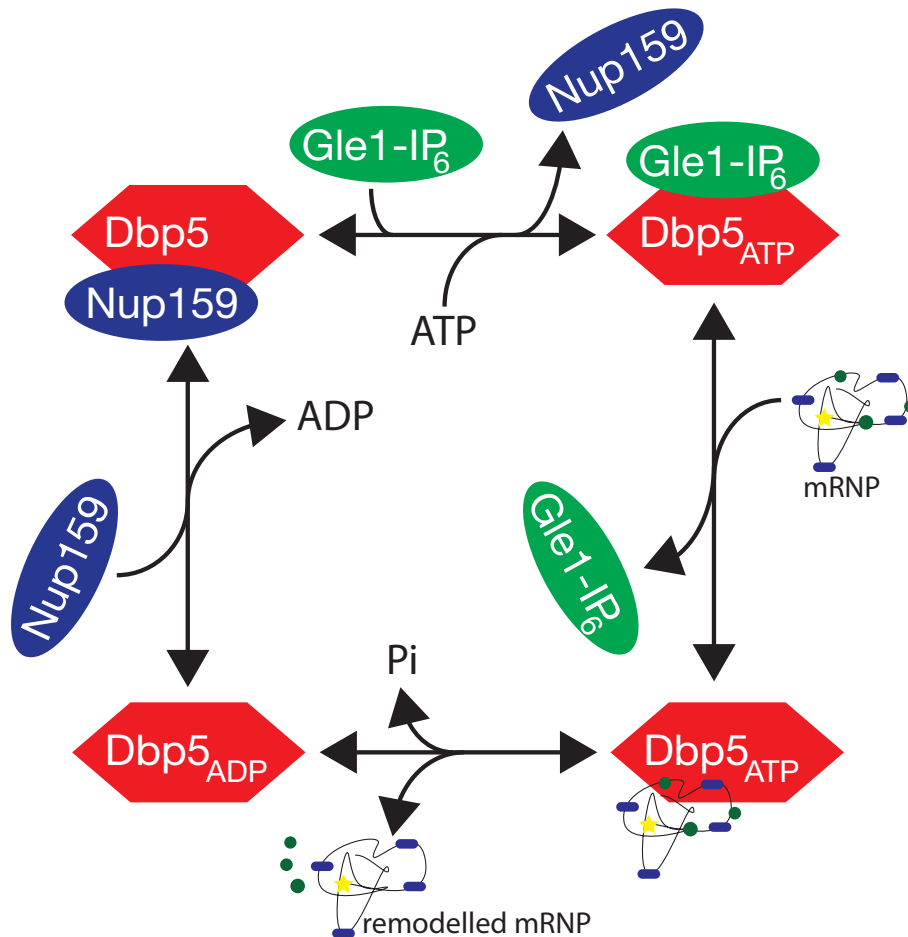


**Figure 1.5: Dbp5 reaction scheme.** *Dbp5-ATP efficiently binds to mRNA. Dbp5-ATP bound to an mRNA-protein complex is capable of inducing a conformational change of Dbp5 driven by ATP hydrolysis. This conformational change is translated via the two RNA binding domains of Dbp5 to the mRNA. Gle1-IP<sub>6</sub> stimulates the ATP-hydrolysis. After remodeling, Dbp5-ADP dissociates from the RNA. The Nup159 stimulated ADP release triggers another conformational change of Dbp5 to apo-Dbp5. Promoted by Gle1-IP<sub>6</sub> Apo-Dbp5 can be loaded with ATP again and is ready for another cycle of mRNA-export. Figure is modified from Noble et al.<sup>[95]</sup>*

## 1.4 Aim and Measurement Principles

The aim of this thesis was to analyse the kinetics and dynamics of nuclear export of native mRNP-particles. Therefore, the transit of mRNP-particles through the NPC were imaged at single molecule level in explanted salivary glands of *C. tentans*. The transit of single mRNP-particles through the NPC was to be measured and its trajectories tracked.

To track single particles, their concentration has to be as low that the single particles are distinguishable (Fig. 1.6). Here, fluorescently labeled Hrp36 was microinjected and thus is incorporated during transcription into mRNP-particles. In *C. tentans* the NPC density is so high that the fluorescently labeled NPCs appear as a closed line, consistent with the NE-position. The microscopical setup, that was used, allows to excite with different wavelengths sequentially. The NE is a rather static structure. Therefore, the position of the NE was imaged in constant intervals. During two NE imaging intervals the labeled mRNP-particles were imaged. Here, the NE-position was used to extract the according pixels of the mRNP-particle image sequences (Fig. 1.6). These pixels were plotted in a kymograph over time. The interaction time of the mRNP-particle and the NE is proportional to the number of pixel it is seen in the kymograph. The frame-wise imaging provides a time discretization and also limits the shortest measurable interaction time. To analyze the mRNP-particle NE interaction kinetics in detail the interaction time distributions were analyzed using advanced statistical methods.

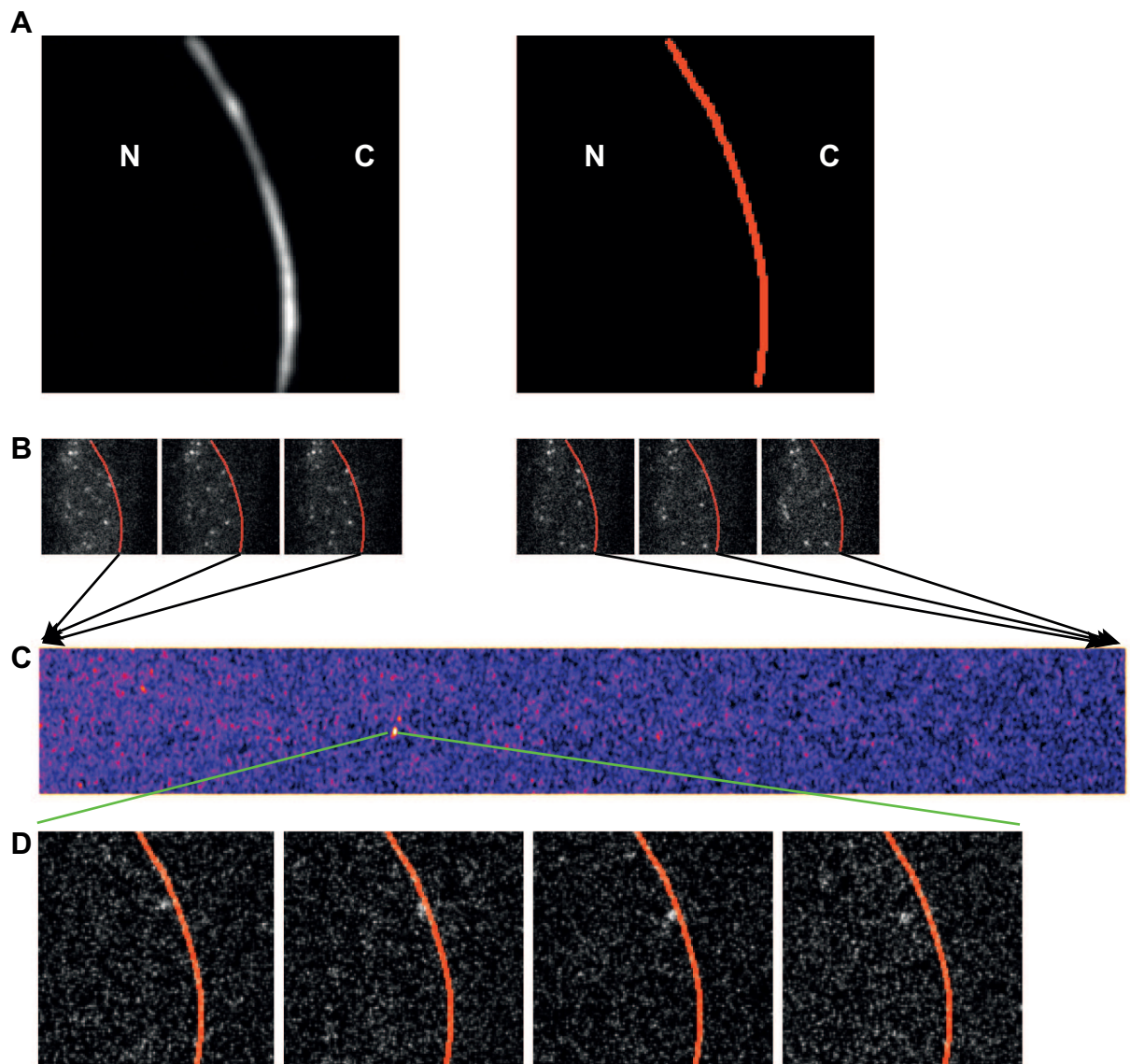


**Figure 1.6: Image analysis procedure.** (A) The stained nuclear envelope was imaged and its position extracted by a gaussian fit. (B) The pixels  $\pm 1$  pixel consistent with the NE (red line) were extracted out of the frames showing the labeled mRNP-particles. (C) These pixels were straightened to a column. According to their temporal order, all columns were aligned along the x-axis to a kymograph. The kymographs were manually inspected for horizontal stripes. The horizontal stripes correspond to an mRNP-particle NE interaction (D) For every detected horizontal stripe the according video frames were inspected to determine if the NE-interaction correspond to a export or probing event. Here a nuclear probing events is shown. The field of view is  $20 \times 20 \mu\text{m}^2$ .

## 1.5 Statistical Analysis

Studying biological processes via single molecule microscopy allows to determine the distribution of a parameter, instead of just measuring its average value as ensemble measurements do. For analysis, the data is usually fitted with a mathematical model. The model used for curve fitting is the mathematical formalization of the qualitative and quantitative characteristics of the process. The parameters extracted by data fitting with a certain mathematical model can give an important insight into a process. A poor mathematical model or incorrect data analysis procedures can cause severe misinterpretations. Therefore, sophisticated testing of the extracted information is needed. Three questions, which have to be answered regularly, are

1. Which model should be used?
2. Does the applied model fit the data appropriately?
3. What is the confidence level of the estimated parameters?

To answer the first question model selection procedures can be used. Model selection procedures compare different models regarding to the trade-off between goodness-of-fit and model simplicity. They are aimed to select a model, which minimizes the information loss.<sup>[12]</sup> A common method for model selection is the usage of the Akaike information criterion (AIC).<sup>[11]</sup> The AIC and other model selection procedures give a relative comparison between different models.

The second question is commonly answered by statistical hypothesis testing. For classical hypothesis testing, the deviation between the observed and expected values according to the null hypothesis are summarized by a test-statistic in a first step. Test-statistics describe this deviation with a single value. If the sampling distribution of the test-statistic is known for the null hypothesis, the test-statistic of the sample can be used to calculate the p-value for a particular observation. The p-value gives the probability to obtain a test-statistic at least as extreme as the observed one, under the assumption that the null hypothesis is true.

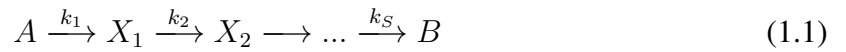
For many widely used probability density functions (PDFs), such as normal distribution, exponential distribution, Poisson distribution, the sampling distributions of different test-statistics are known *a priori*. Biological processes observed by single molecule microscopy often cannot be described by this basic PDFs. Bootstrapping is a method which can be used to estimate the sampling distribution of a test-statistic. This allows to perform hypothesis testing for a large variety of mathematical models. Bootstrapping can also be used to estimate the confidence levels of fit parameters.

Bootstrapping is a resampling method which was published by *Efron* 1979.<sup>[31]</sup>

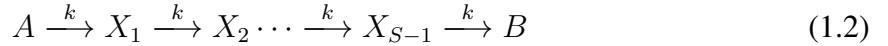
As the main literature source “Bootstrap Techniques for Signal Processing” by *Abdelhak M. Zoubir and D.Robert Iskander* was used in this thesis.<sup>[146]</sup> It will not be referenced explicitly throughout the text to avoid a disruption of readability. All calculation examples were computed by self-written Matlab scripts.

### 1.5.1 Dwell Time Modeling Using Gamma Distribution

The observed kinetics of biological processes is often based on a reaction scheme with  $S$  reaction steps.



Here, the dwell time kinetics were modeled as a uni-directional reaction and every single reaction step is seen as a Poisson process with the rate constant  $k_i$ . Only rate limiting reaction steps will contribute to the reaction kinetics. By taking into account that the kinetics of the slowest reaction step(s) will govern the observed kinetics  $p_{A \rightarrow B}$ , it is plausible to assume that all observed rate limiting reaction steps share the same rate constant.<sup>[33]</sup> This assumption simplifies the reaction scheme for a reaction with  $S$  rate limiting steps to



The PDF of this reaction is an exponential decay with the rate constant  $k$  convoluted  $S - 1$  fold with itself.<sup>[33]</sup>  $S$  denotes the number of reactions steps. The  $S - 1$ -fold convolution of an exponential distribution results in a gamma distribution with the parameters  $S$  and  $k$ .<sup>[78]</sup>

$$p_\gamma(t; k, S) = \frac{k^S t^{S-1}}{\Gamma(S)} e^{-tk} \quad (1.3)$$

For  $S = 1$ ,  $\frac{k^S t^{S-1}}{\Gamma(S)} = k$ , the equation  $p_\gamma(t; k, S)$  reflects an exponential density distribution (Fig. 1.7).

With increasing  $S$  the changes of the shape are more subtle and the correct estimation of the number of rate limiting steps becomes less probable. The uncertainty or the standard deviation of the number of rate limiting steps estimation  $\sigma_S$  depends on the true number of rate limiting steps and the number of observations  $n$ <sup>[33]</sup>

$$\sigma_S = \frac{2\sqrt{S} + S\sqrt{2}}{\sqrt{(n)}} S \quad (1.4)$$



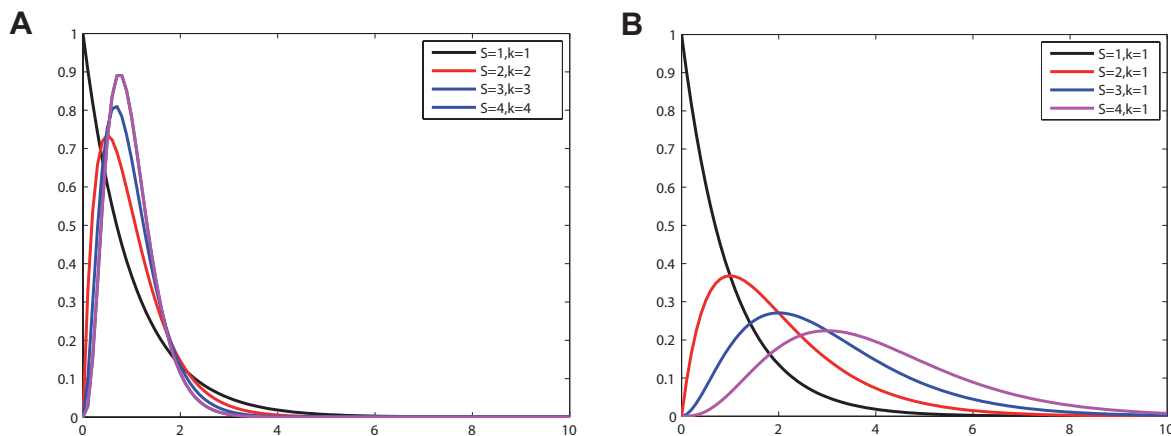


**Figure 1.7:** *Examples of gamma distributions with varying  $S$  and  $k$ . The mean of the gamma distribution is  $S/k$  and its variance  $S/k^2$ . (A) If  $S/k$  is constant and the number of steps  $S$  is increased, the gamma pdf becomes narrower and more symmetric around its mean value. (B) The gamma pdf is shifted to the right and becomes broader if  $k$  is constant and the number of rate limiting steps  $S$  is increased.*

A table of  $\sigma_S$  for values of  $S$  and  $n$  in the relevant range for this thesis is shown in table 7.3 (p. 121). Here, all kinetics were modeled with single or the sum of up to three independent gamma distributions.

## 1.5.2 Parametric-Bootstrapping Based Hypothesis testing

Parametric-bootstrapping is a method which allows the efficient estimation of a test-statistic sampling frequency. First, the empirical data  $x_i$  with  $i = 1 \dots n$  is fitted by the model function  $F(t; \Theta)$  (Fig. 1.8 ①) to obtain  $\hat{\Theta}$  as estimator of the null distribution parameters  $\Theta_0$  (Fig. 1.8 ②). Based on  $\hat{\Theta}_0$   $m$ -values  $\hat{x}_{0i} = (\hat{x}_{0,1}, \dots, \hat{x}_{0,m})$  following the estimated null distribution  $\hat{F}_0$  are calculated (Fig. 1.8 ③). To estimate the test-statistic sampling frequency of  $\hat{F}_0$  asymptotically correct  $m \rightarrow \infty, \frac{n}{m} \rightarrow 0$  is needed.<sup>[7]</sup> By resampling  $\hat{x}_{0,m}$  with replacement  $\hat{x}_{0,i}^* = (\hat{x}_{0,1}^*, \dots, \hat{x}_{0,n}^*)$  is created giving  $\hat{F}^*_b$ , with  $b = 1, \dots, b = B$  (Fig. 1.8 ④). The test static value  $T_b^*$  is calculated for every  $\hat{F}^*_b$  (Fig. 1.8 ⑤). The pdf of  $T_b^*$  is an estimator for the test statistic sampling frequency assuming that the null distribution is true. Its quantiles can be used to calculate a critical value  $\hat{T}_\alpha$  for hypothesis testing (Fig. 1.8 ⑥ & ⑦). If the test statistic of the observed data  $T$  is smaller than the critical value  $\hat{T}_\alpha$  the null hypothesis is accepted (Fig. 1.8 ⑦).

To demonstrate the performance of this approach, the  $\chi^2$  test-statistic sampling distribution of an exponential distribution ( $S = 1, k = 1$ ) was calculated as described above and compared to the theoretically known test-statistic distribution. Plotting the quantiles of the  $\chi^{2*}$  distri-

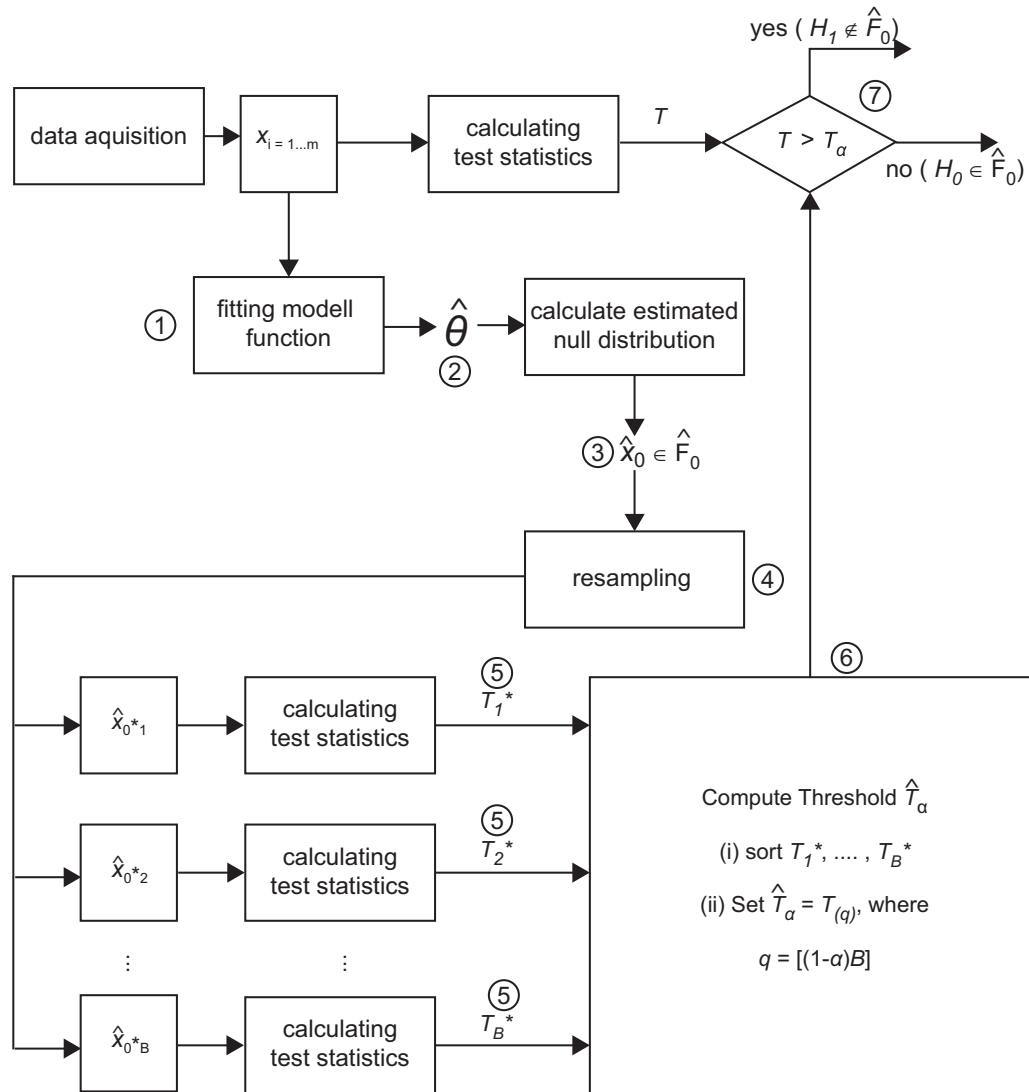


**Figure 1.8: Parametric bootstrapping scheme.** Estimation of the test statistics by parametric bootstrapping. Modified from Zoubir and Iskander<sup>[146]</sup>.

bution obtained by 10,000 bootstrap cycles against the expected  $\chi^2$  quantiles shows that this approach resembles very accurately the theoretical  $\chi^2$  test-statistic distribution.

The accuracy of the test-statistic sampling frequency estimation depends on the number of bootstrap cycles (Fig. 1.10). Parametric bootstrapping requires only little computation power on a current computer (Intel Core i7 3 GHz CPU). 10,000 bootstrap cycles take ~10 s. This makes it easy to achieve an accurate estimation of critical values.

Next to the sufficiently accurate estimation of the critical value, the use of an appropriate function for test-statistic calculation is crucial. Commonly used test-statistic functions belong to the Cressie-Read family as the  $\chi^2$ -test-statistic. If the null distribution shows a very low

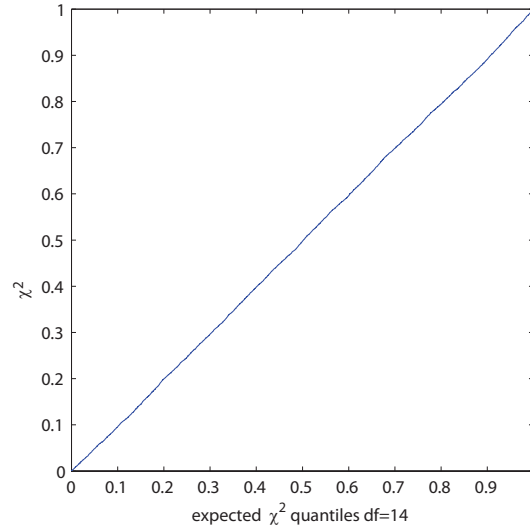


**Figure 1.9:** *Quantile-quantile plot of  $\chi^2_*$  quantiles against theoretical expected  $\chi^2$  quantiles. The sampling frequency of  $\chi^2_b^*$  was calculated by 10,000 bootstrap cycles. The Quantile-quantile plot shows that  $\chi^2_*$  distribution resembles accurately the theoretical expected sampling frequency distribution of the  $\chi^2$  test-statistic.*

probability for some classes (compared to other classes), divisions by- or near-to-zero can occur. This restricts the statistical power of the  $\chi^2$  test statistics severely, even if the boundary conditions of the  $\chi^2$  distribution are fulfilled.<sup>[99]</sup> The Freeman-Tukey test-statistic which also

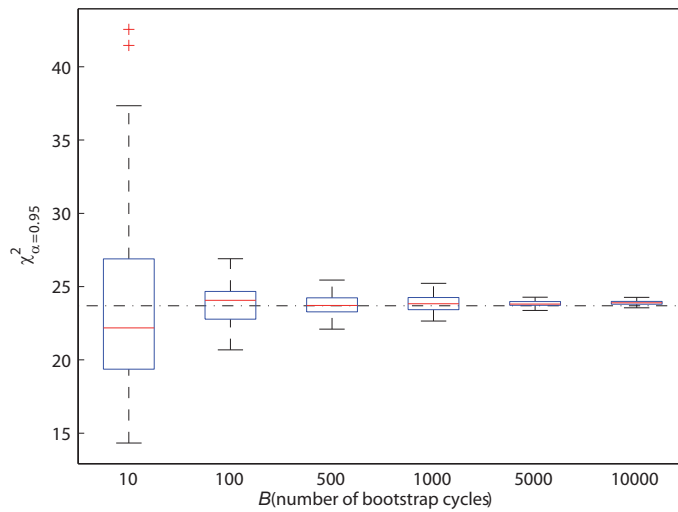


**Figure 1.10:** *Increasing accuracy of critical value estimation with increasing number of bootstrap cycles by parametric bootstrapping. The box plots show the  $\chi^2_{\alpha=0.95}^*$  value obtained by repetitive parametric bootstrapping ( $n=50$ ) with varying numbers of bootstrap cycles. It shows clearly that variance of the  $\chi^2_{\alpha=0.95}^*$  value decreases with increasing number of bootstrap cycles and its convergence to a value close to the theoretically expected  $\chi^2_{\alpha=0.95}$  quantile (black dash-dot line). Bottom and top of the boxes represent 1<sup>st</sup> and 3<sup>rd</sup> quartile and the red line the 2<sup>nd</sup>. The whiskers represent the  $\pm 1.5$  times interquartile range and + the outliers.*

belongs to the Cressie-Read family performs better under these conditions, but the simple Euclidean distance of  $\hat{F}_0^{*b}$  and  $\hat{F}_0$  gives asymptotically correct critical values for hypothesis testing and performs very well with sparse data.<sup>[98]</sup>

### 1.5.3 Non-Parametric-Bootstrapping

Non-Parametric-Bootstrapping allows to estimate the confidence of the fit parameters. It can be used even if the null-distribution is unknown.

The vector  $x_i = (x_1, \dots, x_n)$  is a vector which contains  $n$  observations with the distribution  $F$ . The parameters  $\hat{\Theta}$  are calculated by fitting the distribution function to  $A$  to  $F$ . To analyze the distribution of  $\hat{\Theta}$  the experiment has to be repeated. The distribution of  $\hat{\Theta}$  can be used to give confidence intervals for the estimated parameters. Non-parametric bootstrapping allows to estimate the distribution of  $\hat{\Theta}$  by using only the initial observations  $x_i$ . A new sample  $x_i^*$  is generated by resampling  $n$ -times out of  $x_i$  with replacement (Fig. 1.11 ①). This step is repeated  $B$  times. The same model function  $A$  is fitted to all bootstrap samples  $x_{i^*1} \dots x_{i^*B}$  to calculate  $\hat{\Theta}_{i^*1} \dots \hat{\Theta}_{i^*B}$  (Fig. 1.11 ②). The distribution of  $\hat{\Theta}_{i^*1 \dots B}$  allows to determine the confidence interval of  $\hat{\Theta}$  (Fig. 1.11 ③).

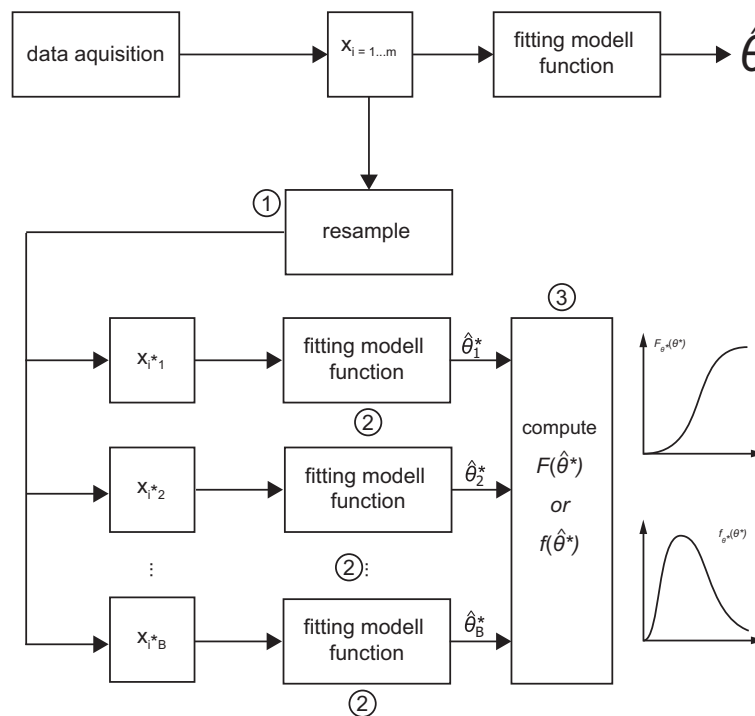


**Figure 1.11: Non-parametric bootstrapping scheme.** Estimation of the distribution of  $\hat{\Theta}$  by non-parametric bootstrapping. Modified from Zoubir and Iskander<sup>[146]</sup>.

## 1.6 *Chironomus tentans*

*Chironomus tentans* is a non-biting midge and belongs to the family of the *Chironomidae*. This family contains around 5000 different recent species with a cosmopolitan distribution. Like other *Chironomus* species, *C. tentans* can be cultivated in the lab.<sup>[54]</sup> The life cycle of *C. tentans* shows four different stages. The egg, larval and pupal stages are aquatic (freshwater), while the adult stage is non-aquatic (Fig. 1.12). The duration of the aquatic stages depends on temperature, access to food and number of light hours and takes four to eight weeks. The adult stage last only a few days. After mating, the female lays an egg strand into shallow water. A single egg strand contains 300-3000 eggs.<sup>[138]</sup>

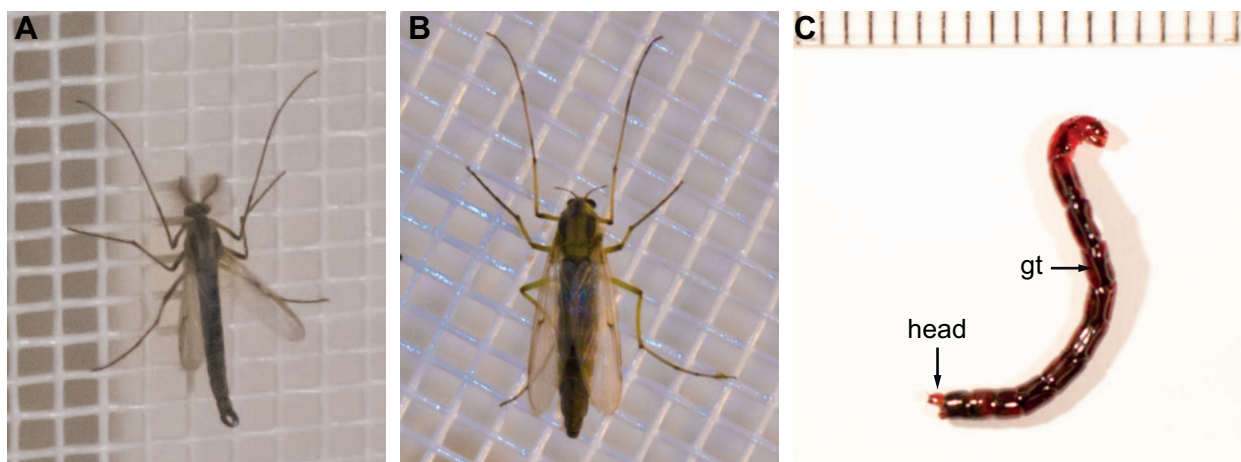


**Figure 1.12:** Adult and larval stage of *C. tentans*. Male (A) and female (B) adult *C. tentans*. The antennas of *C. tentans* show a strong sexual dimorphism. Males have much more complex feather-like antennas. The antennas of female animals look rather rod-shaped. (C) The size of *C. tentans* larvae increase with developmental stage. The shown larva has a length of ~25 mm. The gastrointestinal tract can be recognized by eye. It occupies most of the larval body volume. gt= gastrointestinal tract. Standard ruler length markings with 1 mm distance.

The egg strand consists of a gelatinous mass, in which the eggs are embedded until hatching. The larval development is divided into four instars. After hatching the larvae build a larval tube. The larval tube consists of a thin protein wall, in which surrounding materials are regularly incorporated.<sup>[138]</sup> The proteins, which are used for larval tube building, are secreted by the salivary glands. The secreted protein mix consists of 15 different proteins with molecular masses ranging from 12 kDa to 1000 kDa.<sup>[35,46]</sup> Gene products of the BR-genes make up a major part of the secreted proteins. BR saliva proteins can be modified by post-translational phosphorylation and carbohydrate addition and show a silk like consistency.<sup>[101]</sup> The larvae spend most of the time inside their tubes. The larval tubes are consistently maintained and enlarged to compensate for their growth. Therefore, the salivary proteins are produced throughout

most of the larval stage.<sup>[138]</sup>

*C. tentans* larvae show the characteristic segmental body plan of insect larvae. It has three head, three thoracic and nine abdominal segments (Fig. 1.12).

*C. tentans* larvae have two salivary glands which are located at the second and third thoracic segment. One salivary gland consists of 30-40 cells.<sup>[138]</sup> The cells are placed in one plane.

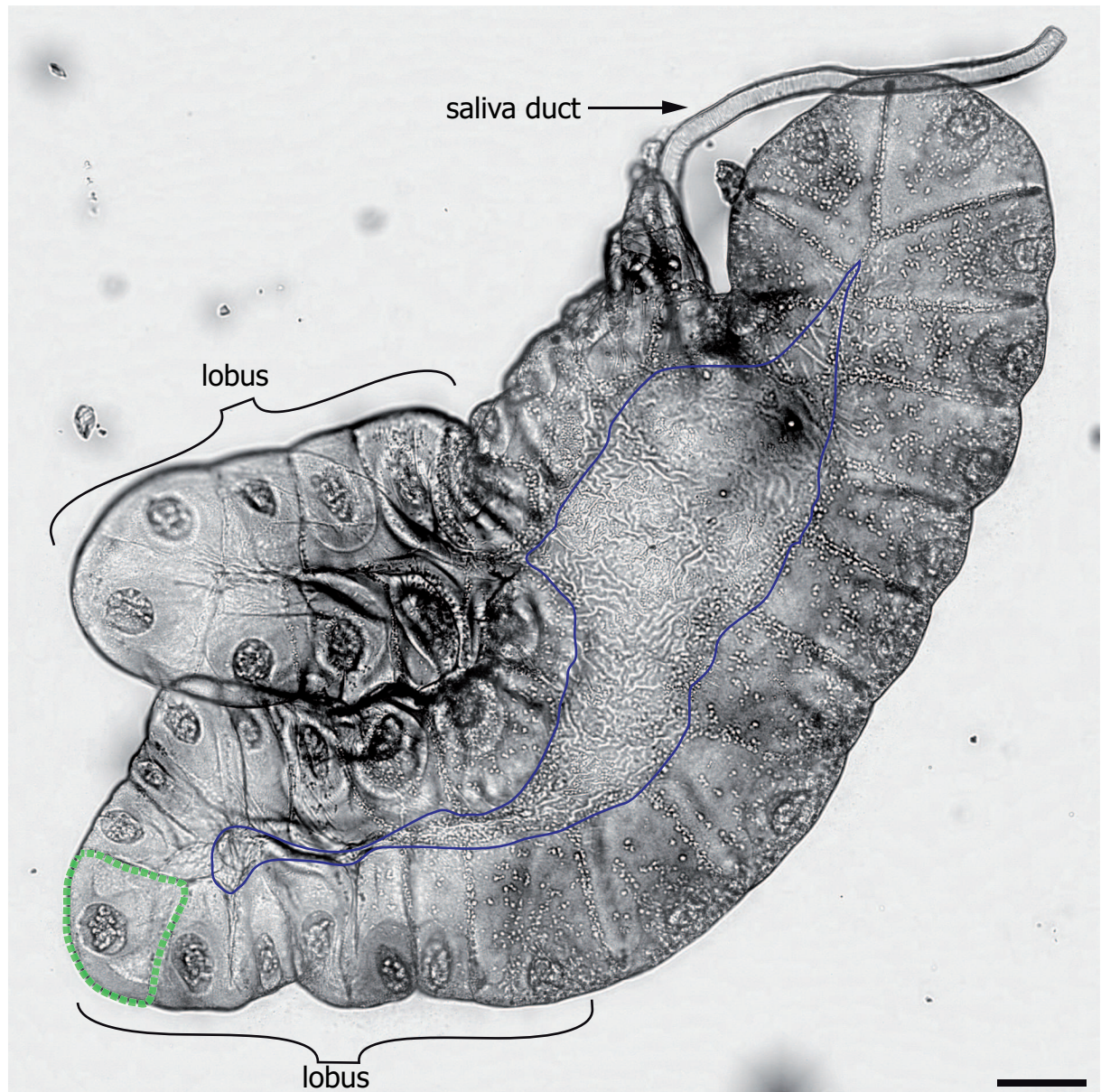


**Figure 1.13:** *Salivary gland of C. tentans* . The salivary gland can be separated into the main body and the two lobes. The saliva duct leads from the main body into the oesophagus. The occupied area of the cells located at the sides (e.g. labeled with dashed green line) is more cubic like. The top and bottom cell are extremely spreaded (blue line). They seal the inter-space between the cells on the side and thereby the gland. Scale-bar is 100  $\mu\text{m}$ .

The top and bottom of the gland is sealed by one single cell each. The cells of *C. tentans* salivary glands and their nuclei are of remarkable size. The nucleus has a diameter of  $\sim 75 \mu\text{m}$ . Seen from the top, the geometry of these cells can be described as saddle-like; from the side as u-shaped (Fig. 1.14). The cells located in the two lobes of the salivary gland show the saddle shape more clearly. Cells located at the main body of the gland are missing this geometry or show it only to a minor extend (Fig. 1.13).

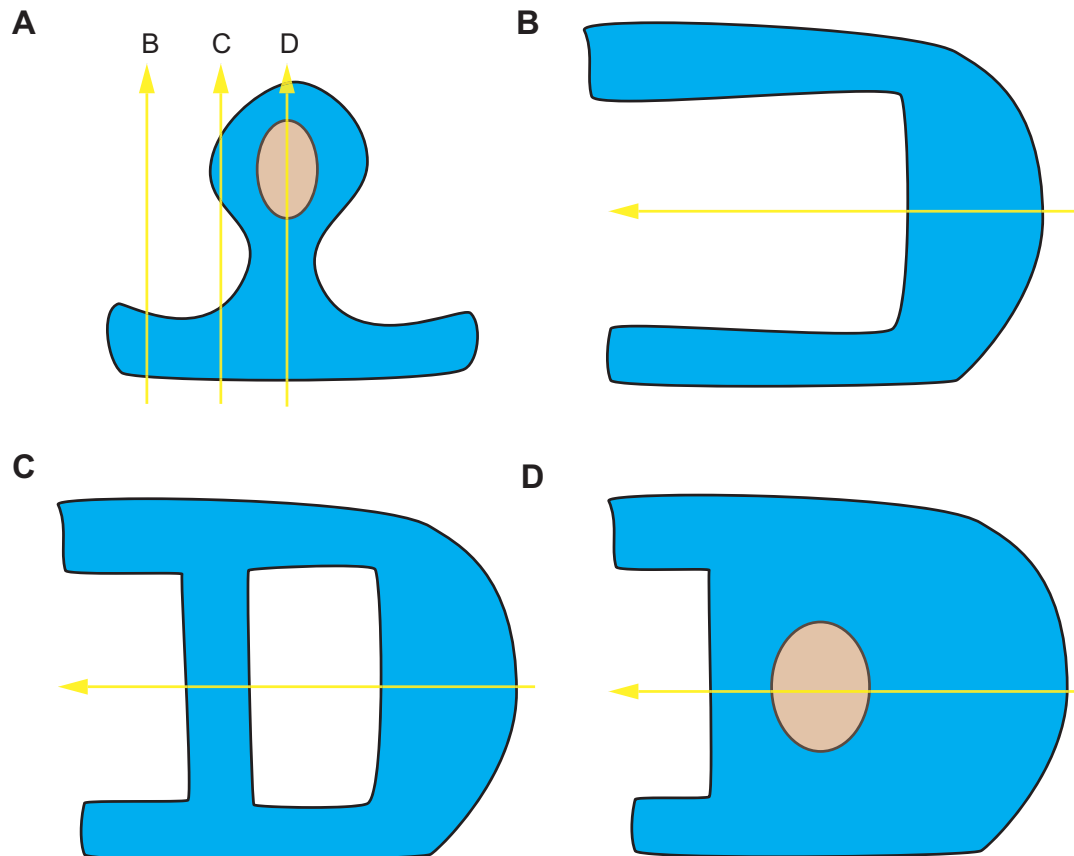


**Figure 1.14:** Sketch of *C. tentans* salivary gland cell geometry. (A) Typical shape of *C. tentans* salivary gland cells from the topview. The sketched cross section (B, C, D) of the top-view along the yellow arrows shows that the cell protrusion which harbors the nucleus is connected to the lower and upper half of the cell body.

A very characteristic feature of salivary gland cells are their polytene chromosomes. Polytene chromosomes consist of numerous, perfectly parallel aligned chromatids. *C. tentans* polytene chromosomes contain 8200 or 16400 chromatids.<sup>[67]</sup> The polytene chromosomes are the result of multiple rounds of replication without cell division. Due to the absence of cell or nucleus dividing activity, the chromatids stay linked after replication. Therefore, these nuclei show a large volume devoid of chromatin.

The spatial organization of the DNA in polytene chromosomes is advantageous for measur-

ing the nuclear export kinetics of mRNP-particles at single molecule level. Even using single molecule fluorescence microscopy, normal chromatin-filled nuclei make it impossible to discriminate the binding of mRNP-particles to chromatin next to an NPC to the binding of these particles to an NPC itself.

During transcription the DNA becomes decondensed. The decondensed and condensed chromosomal sections give the polytene chromosomes their well-known ribbon-like structure. Chromosomal areas with very high transcriptional activity form characteristic DNA puffs. Well known are the Balbiani ring (BR) puffs, which belong to genes coding for saliva proteins.

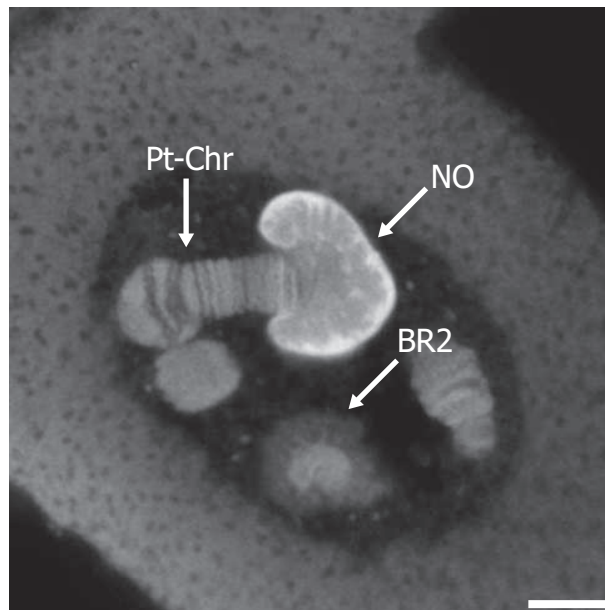


**Figure 1.15:** *Propidium iodide staining of C. tentans polytene chromosomes.* Nuclear RNA was digested by RNase A for background reduction. Since rRNA is more stable against RNase A digestion, the nucleolus (NO) is still visible. The ribbon-like structure of the polytene chromosomes (Pt-Chr) and the large puff formed by the decondensed DNA of the BR2-genes (BR2) are clearly visible. Bar is 10  $\mu\text{m}$ .

*E.G. Balbiani* described these structures for the first time 1881.<sup>[2]</sup> BR2, the largest of the BR puffs, consists of two genes. Their transcripts have a length  $\sim 30$  kb and form giant mRNP-particles with a diameter of 50 nm.<sup>[116]</sup> This large diameter makes the BR2 mRNP-particles easily detectable without affinity labeling using an electron microscope. Years of intense investigations give us numerous snapshots of the fate of BR2 mRNP-particles from transcription to translation. Even the transit of single mRNP-particles through the NPC were observed.<sup>[84,85]</sup> But all these data do not give us information about the dynamics of the nucleocytoplasmic trafficking of mRNPs.

Another characteristic feature of *C. tentans* larvae is their red-colored hemolymph. This



coloration is caused a hemoglobin specific for some insects. *C. tentans* as some of the other *Chironomoid* species, possess this feature. The *C. tentans* hemoglobin consists of 12 subunits and has a very strong affinity to oxygen of 0.1 torr to 0.6 torr depending on temperature and pH-value.<sup>[111]</sup> At 7 torr oxygen partial pressure *C. tentans* hemolymph is still fully saturated. Therefore, it is assumed that the *C. tentans* hemoglobin functions as oxygen storage and not as oxygen transporter as in vertebrates.<sup>[92]</sup> Exposure to air for too long leads to clotting of *C. tentans* hemolymph.

### 1.6.1 The BR Genes of *Chironomus tentans*

The BR-gene family contains four homologous genes (BR1, BR2.1, BR2.2, BR6).<sup>[97]</sup> The BR-gene nomenclature is not consistent throughout literature. This nomenclature will be used, here. All Br-genes encode for large secreted saliva proteins. The BR genes have five exons and four introns (see table 1.1). Exon 4 contains a high number of short repetitive sequences (Fig. 1.16)

	BR1	BR2.1	BR2.2	BR6
Exons (bp)				
1	409	445	373	376
2	18	6	18	15
3	49	43	46	49
4	35000-39000	26000-31000	29000-38000	27000-30000
5	607	609	609	571
Introns (bp)				
1	1790	1009	529	131
2	904	108	1377	67
3	67	1380	520	69
4	55	55	55	62
sum exons (bp)	36083-40083	27103-32103	30046-39046	28011-31011
Translation product (MDa)	1.3-1.4	1.0-1.2	1.1-1.5	1.0-1.1

**Table 1.1:** Exon and intron length of the BR-genes of *C. tentans*. The table is based on Paulson et al.<sup>[97]</sup>

The major part of the BR-genes consists of repetitive basic repeat units.<sup>[101]</sup> The basic repeat unit has a length of 180 bp to 300 bp. The basic repeat unit is subdivided into the constant region and the sub-repeat region (Fig. 1.16 B). While no substructure was found for the constant region, the sub-repeat region can be subdivided further. It contains 3-9 short (9 bp to 33 bp) sub-repeats. The sub-repeat region itself is built up of duplicates of a shorter sequence motif.<sup>[120]</sup> It

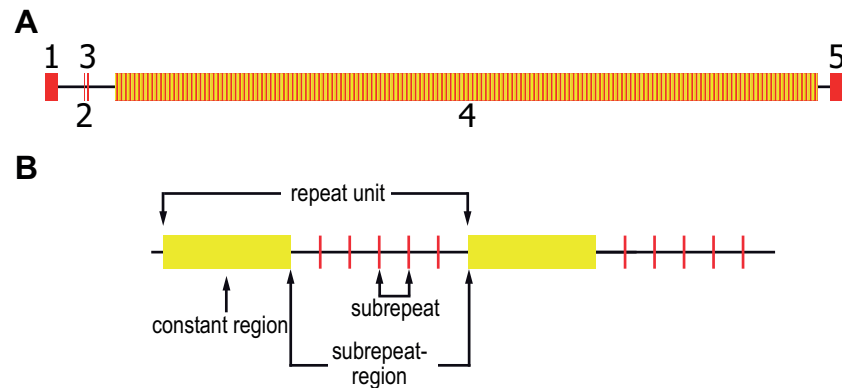


**Figure 1.16: Structure of the BR-genes.** (A) All BR-genes share the same organization. Exon 4 is built up of highly repetitive sequence motifs (red-yellow stripes). The drawing of the exon-intron lengths is scaled according to the BR2.1-gene. For Exon 4 a length of 26 kbp is assumed. The exon numbers are denoted above or below the exons. (B) The repeat units are mainly located in exon 4 and show a nested repetitive structure. The constant region is highly conserved throughout different repeat units. The sub-repeat region is more diverse and contains different numbers of sub-repeats with varying length. (B) is modified from Pustell *et al.*<sup>[101]</sup>

is assumed that the BR-genes are the result of multiple rounds of duplication, divergence and translocation.<sup>[101]</sup>

### 1.6.2 Transcription of the *BR2.1* and its Regulation

The BR2.1 gene is located at the BR2-puff on chromosome IV, the smallest of the four *C. tentans* chromosomes.<sup>[4]</sup> It harbors the BR2.1 and BR2.2 gene. The puffing of the DNA is easily observable by light microscopy. Changes of the BR-puff and indirectly the transcriptional activity of the BR-genes depending on the larval developmental stage or external influence, were studied even before the DNA structure, genes or the existence of transcription was known.<sup>[4,37,133]</sup> It is one of the oldest model systems, in which transcriptional regulation was studied. As already described the larvae maintain and enlarge their larval tube constantly and therefore require saliva proteins constantly. Meyer *et al.* reported for the BR2 genes a constant transcriptional activity throughout larval development. BR1 shows a higher, but more fluctuating transcriptional activity.<sup>[86]</sup>

Upon transcription of the BR-genes, these chromosomal regions expand and form characteristic puffs, which can extend up to ~20  $\mu\text{m}$  into the nucleoplasm. The extent of the BR2 puff was linked to transcriptional activity.<sup>[4]</sup> The extend of the BR2-puff is anti-proportional to the gland lumen degree of filling.<sup>[86]</sup> The transcriptional activity of the BR2-genes can be manipulated with substances like pilocarpine, galactose and ecdysone.<sup>[3,74,80]</sup> By applying a heat-shock to larva or explanted salivary glands the transcriptional activity at the BR2 puff

is reduced rapidly<sup>[75]</sup>. The temperature-dependent reduction of BR2 transcription activity begins at 25 °C. At ~37 °C full reduction of BR2 transcription was reported.<sup>[73,142]</sup> Increasing the temperature further, the BR2 transcription activity begins to increase in comparison to 37 °C. *Yamamoto et al.* showed that heat-shocking larvae for only five minutes is sufficient to induce a reduction of transcriptional activity.<sup>[142]</sup> *Lezzi et al.* reported that minutes after heat-shock release a regaining of transcriptional activity at the BR2-puff<sup>[75]</sup>

As transcription in general, the transcription at the BR2-puff was intensively studied by using transmission electron microscopy. BR2 genes are expressed in a burst-like fashion by so-called transcriptional units. By now these transcriptional bursts are reported for numerous genes in different organisms.<sup>[132]</sup> A single transcriptional unit contains ~123 RNAPII with a distance of ~200 bp in between and is therefore covering more than half of the gene (~69%).<sup>[67]</sup> Therefore, a single transcriptional unit has a mean length of 7.7  $\mu\text{m}$ . On average, a single transcriptional unit is present at a single BR2.1 gene. RNAPII needs ~20 minutes to synthesize the complete BR2.1 mRNA of the 30 kbp to 35 kbp long BR2.1 gene.<sup>[67,97]</sup>

Due to their exceptional size, BR mRNP-particles are easily recognizable without any affinity labeling using transmission electron microscopy. Their size and abundance made them an ideal system to study the fate of mRNP-particles after release from the transcription site.<sup>[27]</sup> The structure of the BR mRNP-particles was studied in detail using electron microscopy tomography.<sup>[116]</sup> This analysis showed with a resolution of 8 nm to 9 nm, that the different BR mRNP-particles have a strikingly similar structure. It has a diameter of  $\approx 50$  nm. It has an asymmetric, four domain ring-like structure with a central slit and its 5' and 3'-end containing domains are close together. Electron micrographs showed that packing of the BR mRNP-particles into their final conformation begins co-transcriptionally.<sup>[116]</sup> The synthesized mRNA shows first a less ordered conformation but is directly associated with proteins to form an initial fibril with a diameter of 10 nm. This fibril is packed later into its final conformation.<sup>[26]</sup> The packaging of the BR mRNP-particle is not completed after release from the transcription site. Before it can be exported out of the nucleus, the packaging and processing of the mRNP-particle has to be finished. After release from the transcription site the BR mRNP-particles diffuse through the nucleus.<sup>[114,130]</sup>

In the nucleus the BR mRNP-particles were found equally distributed.<sup>[26]</sup> The transit of the BR mRNP-particles through the nuclear pore complex was intensively studied using electron microscopy. First the BR mRNP-particle binds to the nuclear basket of a NPC. While it is attached to the nuclear basket its conformation stays unchanged. After entering the nuclear basket and further approaching to the central framework, the BR mRNP-particle is unfolded and elongated during its translocation through the NPC. The rod-shaped BR mRNP-particle is

not repacked into a globular shaped particle after exiting the NPC at the cytoplasmic side. BR mRNP-particles translocate with their 5'-end ahead through the NPC.<sup>[84]</sup> It was furthermore observed that the 5'end can already be bound by ribosomes, while the export process of the BR mRNP-particle is not finished. During the export process some proteins dissociate from the mRNP-particle. Others like Hrp36 accompany the mRNA from transcription through the nucleoplasm on its way to the NPC, during translocation and is still present when the BR mRNP-particle reaches the polysomes.

# 2 Materials and Methods

## 2.1 Buffers

### 10x TBE-Puffer,ph 8,0

- 108 g
- 55 g boric acid

add to 1000 ml with water

### 1x PBS+sugar

- 0.4 mg glucose
- 0.2 mg sucrose
- 0.4 mg trehalose

add to 1 ml with PBS

### 1x PBS+AA

- 20  $\mu$ L Non essential Amino Acid Mix (Biochrom AG, Germany)

add to 1 ml with PBS

### 1x PBS+AA+sugars

- 20  $\mu$ L 50X Non essential Amino Acid Mix (Biochrom AG, Germany)
- 0.4 mg glucose
- 0.2 mg sucrose
- 0.4 mg trehalose

add to 1 ml with PBS

**1x Buffer-K** modified from *Cannon*<sup>[13]</sup>

- 4 mL 50X Non essential Amino Acid Mix (Biochrom AG, Germany)
- 220 mg  $\text{NaH}_2\text{PO}_4$
- 608 mg  $\text{MgCl}_2 \cdot 6 \text{H}_2\text{O}$
- 740 mg  $\text{MgSO}_4 \cdot 7 \text{H}_2\text{O}$
- 596 mg KCl
- 162 mg  $\text{CaCl}_2$
- 140 mg glucose
- 80 mg sucrose
- 1000 mg trehalose
- 80 mg fructose
- 0.004 mg riboflavin
- 0.004 mg nicotinic acid
- 0.004 mg pantothenic acid
- 0.004 mg biotin
- 0.004 mg folic acid
- 0.004 mg inositol
- 0.004 mg choline

add to 1 ml with sterile desalted water

**stop solution**

- 100  $\mu\text{L}$  1  $\frac{\text{mol}}{\text{l}}$  Tris-HCL pH7.5
- 20  $\mu\text{L}$  5  $\frac{\text{mol}}{\text{l}}$  Tris-HCL pH7.5
- 400  $\mu\text{L}$  0.5  $\frac{\text{mol}}{\text{l}}$   $\text{Na}_2\text{EDTA}$  pH8
- 500  $\mu\text{L}$  10% SDS
- 280  $\mu\text{L}$   $\beta$ -MeOH
- 3.7 mL  $\text{H}_2\text{O}$

## 2.2 Materials

Name	Order-ID	Manufacturer
Acrylamid/Bisacrylamid(19:1)	A516.1	Carl Roth (Germany)
ActinomycinD	A1410	Sigma-Aldrich (Germany)
Atto488-dUTP	PP-302S-488	JenaBioscience (Germany)
Biotin	B4501	Sigma-Aldrich (Germany)
Boric acid	Boric acid	Applichem (Germany)
$\beta$ -MeOH	M6250	Sigma-Aldrich (Germany)
Choline chloride	C7017	Sigma-Aldrich (Germany)
EDTA	A8090	Carl Roth (Germany)
Folic acid	7876	Carl Roth (Germany)
Flavopiridol	Cay10009197-5	Biomol (Germany)
Fructose	4981	Carl Roth (Germany)
GelRed	41003	Biotum (USA)
Glucose	6754	Sigma-Aldrich (Germany)
Herculase II	600675	Agilent Technologies (USA)
Inositol	I5125	Sigma-Aldrich (Germany)
KCl	6781	Carl Roth (Germany)
MgCl <sub>2</sub> · 6 H <sub>2</sub> O	A537	Carl Roth (Germany)
MgSO <sub>4</sub> · 7 H <sub>2</sub> O	P027	Carl Roth (Germany)
Mineral Oil	M5904	Sigma-Aldrich (Germany)
NaH <sub>2</sub> PO <sub>4</sub>	T879	Carl Roth (Germany)
Nicotinic acid	72310	Fluka (Germany)
Non essential Amino Acid Mix		Biochrom (Germany)
Pantothenic acid	P3161	Sigma-Aldrich (Germany)
PBS	L 182-01	Biochrom (Germany)
Phenol:chloroform	A156.3	Carl Roth (Germany)
Piperidine	8.22299	MerckMillipore(Germany)
Poly-L-lysine	P8920	Sigma-Aldrich (Germany)
Potassium permanganate	12056	Grüssing (Germany)
Riboflavin	R4500	Sigma-Aldrich (Germany)
Sample chamber light sheet microscope	105.044, Version 2	Hellma GmbH & Co. KG (Germany)
SDS	4360	Carl Roth (Germany)
SlowFade Gold	S36936	Life Technologies (Germany)
Sucrose	3935	Carl Roth (Germany)
Trehalose	309871000	Acros Organics (Belgium)
Tris-HCL	9090	Carl Roth (Germany)
Tween20	9127	Carl Roth (Germany)
ZO-Medium		Statens veterinärmedicinska anstalt (Sweden)

**Table 2.1:** *Used materials.*

## 2.3 Antibodies

Antigen	host	concentration	label	manufacturer	order no.
RNAPII	mouse	1:100	-	Merck-Millipore	CBL221
RNAPII-CTD phospho S2	rabbit	1:250	-	Abcam	ab5095
RNAPII-CTD phospho S5	rabbit	1:250	-	Abcam	ab5131
mouse IgG1	goat	1:500	AF647	Invitrogen	a-21240
mouse IgG1	goat	1:500	AF532	Invitrogen	a-11002
goat IgG	rabbit	1:500	AF647	Invitrogen	a-21086

**Table 2.2:** *Used antibodies.*

## 2.4 Immunostaining of *C. tentans* Larval Salivary Glands

1. Perform steps 1 to 10 as described in 2.5.
2. Incubate primary antibodies overnight at 37 °C. For used antibodies and concentrations see table 2.2 p. 36.
3. 5x45 min PBT wash.
4. Block with PBS+3%BSA for 4 h.
5. Incubate secondary antibodies overnight at 37 °C. For used antibodies and concentrations see table 2.2 p. 36.
6. 5x45 min PBT wash.
7. Place two 20 mm long adhesive transfer tape stripes parallel with 10 mm space between on a microscope slide.
8. Pipette 38 µL SlowFade®Gold between tape stripes.
9. Remove liner from adhesive transfer tape.
10. Place cover slip on tape stripes.
11. Seal all edges with nail polish.
12. After nail polish hardened store microscopic slides at 4 °C .

## 2.5 Fluorescence *in situ* Hybridization

1. Coating cover slips with 30 µl poly-L-lysine.



2. Transfer dissected glands (see 2.6) onto cover slip.
3. Remove remaining buffer from cover slip.
4. Fixation for 20 min fixation with 80  $\mu$ l PBT+4% (PFA).
5. 5x15 min washing with 80  $\mu$ l PBT.
6. 5 min permeabilization with 80  $\mu$ l TE(10  $\frac{\text{mmol}}{\text{l}}$  Tris, 1  $\frac{\text{mmol}}{\text{l}}$  EDTA) + 50  $\frac{\text{mg}}{\text{mL}}$  Proteinase K.
7. Stop permeabilization by 2x washing with 80  $\mu$ l PBT+ 2  $\frac{\text{mg}}{\text{l}}$  glycine.
8. 2x10 min PBT wash.
9. 20 minutes fixation with 80  $\mu$ l PBT+4% (PFA).
10. 5x10 min PBT wash.
11. 20 min SSC-formamide incubation.
12. Hybridization overnight 1  $\frac{\mu\text{g}}{\text{mL}}$  hybridization probe + 1  $\frac{\text{mg}}{\text{mL}}$ . To label BR2.1-mRNA 2'-O-Methyl-RNA oligos (ACU UGG CUU GCU GUG UUU GCU UGG UUU GCU) and the complete mRNA pool poly-dU (dU<sup>20</sup>) labeled with ATTO647N (IBATagnology, Germany) were used.
13. 2x30 min SSC +40 % formamide wash.
14. 2x SSC-PBS wash.
15. Place two 20 mm long adhesive transfer tape stripes parallel with 10 mm space between on a microscope slide.
16. Pipette 38  $\mu$ l SlowFade®Gold between tape stripes.
17. Remove liner from adhesive transfer tape.
18. Place cover slip on tape stripes.
19. Seal all edges with nail polish.
20. After nail polish hardened store microscopic slides at 4 °C .

## 2.6 Dissection of *C. tentans* Larval Salivary Glands

The dissection procedure with subsequent *in vivo* experiments was described previously.<sup>[54]</sup> Here additionally the slight differences for subsequent *in vivo*, immunostaining and *in situ* experiments are described.

1. Collect appropriate amount of larvae and transfer into a beaker with water of the growth dishes.
2. a. For subsequent *in vivo* experiments fill 40 mm  $\varnothing$  petri dish with room temperature PBS.

- b. For subsequent immunostaining and *in situ* hybridization experiments fill 40 mm  $\varnothing$  petri dish with ice cold PBS and add pieces of frozen PBS to keep temperature constant during dissection.
3. Transfer larvae into petri dish and place it under a stereoscopic microscope.
4. Grab the larvae with a Dumont 3c forceps at the abdominal third.
5. Stretch the larvae by scrubbing the body cranial with a No. 10 scalpel.
6. Place scalpel blade between the first and second segment and decapitate the larva. During cutting try to keep the larva strained by pressing the scalpel slightly cranial.
7. Make a second cut 3-4 segments abdominal from the first cut.
8. If the salivary glands are already visible dissect them carefully. The glands are innervated and fixed by several ligaments. Cut the nerve and the ligaments carefully away. If the glands are not visible, try to grab the gut and pull it slightly out, which will push the glands out.
9.
  - a. For subsequent *in vivo* experiments transfer the salivary gland with a transfer tip to a sample chamber, which was previously coated with poly-L-lysine coated and filled with PBS. To reduce needed volume of incubation buffer small black PTFE-blocks can be placed at the sample chamber sides.
  - b. For subsequent immunostaining and *in situ* hybridization experiments transfer the salivary gland with a transfer tip to poly-L-lysine coated cover slips.
10. Remove remaining PBS to adhere salivary glands.
11. Add appropriate incubation media.

## 2.7 Dissection of *C. tentans* Larval Mid Gut

The Mid gut was used as DNA source for control cells, which do not express saliva proteins. To yield DNA with low impurities it is important to avoid contamination of the mid gut tissue with food bolus. The food bolus is enclosed by the peritrophic membrane which makes an separation of the mid gut tissue quite easy. The dissection at 4 °C avoids any change of the expression pattern due to the dissection procedure.

1. Collect appropriate amount of larvae and transfer into a beaker with water of the growth dishes.
2. Fill 40 mm  $\varnothing$  petri dish with ice cold PBS and add pieces of frozen PBS to keep temperature constant during dissection.

3. Transfer larvae into petri dish and place it under a stereoscopic microscope.
4. Grab the larvae with a Dumont 3c forceps at the posterior pro leg.
5. Stitch one scissor blade of a spring scissors (angled to side, 10 mm blade) through the cuticula
6. Rip the larvae by pushing the scissor cranial. This can be supported by cutting with the scissors.
7. Cut the gastrointestinal-tract posterior from the Malpighian tubules and the pharynx.
8. Pull the mid gut tissue and the peritrophic membrane apart with forceps from the posterior end. If Mid gut tissue does not rupture at the gizzard cut it with a scissor.
9. Wash tissue quickly in a petri dish with clean PBS and transfer it into an 2 mL reaction tube. Store tube on ice.

## 2.8 Microinjection of *C. tentans* Larval Salivary Glands

1. Centrifuge injection solution for 20 min to 30 min at 22 000 g.
2. Load 3  $\mu$ L to 5  $\mu$ L injection solution into a Femtotip II with a microloader.
3. Observe the salivary gland with transmitted light and move the top of the salivary gland into focus.
4. Move the salivary gland out of the field of view.
5. Mount the injection needle.
6. Remove air of the needle tip by pressing "clean". To get rid of remaining air bubbles gently knocking on needle.
7. Adjust the compensation pressure to 75 hPa to 100 hPa. This will ensure an constant efflux of the needle.
8. Adjust the injection pressure to 500 hPa and injection time to 0.1 s.
9. Position the needle tip above the objective front glass slightly touching the liquid surface.
10. Move the needle back, forth and left, right. A weak shadowing will appear if the needle is in the field of view.
11. Move the needle tip into the focal plane.
12. Check needle throughflow by pressing "clean" and move needle back by pressing "home".
13. Move a salivary gland into the field of view and focus the euqatorial plane of a nucleus.

14. Move the needle tip 20  $\mu\text{m}$  to 50  $\mu\text{m}$  before the designated injection location on the salivary gland with the tip in the focal plane. Move the needle now into cytoplasm or nucleoplasm and press the joystick button. If no injection can be seen increase the injection time as required. If still no injection can be seen the injection pressure can be increased. Too high injection pressures can damage the cell. Therefore, a prolonged injection time is desirable.
15. Optionally the PBS can be replaced by hemolymph with a gel loading tip.
16. Cover the hemolymph with mineral oil.

## 2.9 Collection of *C. tentans* Hemolymph

1. Collect appropriate amount of larvae and transfer into a beaker with water of the growth dishes.
2. Transfer larvae onto a cover slide.
3. Grab the larvae with a Dumont 3c forceps at the posterior pro leg.
4. Stitch one blade of a scissor through the cuticle. The gut may not be punctured.
5. Rip the larvae by pushing the scissor cranial.
6. Collect the hemolymph with a gel loader tip and transfer into a reaction tube.
7. Spin collected hemolymph of 3-4 larva down for 30 s at maximal g and transfer supernatant into new reaction tube and store on ice.
8. Shock-freeze with liquid nitrogen and store at  $-80\text{ }^{\circ}\text{C}$

## 2.10 DNA Extraction

1. Spin collected cells or tissue down for 30 s to 60 s with 6000 g at  $4\text{ }^{\circ}\text{C}$  in a 2 ml reaction tube.
2. Discard supernatant and add 200  $\mu\text{L}$  PBS + 20  $\mu\text{L}$  Proteinase-K 50  $\frac{\text{g}}{\text{L}}$ .
3. Incubate samples at  $56\text{ }^{\circ}\text{C}$  until digestion is complete.
4. Add 440  $\mu\text{L}$  phenol:chloroform.
5. Invert reaction tube several times.
6. Centrifuge at 16 000 g for 30 s to 60 s
7. Transfer upper phase into a fresh 2 ml reaction tube.
8. Repeat steps 4-6 until inter phase is clear.

9. Add 440  $\mu$ l chloroform.
10. Centrifuge at 16 000 g for 30 s to 60 s
11. Transfer upper phase into a fresh 2 ml reaction tube.
12. Add 440  $\mu$ L ice cold ethanol.
13. Invert reaction tube several times.
14. Samples
15. Centrifuge at 16 000 g for 10 min to 30 min at 4 °C.
16. Discard supernatant and air dry DNA-pellet.
17. Resuspend DNA-pellet in an appropriate amount of TE-buffer.

## 2.11 Potassium Permanganate Foot-Printing

Single stranded DNA is much more sensitive to the oxidation by potassium permanganate than double stranded DNA. Therefore, potassium permanganate allows to specifically modify thymidines in the melted sections of the DNA as e.g. induced by RNA-polymerases. A piperidine treatment of the modified DNA introduces single strand breaks at the modified thymidines. In combination with a linker mediated PCR this technique allows a foot-printing of DNA melting proteins like RNA-polymerases (Figure 2.1)

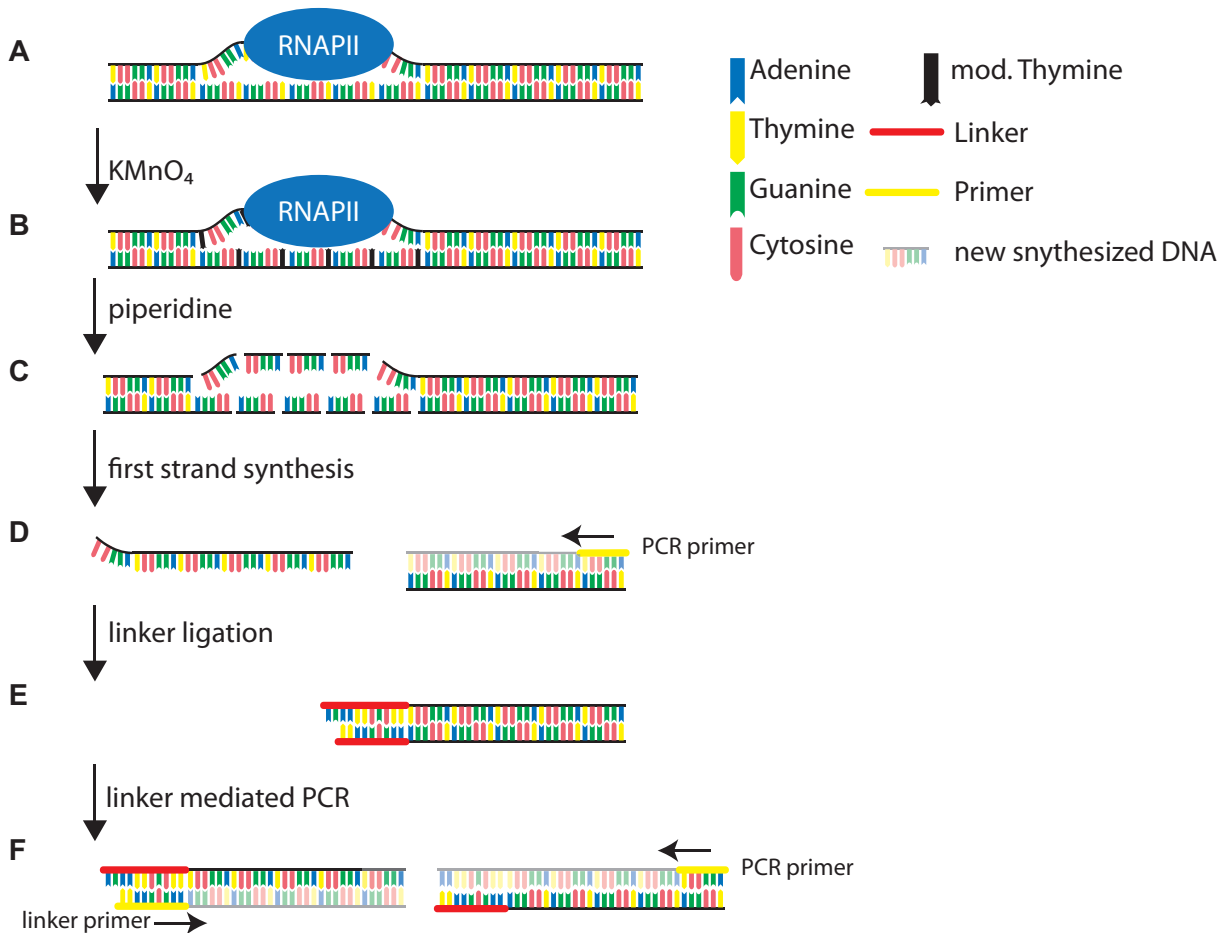


**Figure 2.1:** *Potassium permanganate foot-printing of RNA-Polymerase II. (A) During transcription RNAP II melts DNA locally. (B) Thymidines in short single strand DNA sections are modified by potassium permanganate. (C) Piperidine introduces single strand breaks at the modified thymidines. (D) To detect the single strand breaks a primer upstream of the sequence of interest is used for the first strand synthesis. The result of the first strand synthesis is a mixture of blunt-end DNA-pieces of varying size. (E) To amplify this short DNA pieces a linker with a sticky- and a blunt-end is ligated to the sample DNA. The linker design ensures a defined orientation of the linker in the ligation product. (F) The known linker sequence allows by a single PCR-reaction to efficiently amplify all sequences of interest fused to the linker.*

1. Spin collected cells/tissue down for 30 s to 60 s with 6000 g at 4 °C in a 2 ml reaction tube.
2. Discard supernatant
3. Add 100  $\mu$ L ice cold PBS and vortex for 5 s.
4. Add 100  $\mu$ L 40  $\frac{\text{mmol}}{\text{l}}$  ice cold potassium permanganate and incubate for 30 s on ice.
5. Add 200  $\mu$ L stop solution (2.1 p. 34) and shake until all coloration is vanished.
6. Extract DNA like described (2.10 p. 40) and resuspend DNA-Pellet in 50  $\mu$ L TE-buffer.
7. Dilute 10  $\mu$ g to 20  $\mu$ g DNA to 15  $\mu$ L and add 75  $\mu$ L water + 15  $\mu$ L piperidine in a 1.5 mL reaction tube.
8. Incubate for 30 min at 90 °C in a hood.
9. Spin down condensate and add 200  $\mu$ L water.
10. Extract two times piperidine by adding 700  $\mu$ L isobutanol, invert sample several times and discard upper phase.
11. Final piperidine extraction by adding 700  $\mu$ L ether, invert sample several times and discard upper phase.
12. Add two volumes ice cold ethanol and store for 10 min at  $-80$  °C.
13. Spin down DNA with 16 000 g for 30 min at 4 °C.
14. Discard supernatant and resuspend DNA-pellet in 10  $\mu$ L TE-buffer.

#### 1. Preparation of Linker-DNA

- a. Prepare 20  $\mu$ mol unidirectional linker by mixing 20  $\mu$ mol linker 1 + 20  $\mu$ mol linker 2 in 250  $\frac{\mu\text{mol}}{\text{l}}$  Tris-HCL pH 7.7.
- b. Denature for 5 min at 95 °C.
- c. Briefly spin down condensate.
- d. Incubate linker mix at 70 °C and cool down slowly to room temperature.
- e. Incubate linker mix at 4 °C overnight.
- f. Optionally aliquots can be prepared and stored at  $-20$  °C.

#### 2. First Strand Synthesis

- a. Add 1  $\mu$ g to 2  $\mu$ g piperidine digested DNA to a PCR tube and add to 5  $\mu$ L with water.
- b. Add PCR-mix consisting of 5  $\mu$ L 5x Herculase II reaction buffer, 0.625  $\mu$ L dNTP (10  $\frac{\mu\text{mol}}{\text{l}}$ ), 0.5  $\mu$ L of 1  $\frac{\mu\text{mol}}{\text{l}}$  PCR-Primer, 0.2  $\mu$ L HerculaseII and add to 30  $\mu$ L with water.

- c. Perform first strand synthesis in a thermo-cycler with 5 min at 95 °C denaturation, 30 min at 60 °C annealing and 10 min at 72 °C elongation.
3. Linker Ligation
  - a. Add to the first strand reaction 10 µL of 10x T4 DNA Ligase Buffer, 10 µL 50% PEG 4000 solution, 5 µL of Linker-Mix, 2U T4 DNA ligase and add to 50 µL total volume with water.
  - b. Incubate overnight at 4 °C.
  - c. Add 9 µL of 3  $\frac{\text{mol}}{\text{l}}$  sodium acetate pH 7, 220 µL ice cold ethanol and store at –80 °C for 10 min.
  - d. Spin down DNA with 16 000 g for 30 min at 4 °C.
  - e. Discard supernatant and resuspend DNA-pellet in 10 µL TE-buffer.
4. Linker Mediated PCR with subsequent polyacrylamide gel electrophoresis (PAGE)
  - a. Add following components in order 36.85 µL water, 10 µL 5x HerculaseII II reaction buffer, 1.25 µL dNTPs(10  $\frac{\mu\text{mol}}{\text{l}}$ ), 0.2 µL Linker-Primer(100  $\frac{\mu\text{mol}}{\text{l}}$ ), 0.2 µL PCR-Primer(100  $\frac{\mu\text{mol}}{\text{l}}$ ), 1 µL redissolved ligation reaction, 0.5 µL HerculaseII II. For fluorescent labeling of PCR-products 5 µL of ATTO488-UTP 1  $\frac{\mu\text{mol}}{\text{l}}$  can be added (28 % UTP labeling ratio).
  - b. Thermocycling with initial denaturation 5 min 98 °C and 60 cycles of (1 min 98 °C denaturation, 2 min annealing (annealing temperature according to polymerase manufacture guide), 15 s 72 °C elongation and a final elongation of 5 min 72 °C.
  - c. Add 5 µL of 3  $\frac{\text{mol}}{\text{l}}$  sodium acetate pH 7, 150 µL ice cold ethanol and store at –80 °C for 10 min.
  - d. Discard supernatant and resuspend DNA-pellet in 5 µL TE-buffer.

## 2.12 DNA Fragment Length Analysis

1. Add two volumes ice cold ethanol and store for 10 min at –80 °C.
2. Spin down DNA with 16 000 g for 30 min at 4 °C.
3. Resuspend in 5 µL Tris-HCL+0.1  $\frac{\text{mmol}}{\text{l}}$  EDTA.
4. For electrophoretic PCR-product separation by handcast Polyacrylamid gel follow (a-e).
  - a. Cast a 10-16% Acrylamid/Bisacrylamid (19:1, Carl Roth) gel following the instruction supplied by the electrophoresis chamber ( PROTEAN II XL Cell, Bio-Rad, Germany) manufacturer.



- b. Load complete resuspended DNA to the gel.
- c. Run gel at maximum available voltage. Take care that the gel temperature is in the range suggested by the manufacturer.
- d. Stain Gel for 1 h in a 3xGelRed-solution (Biotum Inc., USA).
- e. Image Gel with a gel documentation system suitable for Ethidium-Bromide stained gels.
- f. For PCR-product length analysis by capillary electrophoresis follow (I-IV).

I Dilute fluorescent PCR-products according to the instruction of the capillary electrophoresis device. By random incorporation of fluorescent multiple nucleotides the degree of labeling is much higher compared to samples used for sequencing. Using a 3130xl Genetic Analyzer (life technologies, Germany) the PCR reaction was diluted to a DNA-concentration of  $5 \frac{\text{ng}}{\mu\text{L}}$ .

II Add appropriate size standard. Here Internal Lane Standard 600 (Promega, Germany) was used.

III Electrophoresis properties depend on device and configuration. Here a POP7 36 cm capillary was used.

IV Analyze fluorescence traces by e.g. Matlab.

## 2.13 Kinetic Data Fitting

As introduced the dwell time kinetics of particles at the NE were measured by single molecule microscopy. The dwell-time  $t_{dwell}$  is proportional to the number of frames, in which the particle is present at the NE. The frame-wise image acquisition provides a time discretization. The images were acquired in the frame-transfer mode. In the frame transfer mode between two frames only for less than  $200 \mu\text{s}$  no photons are collected. Therefore, the image sequence can be seen as a continuous sequence. To compensate the fact that a particle is not necessarily present the complete first and last frame at the NE for dwell time  $t_{dwell}$  calculation it is assumed that the particle was present in 75% the frame cycle time  $t_{ct}$  in these frames. Based on this assumption the dwell time is  $t_{dwell} = \frac{t_{ct}}{2} + (d - 1)t_{ct}$ . The routine for kinetics data fitting was written in Matlab. First all events which lasted at least three frames were selected and their cumulative distribution  $F$  determined.

The empirical dwell time distribution functions were model by a single, referred as single modal, or the sum of up to three, referred as multi-modal, gamma distributions. The number of modes is denoted by  $M$ . The number of modes  $M$  was varied between  $M \in [1, 2, 3]$ . The fit function of Matlab requires that all fit parameters are continuous. The number of rate limiting  $S$  steps is an integer value. Therefore, it was supplied as fit independent parameter  $S_b \in [1, 2, \dots, 30]$ . According to equation 1.3 with  $a_b$  denoting a scaling factor for each single gamma distribution, equation 2.1 was fitted to the data.

$$cdf_{\gamma fit}(t; a, b, k_b, S_b) = \sum_{b=1}^M \left( a_b \frac{\gamma(t; k_b, S_b)}{\Gamma(S_b)} \right) + b \quad (2.1)$$

For every fit the  $AIC_c$  was calculated as described below (see 2.14).

## 2.14 Model Selection

For model selection the Akaike Information criteria was calculated as

$$AIC = n \ln(RSS/n) + 2k + C \quad (2.2)$$

$n$  is the number of observations  $RSS$  the residual sum of squares and  $k$  the number of fitted parameters.  $C$  depends only on the particular data points and not on the tested model.<sup>[11]</sup> By the  $AIC$  to the same empirical data set it can be simplified to

$$AIC = n \ln(RSS/n) + 2k \quad (2.3)$$

For finite sample size the  $AIC$  has to be corrected. Even with large  $n$  and small  $k$  the use of the corrected Akaike Information Criterion ( $AIC_c$ ) is recommended.<sup>[11]</sup>

$$AIC_c = AIC + \frac{2k(k+1)}{n-k-1} \quad (2.4)$$

The model giving the lowest  $AIC_c$ -value is considered as best fitting model.

## 2.15 Goodness-of-Fit Test by Parametric Bootstrapping

The parametric bootstrapping based goodness-of-fit test was realized by a short matlab script. The best fit to the data set  $x_i$  with  $n$  elements was used as an estimator for the parameters  $\hat{\theta}$

of the null distribution. With  $\hat{\theta}$  the vector  $\hat{x}_0$  with  $m$  elements following the estimated null distribution was calculated. The number of elements  $m$  was  $\sim 1.5 \cdot 10^4 n$ . By resampling with replacement out of  $\hat{x}_0$ ,  $5 \cdot 10^4$  vectors  $\hat{x}_{0*i}$  with  $m$  elements were created. For all  $\hat{x}_{0*i}$  the divergence  $T_{m,b*}$  to the zero distribution was calculated by the used test statistics (see below). For hypothesis testing the 0.95 quantile value of  $T_{m,b*}$  was used as critical value.

$$\begin{aligned}\chi^2 &= \sum_{i=1}^{i=k} \frac{(X_i - E_i)^2}{E_i} \\ FT^2 &= 4 \sum_{i=1}^{i=k} (\sqrt{X_i} - \sqrt{E_i})^2 \\ X &= \sum_{i=1}^{i=k} \sqrt{(X_i - E_i)^2}\end{aligned}$$

## 2.16 Non-Parametric Bootstrapping

First the empirical data set  $x_i$  with  $n$  data points was resampled  $n$  times with replacement to construct the bootstrap sample  $x_{i*}$ . The bootstrap sample was fitted by the model which was selected as best model according to the empirical data (see 2.14 p. 47). This was repeated  $B = 10000$  times and the resulting fit parameters denoted as  $\hat{\Theta}_{i*}$ .

## 2.17 mRNP-Particle Export Analysis

To screen the large amount of data efficiently for mRNP export events a kymograph based approach was used. The basic idea is to plot the pixels congruent with the nuclear envelope over time (Fig. 2.2). This was realized by three custom-programmed ImageJ plugins (GaussProfiler, Kymograph mt\_2 and KymoReader)<sup>1</sup>. The GaussProfiler plug-in determined the nuclear membrane position with subpixel accuracy.<sup>[54,113]</sup>

First an average image is calculated from the nuclear membrane substack. In this average image the brightest pixel of every line was determined and a Gaussian was fitted perpendicular to the nuclear membrane contour. The pixels covered by the membrane contour are used for the kymographs. The single kymographs are screened manually for mRNP NE interactions. With the KymoReader plug-in the duration of the NE interaction is determined. Therefore, the intensity of a manually selected ROI above the background intensity +  $3\sigma$  was measured.<sup>[54,113]</sup> To track the NE interactions events a custom-built Matlab based manual tracking program was

<sup>1</sup>The plugin design and code of the kymograph approach was developed by Dr. Jan-Peter Siebrasse and is not part of my work.

used, with a subsequent high throughput data visualization. The single mRNP-particle NE interaction events were categorized according to Fig. 3.6 (p. 59).

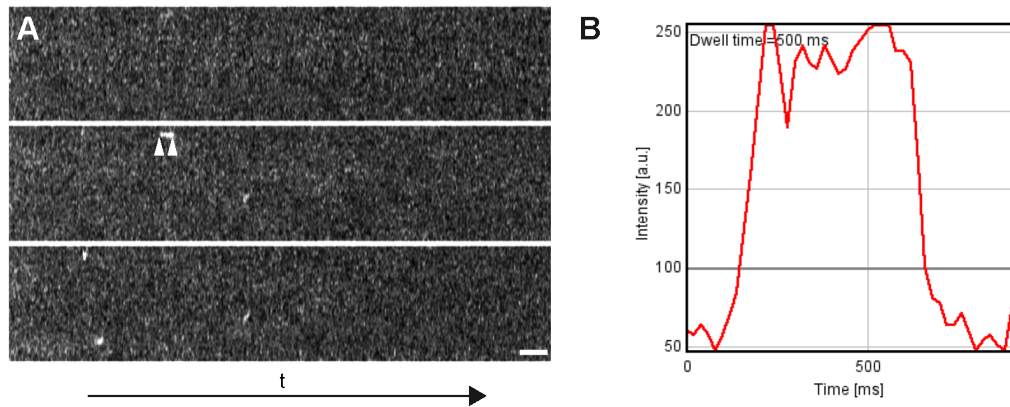


**Figure 2.2: Kymograph analysis.** (A) The averaged pixels congruent with the NE (middle)  $\pm 1$  pixel and shifted 1 pixel to the nucleus (upper kymograph) and shifted 1 pixel to the cytoplasm (lower kymograph) were plotted over time (x-axis). The scale bar represents 1 second. NE-interaction appeared as horizontal stripes in the kymograph (between arrowheads). Originally it was intended to use the nucleoplasmic and cytoplasmic kymographs to recognize exports events. Since it was not possible to categorize NE-interaction events according to Fig. 3.6 (p. 59) a manual inspection of the according image sequence had to be used. (B) The length of an interaction event was determined as the time the signal was above a threshold (gray line). B shows the output figure of the KymoReader plugin. The arrowheads mark the timepoints marked by arrowheads in A.

## 2.18 Overlay of Export Trajectories and NPC-Structure

To overlay the trajectories with the NPC structure an approach similar to *Lowe et al.*<sup>[77]</sup> was used. The mRNP-particle trajectories were tracked by using a self-written Matlab script. It applies a 2d-Gaussian fit to a user selected ROI to determine the particle position with sub-pixel accuracy. The trajectories were rotated so that the according NE piece was perpendicular to the X-axis. These rotated trajectories were overlaid with a mask resembling the NPC shape of *C. tentans*.<sup>[56]</sup> This mask and a trajectory were moved iteratively in one nanometer steps  $\pm 200$  nm along the X-axis and  $\pm 100$  nm along the Y-axis against each other. For every position the trajectory position inside the NPC-shape was calculated. If more than one configuration gave the highest number of counts inside the NPC-shape, the configuration used for the overlay was randomly selected.

## 2.19 Light Sheet Microscope

The microscope setup was developed, built and described by *Jörg Ritter et al.* <sup>[105]</sup> It is based on a Axiovert 200 microscope (Carl Zeiss Microscopy GmbH, Germany). The setup provided three laser lines with 488 nm (Sapphire-100, Coherent, Germany), 532 nm (LaNova50 Green, Lasos, Germany) later replaced by 532 nm (Pluto PL.P532.400, PEGASUS Optik GmbH, Germany) and 640 nm (Cube 640-40C, Coherent, Germany). The laser lines were combined by dichroic mirrors and guided through an acousto optical tunable filter (AOTF) (AOTFnC-VIS, AA OPTO-ELECTRONIC, France) and a single-mode optical fiber (kineFLEX, Qioptiq Photonics GmbH & Co KG, Germany) to the elliptical beam expander. By a periscope the elliptical beam was guided to the 10x illumination objective (plan apochromat 106, NA 0.28, Mitutoyo, Germany) into the sample chamber (Type 105.044 version 2 edges non chamfered, Hellma GmbH & Co. KG, Germany). The sample holder was positioned in a self-built chamber mount which was moved by a user developed microscopy stage.<sup>[105]</sup> Light from the sample was collected by a 40x, NA 1.2 water immersion objective lens (C-Apochromat, Carl Zeiss Microscopy GmbH, Germany). The collected light was cleaned up from scattered excitation light by a double band pass filter (z532/633m, Chroma Technology Corp, USA) and detected by an EM-CCD camera with 128x128 pixels (iXon BI DV-860, pixel size 24  $\mu\text{m}$ , Andor Technology, United Kingdom). By the installed 4x magnifier in front of the camera the field pixel size was 150 nm. The EM-CCD camera was controlled with the Solis-Software (Andor Technology, United Kingdom).

During this thesis the original laser control hardware was replaced by a network controlled FPGA-module (cRIO-9076, National Instruments, Germany) with an 8-channel digital input/output module (NI 9401, National Instruments, Germany) and a 4-channel analog output module (NI 9263, National Instruments, Germany). The AOTF was controlled via the cRIO-module, which was driven by the EM-CCD camera fire-out signal. The Lab-view (National Instruments, Germany), front-end graphic user interface to set-up the measuring parameters and transfer it to the cRIO-module, was self-written. Programming of the FPGA-module was done by SET GmbH, Allgäu/Germany.

For microinjection a FemtoJet® (Eppendorf, Germany) combined with a InjectMan®NI 2 (Eppendorf, Germany) was mounted to the setup.

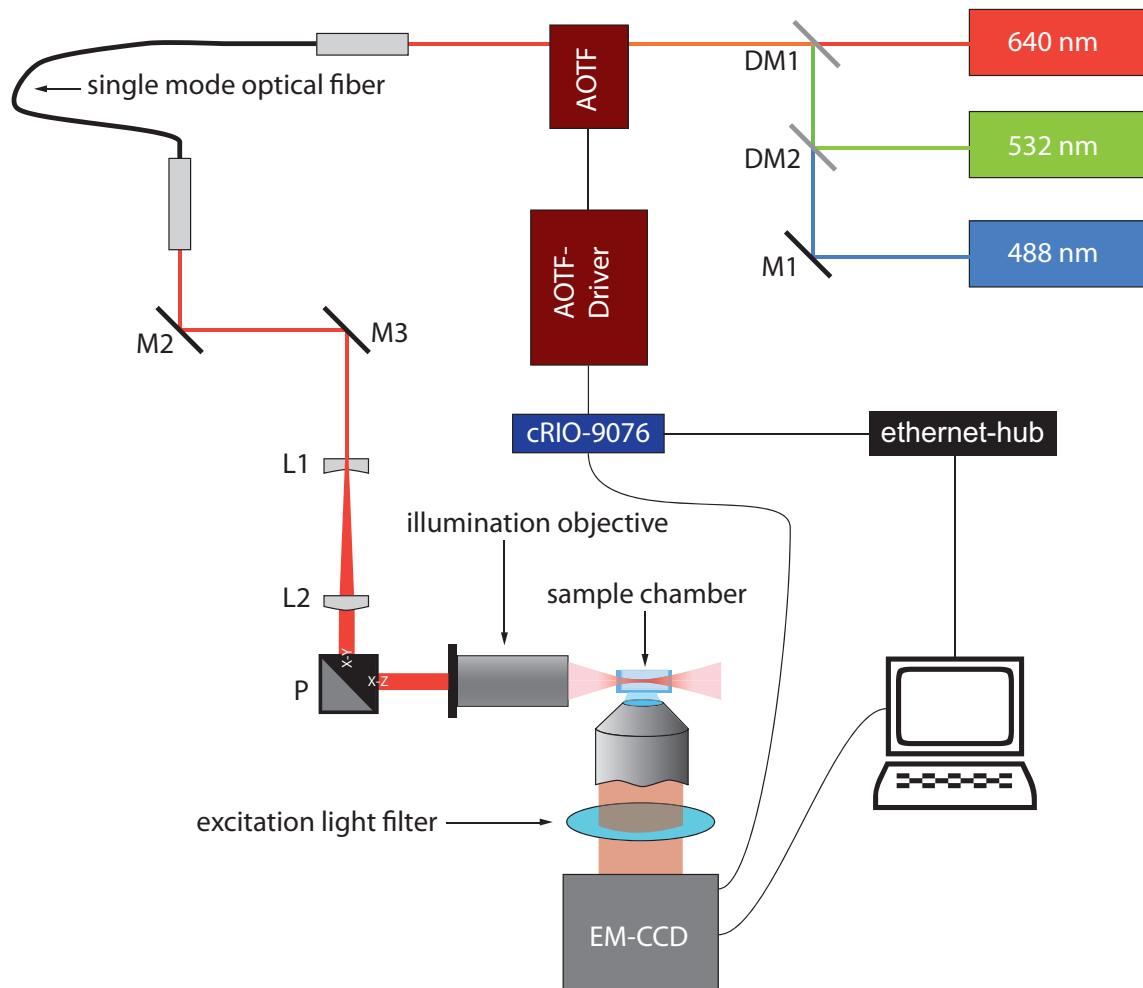


**Figure 2.3:** Schematic drawing of the Light Sheet Microscope setup.

## 2.20 Single Molecule Imaging in *C. tentans* Salivary Glands by Light Sheet Microscopy

To image the export of single mRNP-particle in *C. tentans* salivary glands cell AF647-tc-hrp36 and AF546-tc-NTF2 were co-injected. The concentration of labeled mRNP-particles was chosen so low that the trajectories of single mRNP-particles could easily be followed up ( $40 \frac{\text{pmol}}{\text{l}}$  to  $200 \frac{\text{pmol}}{\text{l}}$ ). The EM-CCD camera was operated in the frame transfer mode with 20 ms integration time, 1 MHz horizontal readout rate and  $0.9 \mu\text{s}$  vertical shift time. In a consecutive sequence 950-980 frames mRNP-particle fluorescence (640 nm excitation), 20-50 frames 532 nm excitation and 950-980 frames 640 nm followed by a 5 s break were imaged. The sequences were interrupted by 5 s without imaging. A gland pair was imaged for a maximum time period of 90 min.

# 3 Results I: Single Molecule Observation of mRNP-Particle Export

## 3.1 Light Sheet Characterization

The microscopical setup was built and described by *J. Ritter et al.*<sup>[104,105]</sup> In this setup a cylindrical beam expander is used to form the light sheet. To image mRNP-particle export a sequential illumination with the wavelengths of 532 nm to image a nuclear envelope marker and 640 nm to image the labeled mRNP-particles was used. To co-localize the nuclear envelope with the labeled mRNPs, the light sheet focus position and thickness should be approximately the same at both illumination wavelengths. The cylindrical beam expander consists of chromatic lenses, which introduce a chromatic error to the illumination. The chromatic shift of the light sheet focus was measured and corrected by readjustment of the cylindrical beam expander. To measure the light sheet geometry a procedure and software developed by *J.-H. Spille* was used. As sample fluorescent beads embedded in an agarose matrix were used.

The light sheet thickness before realignment was  $\text{FWHM}_{532} = 3.3 \mu\text{m}$  and  $\text{FWHM}_{640} = 2.9 \mu\text{m}$ . The distance between the two illumination foci was  $\Delta X_{0532,640} = 69.2 \mu\text{m}$  (Fig. 3.1 A). Due to the chromatic error the light sheet thickness of the two illumination wavelengths differed significantly at the focus position of the other wavelength ( $X_{0532}$  and  $X_{0640}$ ). The chromatic error was reduced by changing the distance between the cylindrical lenses slightly.

The new positioning of the cylindrical lenses decreased the chromatic focus shift dramatically from  $\Delta X_{0532,640} 69.2 \mu\text{m}$  to  $6.8 \mu\text{m}$ . The light sheet thickness at the appropriate focus positions changed to  $\text{FWHM}_{532} = 3.1 \mu\text{m}$  at  $X_{0640}$  and  $\text{FWHM}_{640} = 2.2 \mu\text{m}$  at  $X_{0532}$ .

Agarose is an optically very homogenous sample in comparison to *C. tentans* salivary glands. To evaluate the chromatic shift under experimental conditions the nuclear envelope of *C. tentans* salivary gland cells was labeled simultaneously by NTF2-AF546 and NTF2-AF647. Such labeled nuclear envelopes were imaged with both illumination wavelengths alternating for 200

frames. This stack was subdivided in two stacks, each of them corresponding to one illumination wavelength. A 2D-cross-correlation of the averaged sequences of four nuclei shows that the mean deviation was below 1 pixel at all four nuclei. A Gaussian fit to the membrane of a single nucleus as performed to analyze the mRNP-particle export, resulted in an average deviation of  $75 \pm 35$  nm (Fig. 3.2).

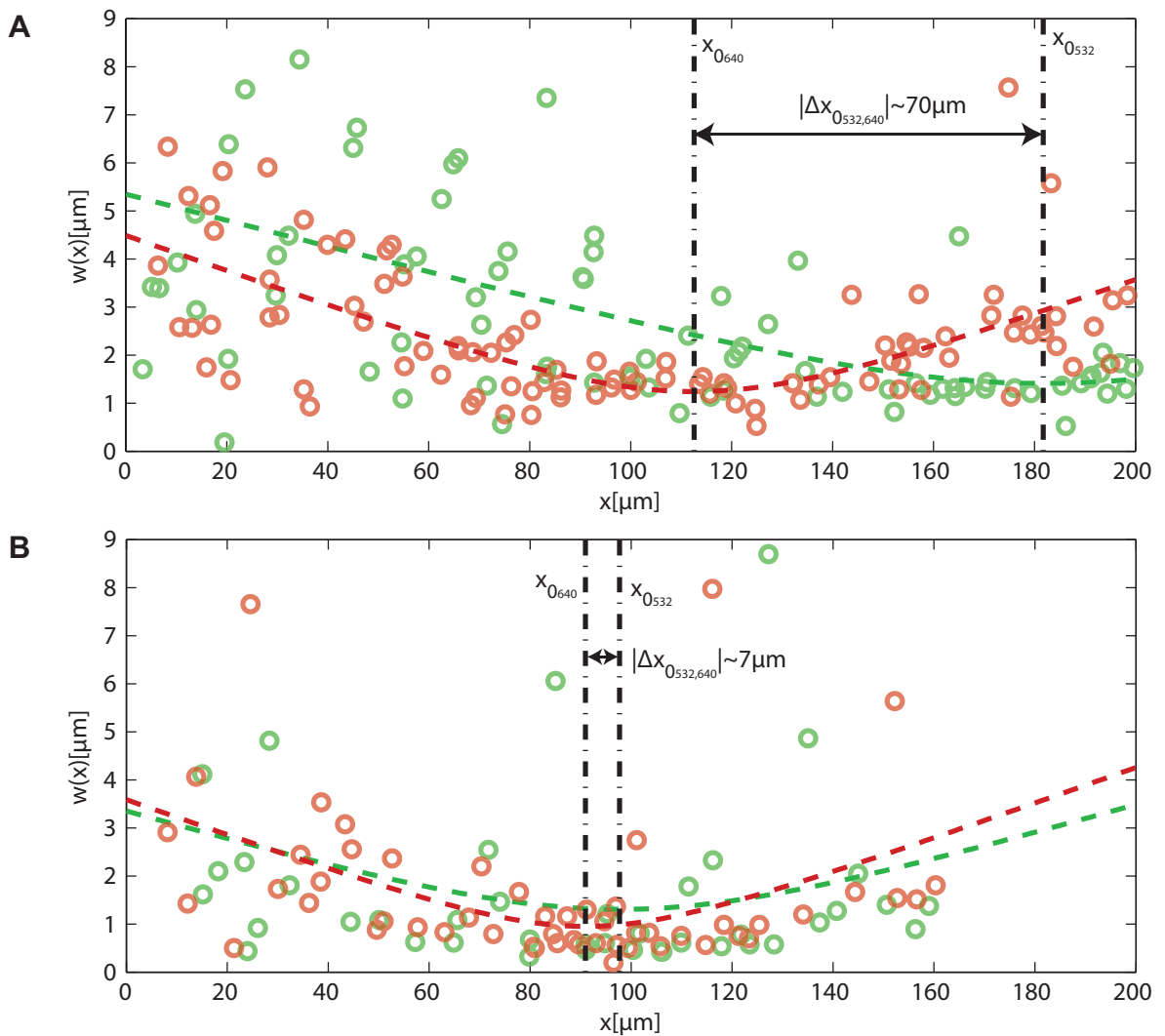


**Figure 3.1:** *Chromatic shift and geometry of the light sheet. (A) Light sheet geometry before readjustment. The focus positions of the wavelengths used differed more than one FOV from the EM-CCD camera ( $18 \times 18 \mu\text{m}^2$ ) used. (B) After readjustment the focal shift was significantly reduced.*



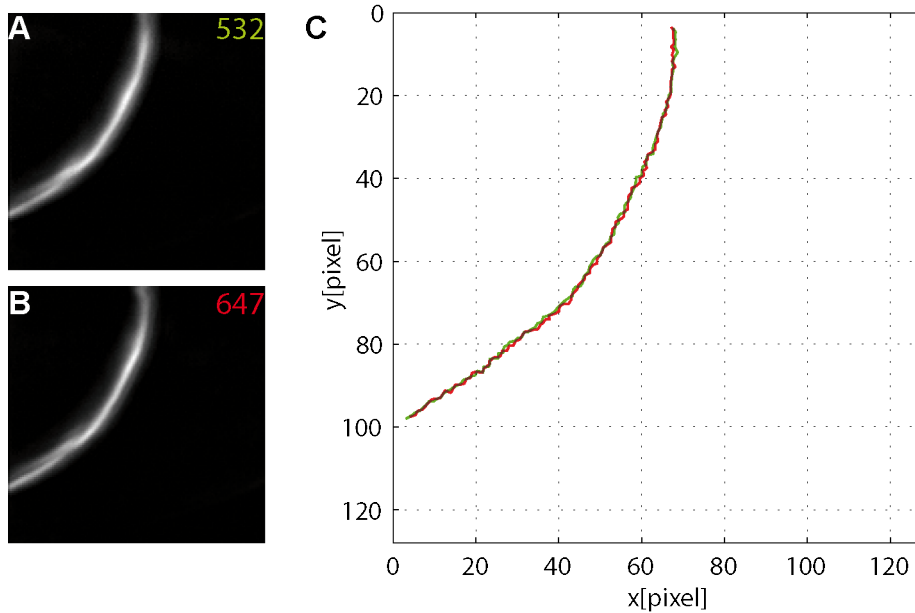


**Figure 3.2: Lightsheet chromatic shift.** *AF546-tc-Ntf2* and *AF647-tc-Ntf2* were co-injected in *C. tentans* salivary glands cells and imaged with frame-wise alternating excitation of 532 nm and 640 nm. (A) and (B) shows the averaged of the appropriate channels as described in the text. By eye no differences can be detected between A and B. (C) To determine the chromatic shift the averaged images were analyzed by the Gauss profiler plug-in (see section 2.17 p. 47) and the resulting polygon is plotted. No systematic shift between the two images is recognizable. In average the NE position differed by  $75 \pm 35$  nm. Pixel size 150 nm.

## 3.2 Establishing Whole Mount Fluorescence *in situ* Hybridization

*In situ* hybridization is a classical technique to detect specific RNAs. For *C. tentans* salivary glands several *fluorescence in situ hybridization* (FISH) procedures are described.<sup>[64,66]</sup> All described procedures section the salivary glands physically. Since this is time consuming and disrupts the 3D-structure of the salivary gland a whole mount FISH procedure was developed. It is easy to perform, preserves the sample 3D-structure, requires less hands-on time and is inexpensive. The only disadvantage is that a sectioning microscope is needed to yield images of comparable quality to physically sectioned FISH samples. The development of the whole mount FISH is based on a protocol for *Drosophila (Sophophora) melanogaster* salivary glands by Mee *et al.*<sup>[83]</sup> The protocol was adapted to the increased size of the *C. tentans* salivary glands.

Labeling with BR2.1-mRNA complementary oligonucleotides resulted in a strong staining of the BR2-puff and cytoplasm and a weaker staining of the nucleoplasm (Fig. 3.3 a). This staining was strongly diminished by a one-hour RNase-A digestion prior to hybridization (Fig.

3.3 b). A control oligonucleotide with the sense sequence of the BR2.1-mRNA did not label the BR2-puff but stained the cytoplasm (Fig. 3.3 C). Since the complete genomic sequence of *C. tentans* is not published, it cannot be ruled out that the control oligonucleotide is partially complementary to other RNAs. An unspecific binding to other cellular structures is improbable since by RNase-A digestion the cytoplasmic and nucleoplasmic staining was strongly diminished for the BR2.1 specific.

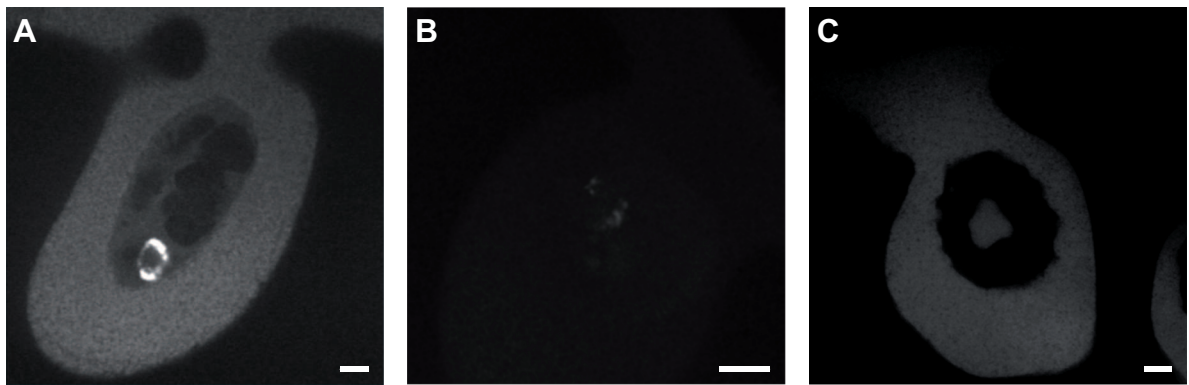


**Figure 3.3:** Whole mount fluorescence in situ hybridization of *C. tentans* salivary glands. (A) FISH staining of BR2.1-mRNA. The BR2-puff is clearly visible as a bright nearly closed circular structure. (B) After 1 h RNase-A digestion no nuclear and cytoplasmic staining can be detected. This suggests that the used BR2.1-oligonucleotide bind to RNA and shows no unspecific binding to other cellular structures. (C) Using a FISH probe with the sense sequence of the probe used in (A) weakly stains the cyto- and nucleoplasm. Scale-bar = 10  $\mu$ m.

### 3.3 Testing of Different Incubation Media

The aim of this work was to study the export of native mRNP-particles through the NPC. Therefore, a strategy for mRNP-particle labeling was used which presumably disturbs the mRNP-particle export kinetics as little as possible. The incubation medium of the salivary glands was carefully chosen, to avoid an artificial influence on mRNP-particle export. To monitor the effect of different incubation media on mRNP-particle export, the BR2.1-mRNA distribution was analyzed by FISH. An analysis of the export kinetics at the level of single mRNP-particles using different incubation media would be to time consuming.

Numerous different incubation media to maintain *C. tentans* salivary glands viable for prolonged time periods are described<sup>[13,32,140]</sup>. PBS, PBS+sugars, PBS + amino acids, PBS + sugar + amino acids, ZO-medium, Buffer-K, hemolymph diluted with PBS and pure hemolymph were tested. An increase of the nucleoplasmic /cytoplasmic BR2.1-mRNA ratio was interpreted as impaired mRNA-export and an undetectable BR2-puff as impaired transcription. The

nucleoplasmic/cytoplasmic ratio was calculated by using representative ROIs for each of them. For most incubation media salivary glands were incubated for different incubation times. Additionally to exclude variations between different animals the sister glands of one larva were incubated at different conditions. This resulted in more than 40 different experiments and 400 microscopic slides. Therefore, the results are presented consolidated in tabular form (see table 3.1) and representative images are shown in (Fig 3.4). In summary, only pure hemolymph could be used as incubation medium.

The light sheet microscopy sample chamber has a volume of 160  $\mu\text{L}$ . On average 3  $\mu\text{L}$  to 4  $\mu\text{L}$  hemolymph can be obtained from one fourth instar larva. Since it is labor-intensive to collect hemolymph, the amount of hemolymph needed per experiment was reduced. First PTFE-blocks were placed in the sample chambers edges as spacers. To ensure the sample accessibility with the micro-injection needle one spacer was wedge-shaped. To seal the sample a cover glass was placed on top of the sample chamber. This configuration was prone to air bubble inclusion which resulted in clotting of the hemolymph. Clotted hemolymph is strongly scattering and absorptive. Under these conditions single molecule imaging was not possible. The use of mineral oil as sealing reduced the amount of required hemolymph further to  $\sim 20 \mu\text{L}$ . With this procedure no air bubbles are trapped which avoids the clotting efficiently. After using mineral oil for sealing, hemolymph clotting did not occur anymore.

Medium	nuc. BR2.1	BR2-puff	transcription	export
15 min PBS	+	0	+	+
30 min PBS	++	0	+	-
45 min PBS	+++	0	+	-
50 min PBS	+++	0	+	-
50 min PBS+sugar	- - -	- - -	-	+
50 min PBS+AA	-	0	-	-
50 min PBS+AA+sugar	-	0	-	-
50 min ZO-medium	-	0	-	-
50 min Buffer-K	-	0	-	-
50 min diluted hemolymph	-	0	-	-
50 min hemolymph	0	0	+	+
50 min PBS+15 min hemolymph	+	0	+	+

**Table 3.1:** Overview of the different incubation media tested and their influence on mRNA-export and transcription activity. Plus and minus signs describe the subjective observation of BR2.1 concentration change or change of transcription and mRNA-export activity at the respective. Zeros indicate no change.

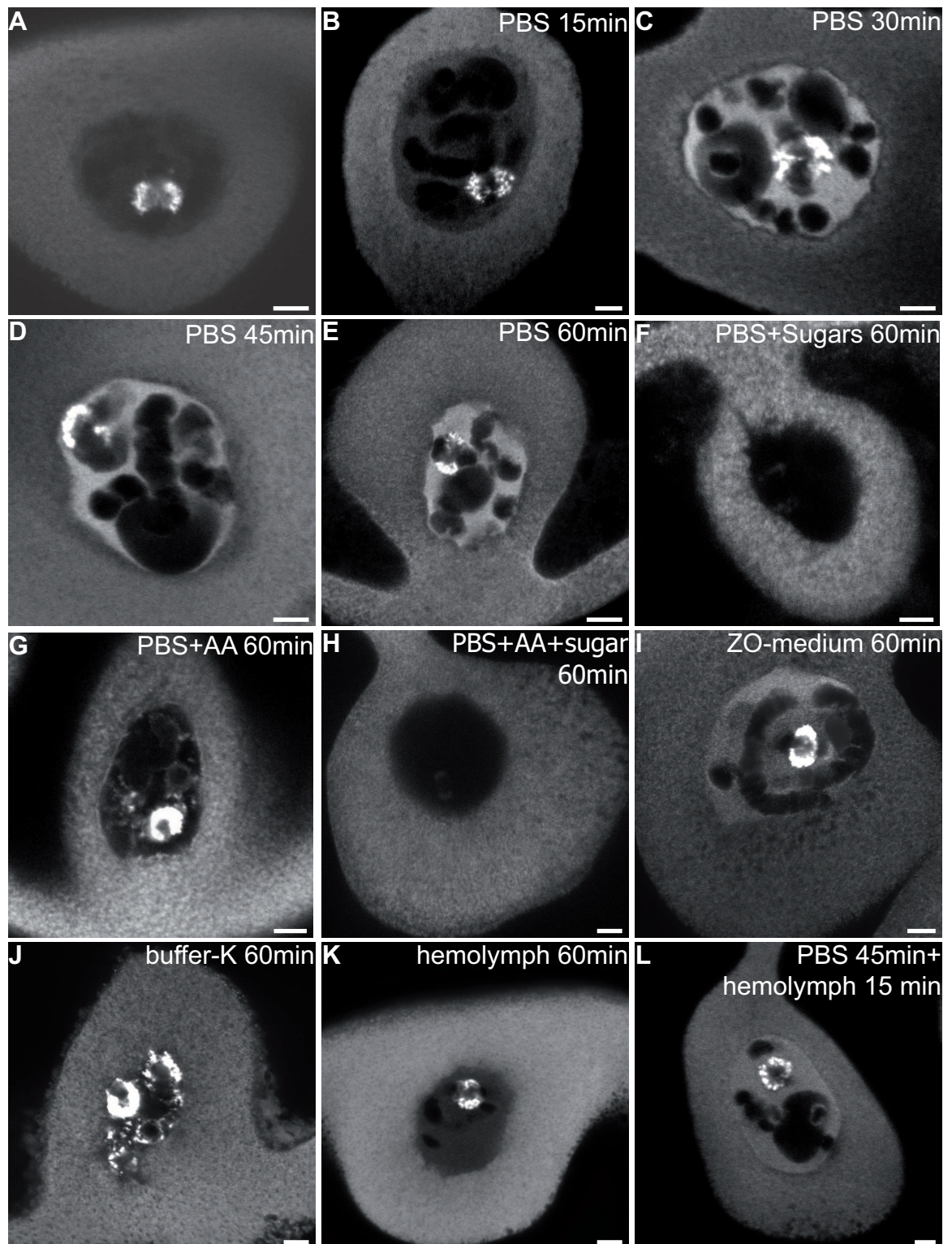


**Figure 3.4:** *Representative images of the BR2.1-mRNA distribution after incubation in different media. The incubation conditions are noted in the sub-figures. Scale bars = 10  $\mu\text{m}$*

### 3.4 Single Molecule Observation of mRNP-Particle Export

Only recently the kinetics of the mRNA-export were published.<sup>[54]</sup> Goal of this study was to observe the mRNA-export at the single molecule level and analyze its kinetics. To image the mRNP-particles crossing the NE through the NPC, fluorescently labeled Hrp36 (AF647-tc-Hrp36) and NTF2 (AF546-tc-NTF2) were micro-injected into the cytoplasm of *C. tentans* salivary gland cells. Hrp36 contains an M9-domain which allows it to shuttle between cytoplasm and nucleus. Due to the higher import rate Hrp36 is enriched in the nucleus.<sup>[115]</sup> AF647-tc-Hrp36 is incorporated into nascent mRNPs like wild type Hrp36. Several minutes after micro-injection the well known ribbon pattern of *C. tentans* polytene chromosomes caused by the distribution of active transcription site along the chromosome becomes visible (Fig. 3.5 A). The AF546-tc-NTF2 is enriched at the NPC.<sup>[50]</sup> Here it is used as NPC marker. The average NPC distance in *C. tentans* salivary gland cells is so small (128 nm center to center) that the labeled NPCs appear as a continuous line representing the position of the NE (Fig. 3.5 B).<sup>[64]</sup>

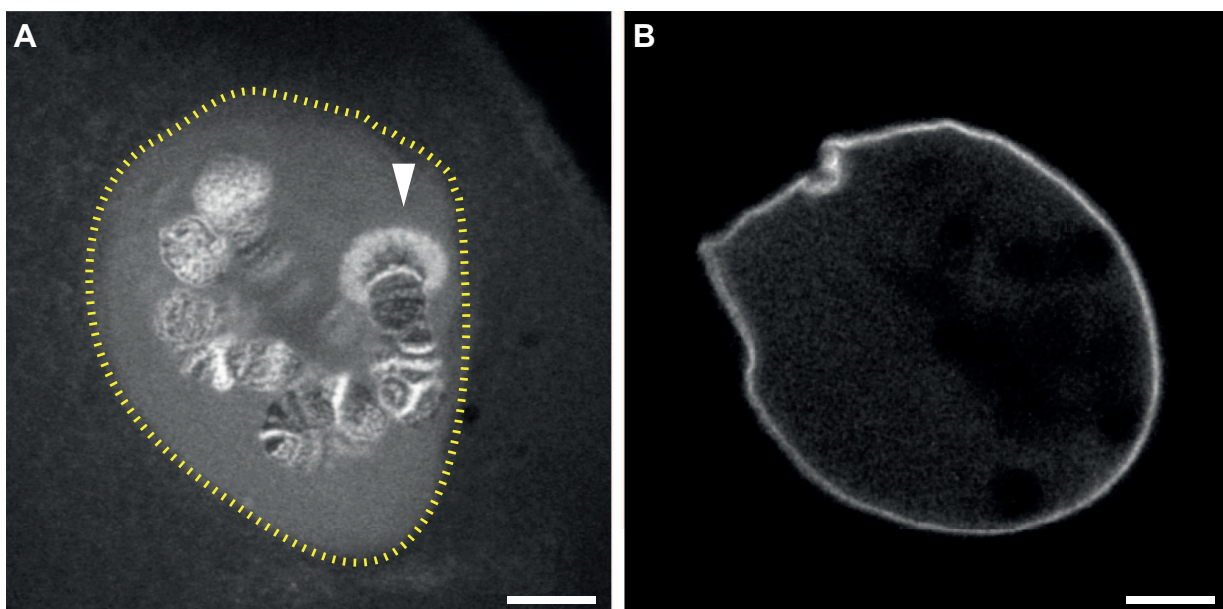


**Figure 3.5:** Labeling of nascent mRNP-particles and the Nuclear envelope. (A) Cytoplasmic injected AF647-tc-Hrp36 accumulates in the nucleus (dashed yellow line) and is incorporated into active transcription sites like the prominent BR2-puff (arrowhead). (B) AF546-tc-Ntf2 binds to NPCs. The NPCs of *C. tentans* salivary gland cells are so dense that they appear as a continuous line. Scale bars = 10 μm.

Data was collected on 140 nuclei from 70 different salivary glands to analyze the interaction of single mRNP-particles with the NE. In total 7180 movies of 20 s duration were analyzed.

This means that over seven million single frames had to be evaluated. To evaluate this amount of image data efficiently a kymograph-based analysis approach was used (see 2.17 p. 47).

### 3.4.1 Image and Kinetic Data Analysis

To image the mRNP-particle export both AF647-tc-Hrp36 and AF546-tc-NTF2 were imaged sequentially with a frame rate of 50 Hz. First AF647-tc-Hrp36 was imaged for 980 frames and subsequently AF546-tc-NTF2 for 20 frames (see 2.20 p. 50). On average an excitation power of  $0.7 \frac{\text{kW}}{\text{cm}^2}$  to  $1 \frac{\text{kW}}{\text{cm}^2}$  was used. As described the AF546-tc-NTF2 image sequence was averaged and used to extract the pixel region congruent with the NE. These pixels were plotted as kymograph. Events, which lasted for several frames at the same NE location appeared as horizontal stripes. The dwell times of these events was determined by measuring the length of the horizontal stripes above the background (see 2.17 p. 47).<sup>[54,113]</sup> The corresponding image sequence of every extracted mRNP-particle NE interaction event was carefully reviewed and categorized according to Fig. 3.6.

All events, for which the attachment to and/or the release from the NE was not observed could be the part of either an export or probing event. Therefore, only the kinetics of complete export or probing events were analyzed in detail. The data analyzed in this thesis are the same as in *Siebrasse et al. 2012*.<sup>[113]</sup> Since an advanced analysis procedure was used in comparison with *Siebrasse et al. 2012* the results here are not the same.

It is obvious that the detection probability of a NE-interaction event increases with its dwell time. Especially if the spatio-temporal density of NE-interactions is high it is very likely that short events are not detected. Therefore, here only events, which were detected at the membrane for at least 3 frames were taken into account to determine the NE-dwell time distribution. The images were acquired with a kinetic cycle time of  $t_{cyc} \sim 20$  ms and the dwell time calculated as  $t_{dwell} = 10 \text{ ms} + (d - 1)10 \text{ ms}$ .  $d$  denotes the number of frames, in which the particle was detected at the NE.

Previously the NE-interaction kinetics were analyzed by fitting a uni- or bimodal exponential growth function to the cumulative dwell time distribution.<sup>[113]</sup> As described in section 1.5.1 (p. 20) the exponential distribution describes the kinetics of a process with a single state transition with a fixed transition rate. It is plausible that mRNP-export and NPC probing of mRNP-particles could go through a reaction path with several rate limiting intermediate states. As outlined before, the kinetics of processes with several intermediate steps can be modeled by a gamma distribution (1.5.1 p. 20). The shape parameter  $S$  represents the number of rate limiting reaction steps and  $\tau$  the average time constant of a single rate limiting reaction step (see eq. 1.3 p.20).<sup>[33]</sup> The exponential distribution is just a special case of the gamma distribution with

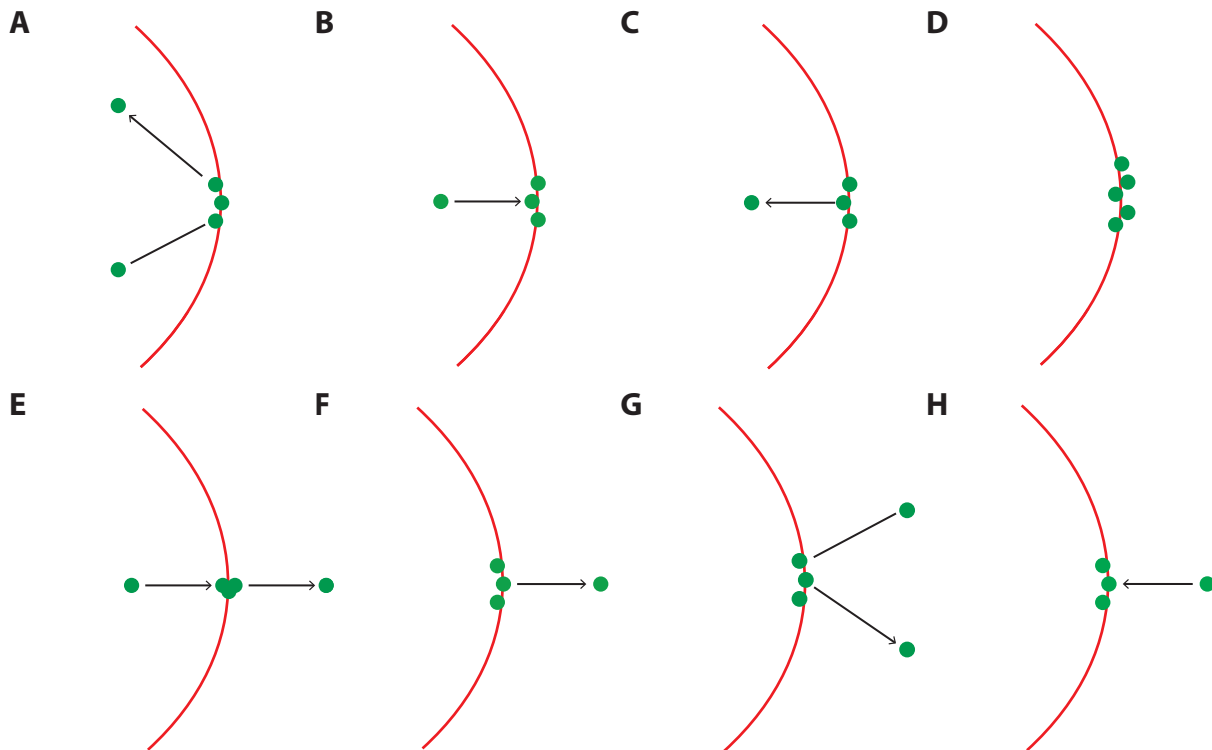


**Figure 3.6:** *Characterization scheme of mRNP NE interaction. (A) Nucleoplasmic probing (B) Nucleoplasm to the NE (C) NE to nucleoplasm (D) NE (E) Export (F) NE to cytoplasm (G) Cytoplasmic probing (H) Cytoplasm to NE.*

$S = 1$ . Therefore, using the gamma distribution is clearly advantageous as compared to fitting only an exponential distribution to the data.

To decide whether a uni- or multimodal gamma distribution is used to describe the NE-dwell time distribution, a model selection procedure was applied (see 1.5.1 p. 20). Therefore, multiple gamma distributions with an increasing number of modes were fitted iteratively to the data (see 2.13 p. 46).

Fitting the NE-dwell time distributions was realized in Matlab, which requires that all fitted parameters are continuous numbers. Since the number of rate limiting steps must have an integer value  $S_b \in [1, 2, \dots, 30]$ , it had to be fixed as a problem-dependent constant (see 2.13 p.46). For every number of modes and shape parameter combination an  $AIC_c$ -value was calculated. The model with the lowest  $AIC_c$ -value was used to describe the data. For all fitted data sets a uni- or bimodal gamma distribution had the lowest  $AIC_c$ -value. Therefore, the  $AIC_c$ -value

parameter space is visualized in the following as a heat map (see e.g. Fig 3.7, 3.11).

The estimation uncertainty of the number of rate limiting reaction steps is described in the following by its theoretical standard deviation. It is proportional to the number of rate limiting steps and inversely proportional to the number of observations (see eq. 1.3 p. 20 and table 7.3 p. 121).

The goodness-of-fit was estimated by hypothesis testing based on a parametric bootstrap. The test statistics were calculated as described at 1.5.2 (p. 21). Since test statistics weigh the fitting result differently, three different test statistics were applied (see 2.15 p. 47). In this context the null hypothesis is that the experimental data are appropriately described by the best model. It was accepted if the test-statistic of the best model was below the 0.95 quantile of the estimated test-statistic sampling frequency distribution (see Fig. 3.9,3.13, 3.16, 3.20, 3.24).

Furthermore, non-parametric bootstrapping was used to describe the quality of the estimated parameters. It allows to estimate the spread of the fit parameters based on the stochastic noise of the data. The narrower the estimated distribution of a fit parameter, the less its fitting result depends on the stochastic fluctuation of the experimental data. As spread indicator for the fitted parameters in the following the 0.25 and 0.75 percentile are used. A small spread does not indicate a good model fit (see 1.5.2 p.21 & 2.16 p.47).

A complete overview of the values extracted by data fitting and non-parametric bootstrapping is given at (Tab 7.2 p. 120).

### 3.4.2 Export Kinetics of Native mRNP-Particles

In total 121 complete export events were extracted, of which 109 lasted for at least three frames. For the mRNP-particle export the lowest  $AIC_c$  were obtained for a bimodal gamma distribution. The corresponding numbers of rate limiting steps are  $S_{1exp} = 21$  and  $S_{2exp} = 1$  (Fig. 3.7) with time constants  $\tau_{1exp} = 3.6$  ms (3.4 ms/3.8 ms) and a fraction of 30% (23% / 36%) and  $\tau_{2exp} = 158$  ms (137 ms/184 ms) and a fraction of 70 % (64% / 77%). This corresponds to an average export time for  $\tau_{1exp}$  of  $t_{1exp} = 76$  ms (71 ms/80 ms) ( $t_{1exp} = \tau_{1exp} S_{1exp}$ ). The empirical CDF  $F_n(t) = \frac{1}{n} \sum_{i=1}^n \{ \frac{5}{2} t_{cyc} < x_i \leq t \}$  does include only events  $x_i \geq \frac{5}{2} t_{cyc}$ . The cumulative gamma distribution is the integral from 0 to  $t$ . Therefore, the y-axis offset parameter  $c$  was introduced to the fit function  $cdf_{\gamma fit}(t; a, c, k_b, S_b)$ .  $c$  is an estimator for the number of events missed during the analysis.

The goodness-of-fit test by parametric bootstrapping shows that the null hypothesis is accepted at the 95% confidence level by all three test-statistics used (Fig. 3.9 p. 63).

The non-parametric bootstrapping shows clear peaks for the distributions of  $\tau_{1exp}^*$  and



$\tau_{2exp}^*$ . While the distribution of  $\tau_{1exp}^*$  shows a sharp peak, the distribution of  $\tau_{2exp}^*$  is much broader. This suggests that the fit result for  $\tau_{2exp}$  is governed to a higher extent by the stochastic fluctuations of the process. This is somehow surprising since the ratio of  $\tau_{1exp}$  and  $\tau_{2exp}$  suggests that the majority of observed export events belong to the slower export process described by  $\tau_{2exp}$ .

The fitted CDF is nearly asymptotic at 500 ms, whereas only  $\sim 90\%$  of the observed events were  $\leq 500$  ms (Fig. 3.8 p. 63). The extremely long lasting export events are not sufficiently described by this bimodal gamma distribution. The  $AIC_c$  shows that there is no gain of information by using a tri- or higher-modal gamma distribution. This is caused by the small number of export events which lasted 500 ms and longer.

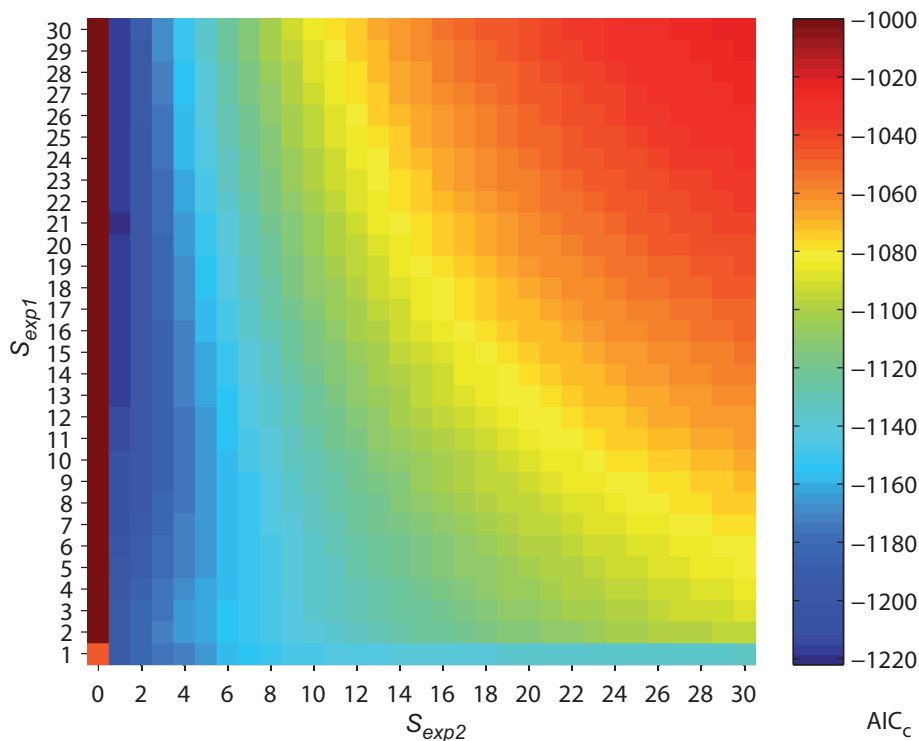


**Figure 3.7: Model selection for mRNP-export based on the  $AIC_c$ .** Color coded  $AIC_c$ -matrix of fitting the mRNP-export kinetics by a uni- or bimodal gamma distribution with varying number of rate limiting steps  $S_{exp}$ . The  $AIC_c$  for the single gamma distributions are located at  $S_{exp2} = 0$ . The model with the lowest  $AIC_c$  was selected. Because of the large variance of the  $AIC_c$  values  $\geq -1000$  are coded by the same color.

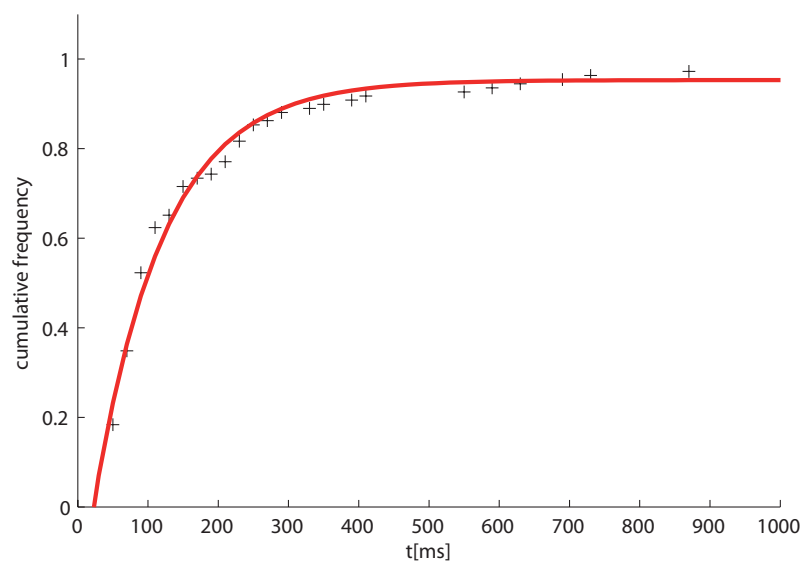


**Figure 3.8:** *Fitting of the cumulative NE-interaction time distribution of all export events. For calculation of the CDF (+) and fitting (red line) only events  $\geq 50$  ms were considered.*

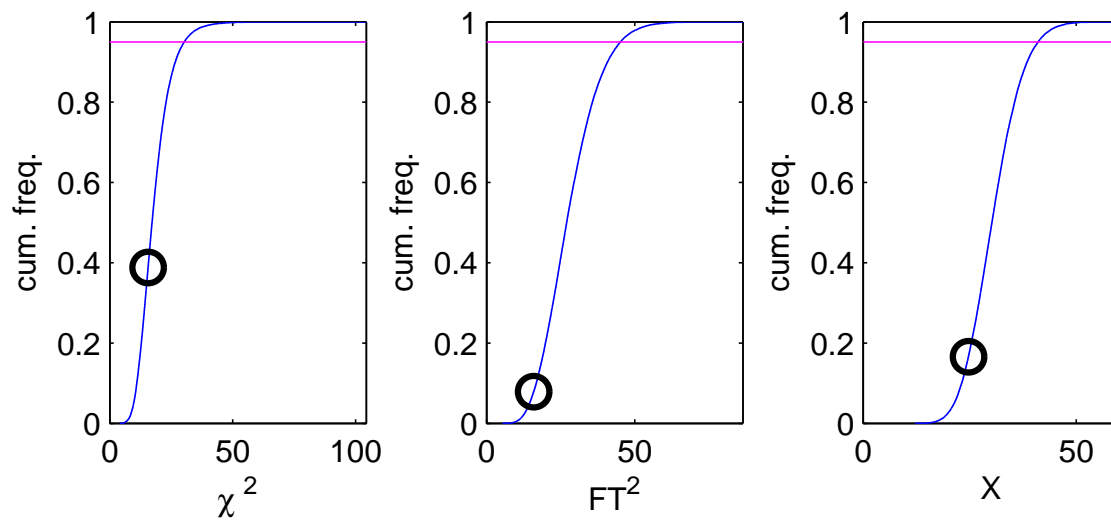


**Figure 3.9:** Goodness-of-fit test of the mRNP-particle export kinetics approximation by parametric bootstrapping. The cumulative test statistic distributions (blue line) were estimated by an  $m$ -out-of- $n$  parametric bootstrap. The null hypothesis is accepted if the test statistic of the best fit (black circle) is below the 0.95 quantile (magenta line).  $\chi^2$  = chi-square-,  $FT^2$  = Freeman-Tukey- and  $X$  = the Euclidean-test-statistic.

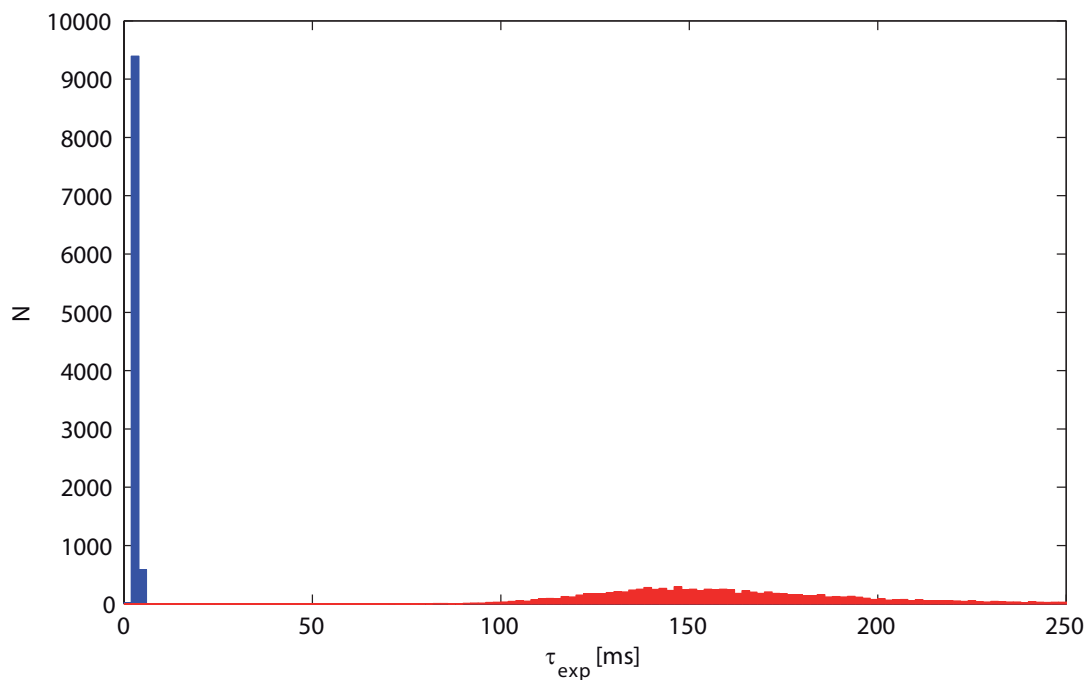


**Figure 3.10:** Variance estimation  $\tau_{1exp}$  (blue) and  $\tau_{2exp}$  (red) by non-parametric bootstrapping. A bimodal gamma-distribution,  $S_{exp1} = 21$  and  $S_{exp2} = 1$ , was fitted 10,000 times to a bootstrap sample of the experimental export kinetics. The histogram shows the distribution of  $\tau_{1exp}^*$  and  $\tau_{2exp}^*$ . The bin size is 2 ms.

### 3.4.3 Nuclear Probing Kinetics of Native mRNP-Particles

The the lowest  $AIC_c$  were obtained by fitting the nucleoplasmic probing kinetics with a bi-modal gamma distribution. The estimated number of rate limiting steps are  $S_{1nprobing} = 3$  and  $S_{2nprobing} = 1$  (Fig. 3.11). The fitted rate constants are  $\tau_{1nprobing} = 22.3$  ms (20.5 ms/23 ms) with a fraction of 93% (75% / 83%) and  $\tau_{2nprobing} = 320$  ms (208 ms/333 ms) with a fraction of 7% (17% / 25%).

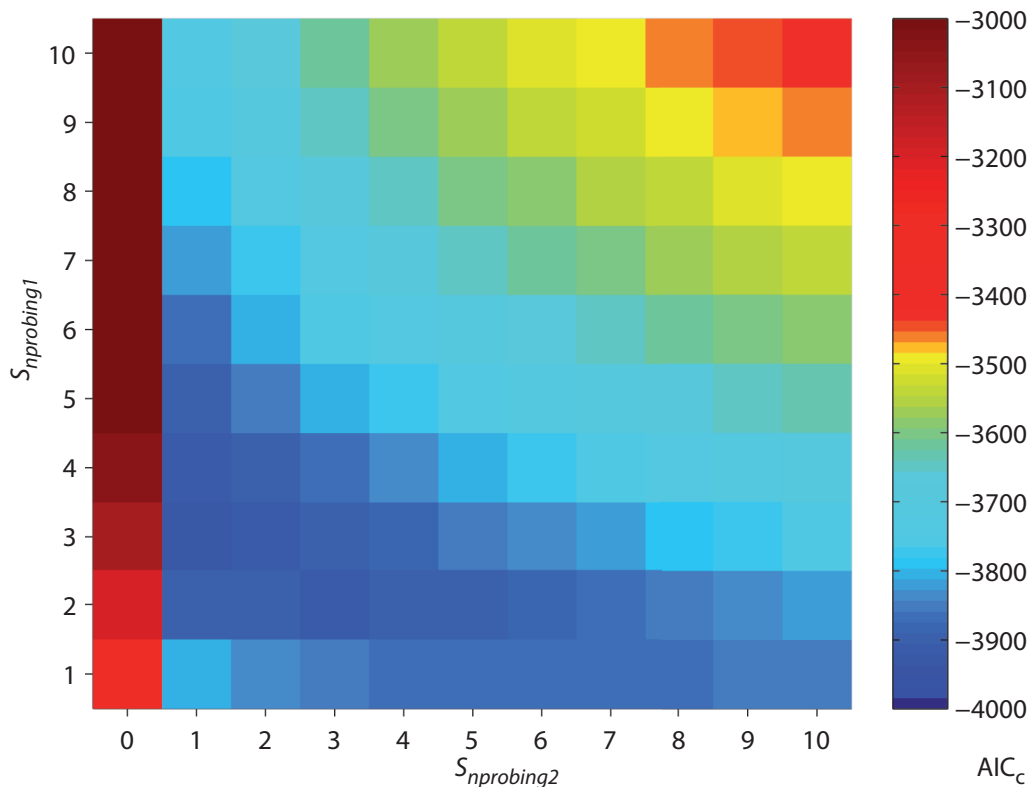


**Figure 3.11:** *Model selection for fitting the nuclear probing kinetics by  $AIC_c$ . Color coded  $AIC_c$ -matrix of approximating the nuclear probing kinetics by a uni- or bimodal gamma distribution with varying number of rate limiting steps. The  $AIC_c$  for the single gamma distributions are located at  $S_{nprobing2} = 0$ . The model with the lowest  $AIC$  was selected. Because of the large variance of the  $AIC_c$  values  $\geq -3000$  are coded by the same color.*

The goodness-of-fit test accepts the null hypothesis at the 95% confidence level (3.13 p. 67). The measured data especially for the long lasting events is very sparse. The  $\chi^2$  and to a minor extend the  $FT^2$  test statistics are sub-optimal with sparse data and overestimate the rare events (see section 1.5.2 p. 21). Therefore, the  $\chi^2$  and  $FT^2$  test statistics are closer to the 0.95 quantile than the simple Euclidean test statistic of the fitted function.

The estimated spread of  $\tau_{1nprobing}$  is very low. The higher estimated spread of  $\tau_{2nprobing}$  can be caused by the low number of observations and the increasing stochastic fluctuations

with increasing time constant.<sup>[106]</sup> As already seen for the mRNA-export kinetics the bimodal gamma-distribution does not reproduce the extremely long lasting nuclear probing events. The fitted bimodal gamma distribution is already close to its asymptotic value at  $t = 400$  ms, while the empirical CDF is still increasing (Fig. 3.12 p. 66). The  $AIC_c$  of a tri-modal gamma distribution is higher than of the best fitting bimodal fit. Adding more modes to the fitting function would increase the goodness-of-fit but the more complex model would not be justified by the  $AIC_c$ .

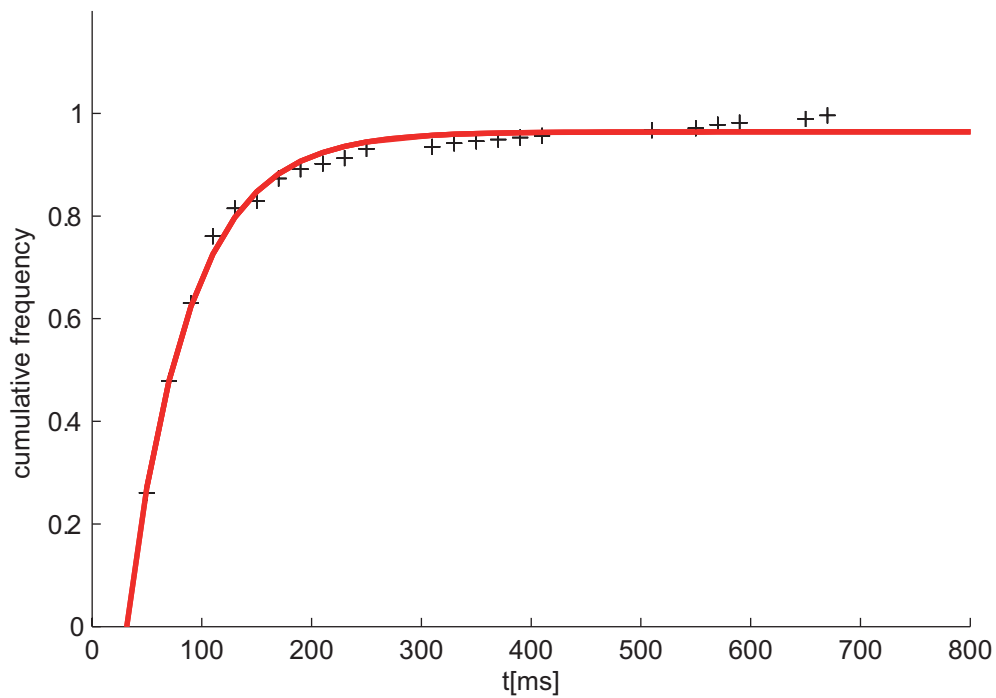


**Figure 3.12:** *Fitting of the cumulative NE-interaction kinetics of the nuclear probing events. For calculation of the CDF (+) and fitting (red line) only events  $\geq 50$  ms were considered.*

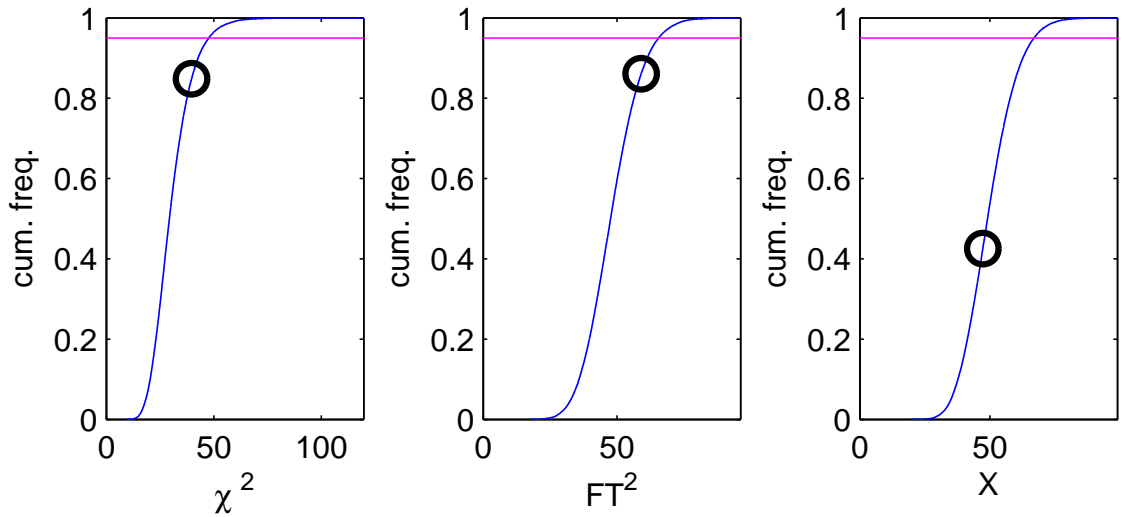


**Figure 3.13:** *Goodness-of-fit test of the nuclear probing kinetics approximation by parametric bootstrapping.* The cumulative test statistic distributions (blue line) were estimated by an  $m$ -out-of- $n$  parametric bootstrap. The null hypothesis is accepted if the test statistic of the best fit (black circle) is below the 0.95 quantile (magenta line).  $\chi^2$  = chi-square-,  $FT^2$  = Freeman-Tukey- and  $X$  = the Euclidean-test-statistic.

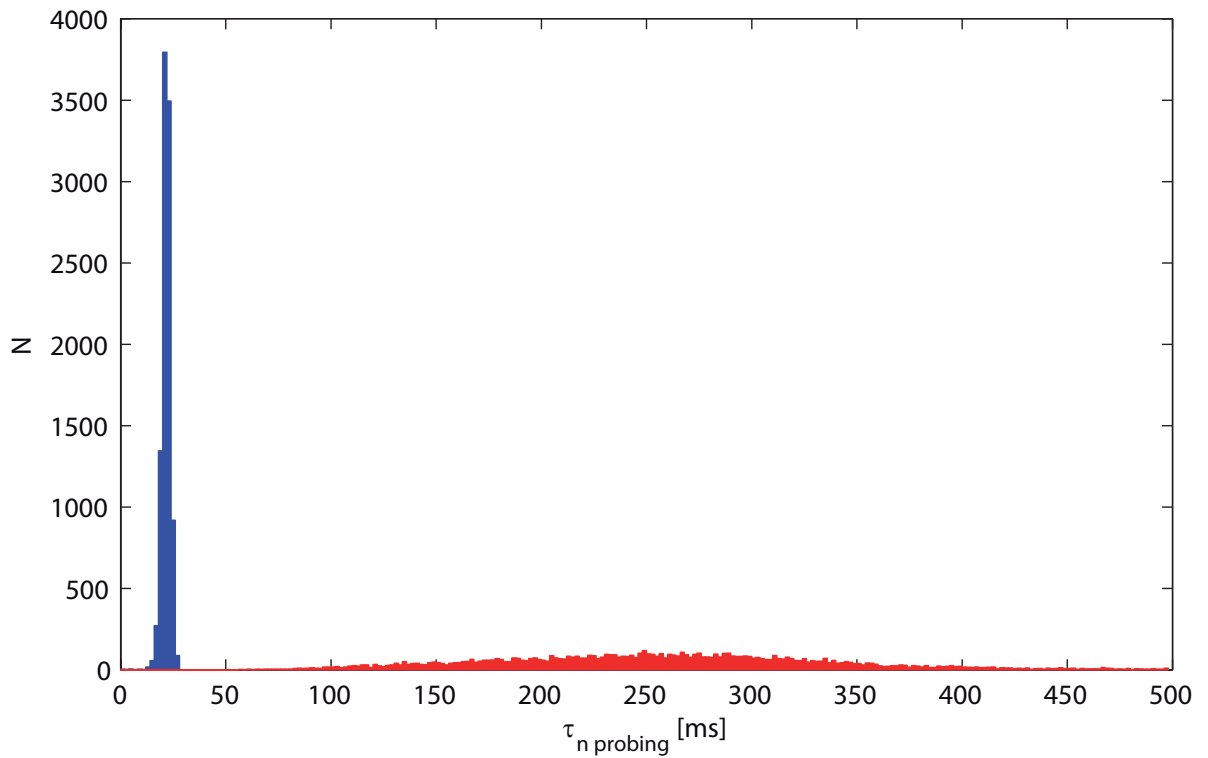


**Figure 3.14:** *Estimation of the Variance of  $\tau_{1nprobing}$  (blue) and  $\tau_{2nprobing}$  (red) by nonparametric bootstrapping.* A bimodal gamma-distribution,  $S_{1nprobing} = 3$  and  $S_{2nprobing} = 1$ , was fitted 10,000 times to a bootstrap sample of the experimental nucleoplasmic probing kinetics. The histogram shows the distribution of the fit parameters  $\tau_{1nprobing}$  and  $\tau_{2nprobing}$ . The bin size is 2 ms.

### 3.4.4 Cytoplasmic Probing Kinetics of Native mRNP-Particles

The lowest  $AIC_c$  for fitting the cytoplasmic probing kinetics were obtained with a uni-modal gamma distribution with a single rate limiting step, so that the gamma distribution is simplified to an exponential distribution. The cytoplasmic probing rate constant was  $\tau_{cprobing} = 86$  ms (81.6 ms/94.5 ms).

For  $t \geq 500$  ms the data density is very sparse. The  $\chi^2$  test statistics performs suboptimal with sparse data. Based on the  $FT^2$  and the Euclidean goodness-of-fit statistics the null hypothesis has to be accepted (Fig. 3.16 p. 69).

The estimated variance of the fitted time constant seems to be higher in comparison to the fast export or nuclear probing. But the divergence of  $\tau_{1exp}$  or  $\tau_{1nprobing}$  has to be multiplied by the number of rate limiting steps to obtain the uncertainty of the estimated mean total interaction time. Taking this into account the variance is comparable to the total mean interaction time of the fast export and nucleoplasmic probing processes. For cytoplasmic probing extremely long lasting events which are not modeled by the uni-modal gamma distribution were observed, too (Fig. 3.15 p. 68). But as before no conclusions can be made regarding the kinetics of these events because of their low frequency.

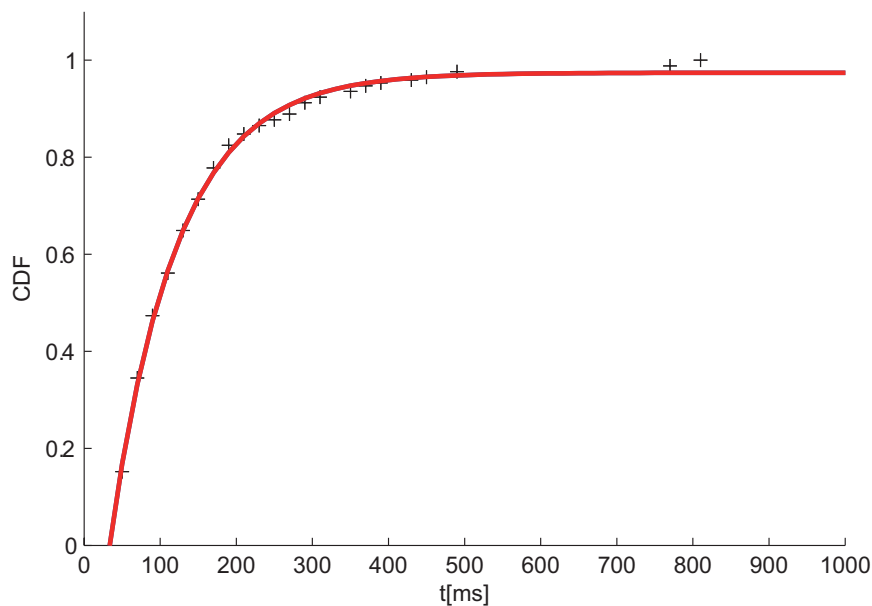


**Figure 3.15:** *Fitting the cumulative NE-interaction kinetics of the cytoplasmic probing events. For calculation of the CDF (+) and fitting (red line) only events  $\geq 50$  ms were considered.*

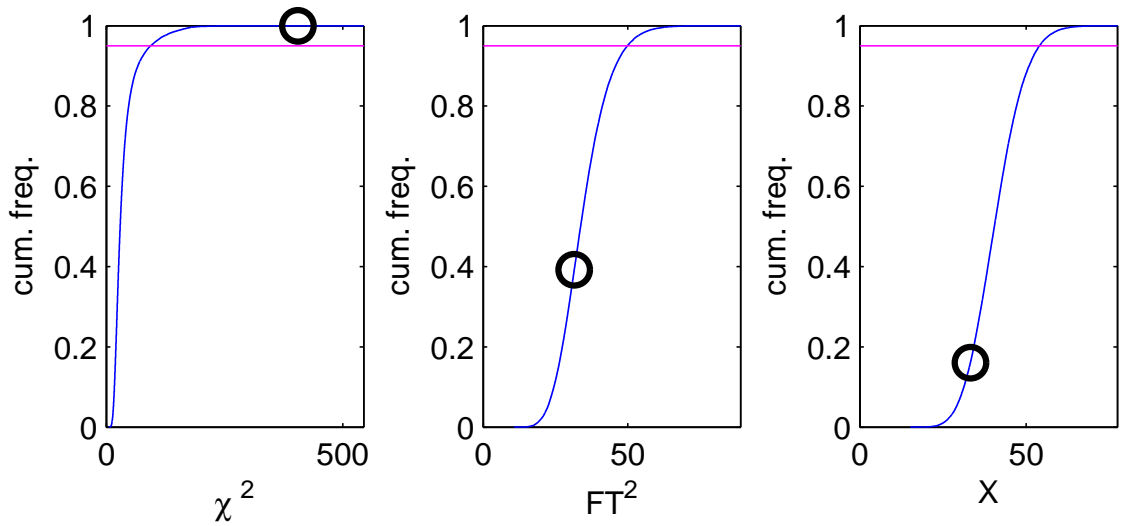


**Figure 3.16:** *Goodness-of-fit test of the cytoplasmic probing kinetics approximation by parametric bootstrapping.* The cumulative test statistic distributions (blue line) were estimated by a  $m$ -out-of- $n$  parametric bootstrap. The null hypothesis is accepted if the test statistic of the best fit (black circle) is below the 0.95 quantile (magenta line).  $\chi^2$  = chi-square-,  $FT^2$  = Freeman-Tukey- and  $X$  = the Euclidean-test-statistic.

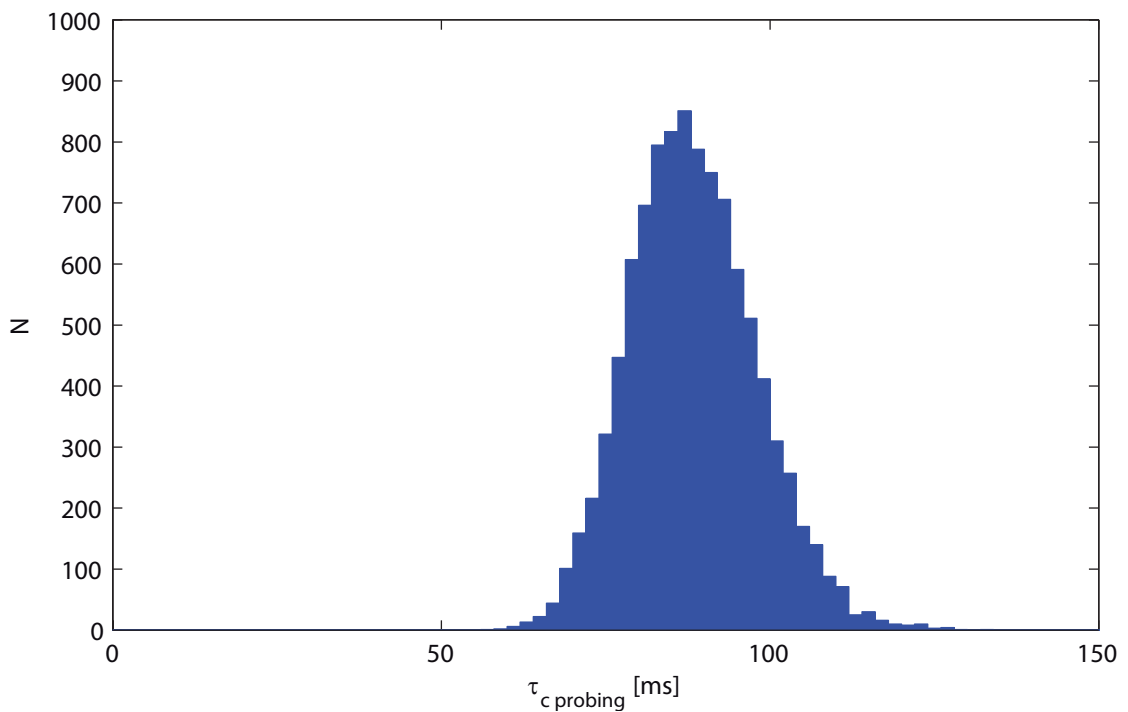


**Figure 3.17:** *Estimation of the Variance of  $\tau_{c\text{probing}}$  by nonparametric bootstrapping.* A unimodal gamma-distribution,  $S_{c\text{probing}} = 1$ , was fitted 10,000 times to a bootstrap sample of the experimental cytoplasmic probing kinetics. The histogram shows the distribution of the fit parameter  $\tau_{c\text{probing}}^*$ . The bin size is 2 ms.



### 3.4.5 Trajectory Analysis

The high signal-to-noise ratio resulted in an average localization precision for single mRNP-particles of  $\sim 10$  nm. This high localization precision allows a detailed analysis of the mRNP-particle trajectories crossing the NPC. The export trajectories, which showed an NE-dwell time of  $\geq 300$  ms were used for this analysis. These trajectories (N=17) were superimposed using a procedure introduced by *Lowe et al.*<sup>[77]</sup>. The best overlay of these trajectories with a virtual scheme of the *C. tentans* NPC shape was determined as described (see 2.18 p. 49).<sup>[56]</sup> The overlay of the coordinate distribution with the NPC dimension suggests that the mRNP-particles lingered predominantly in the nuclear basket and at the nucleoplasmic face of the central channel (Fig 3.18 A).

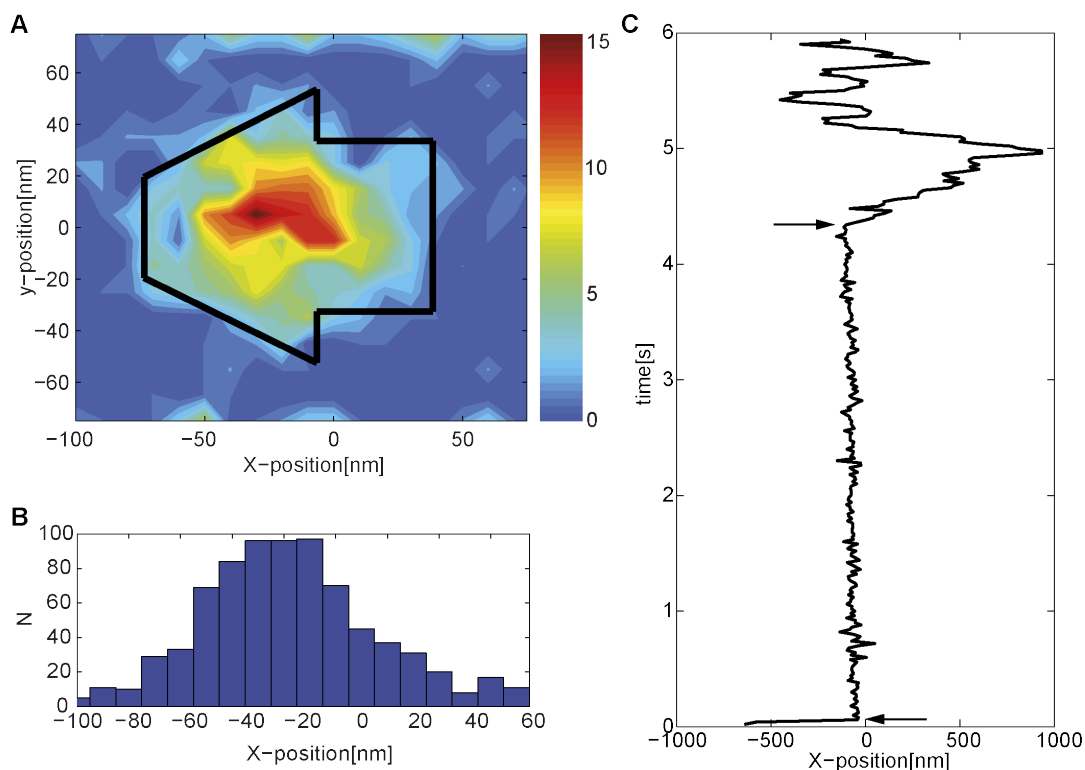


**Figure 3.18: Trajectory analysis of export events  $\geq 300$  ms.** The overlay of the localization density map of export trajectories with the *C. tentans* NPC shape (A) and the histogram of the mRNP-position along the nucleo-cytoplasmic axis (B) suggest that mRNP-particles are preferentially localized at the nuclear basket before being exported. (C) Plotting the x-position of a single export event showing that the mRNP-particle rather is immobile at the NPC than moving progressively through NPC during export (between arrows).

Slow mRNP-export trajectories did not show a constant progression through the NPC as illustrated by the longest export trajectory (Fig. 3.18 C). They rather bind to the NPC and stay stationary for extended time periods.

### 3.4.6 Dbp5-Kinetics at the Nuclear Envelope

Dbp5 is an essential component of mRNA-export. The essential action of Dbp5 during mRNA-export is located at the cytoplasmic face of the NPC.<sup>[47,95]</sup>

As for the mRNP-particle interaction before, here also only events lasting three or more frames at the NE were considered during analysis. Imaging the Dbp5 NE interactions with a framerate of 20 ms 59 of 144 events had to be excluded by this threshold.

For the Dbp5 NE interaction the lowest  $AIC_c$ -value was obtained by a uni-modal gamma distribution with a single rate limiting step  $S_{Dbp5_{50Hz}}=1$  and a rate constant  $\tau_{Dbp5_{50Hz}} = 52$  ms (45.1 ms/62.3 ms). The  $\chi^2$  and  $FT^2$  goodness-of-fit-statistics are close to the critical value for rejecting the null hypothesis and the null hypothesis is rejected by the Euclidean test statistic. This shows that the applied function for modeling is not a good fit for the data even if it represents the best model tested here.

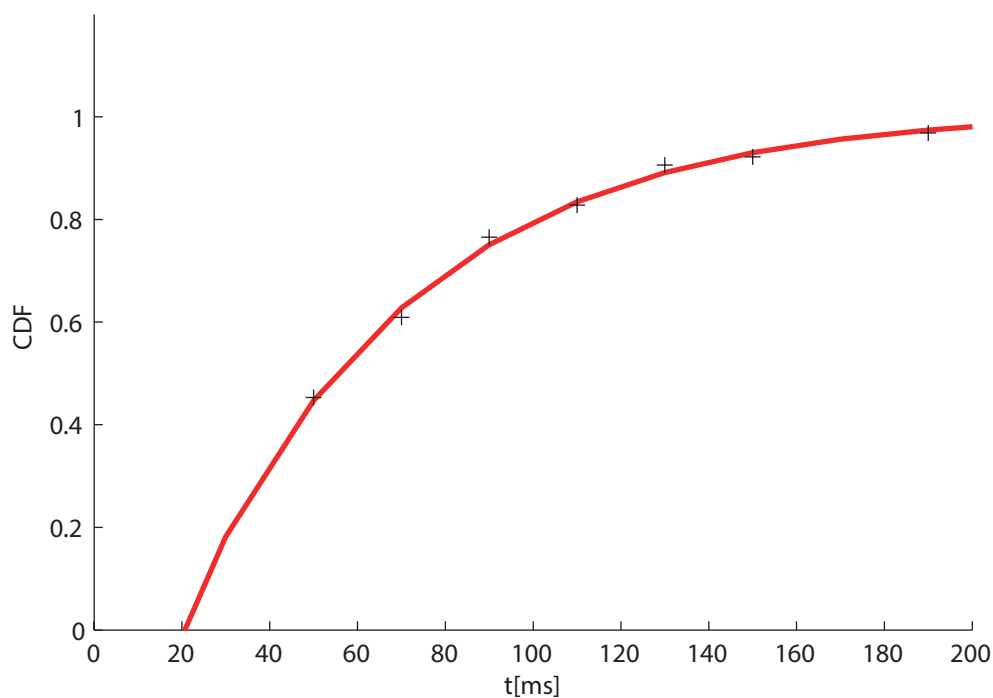


**Figure 3.19:** *Fitting the cumulative NE-interaction kinetics of Dbp5 imaged with 50 Hz. For calculation of the CDF (+) and fitting (red line) only events  $\geq 50$  ms were considered.*

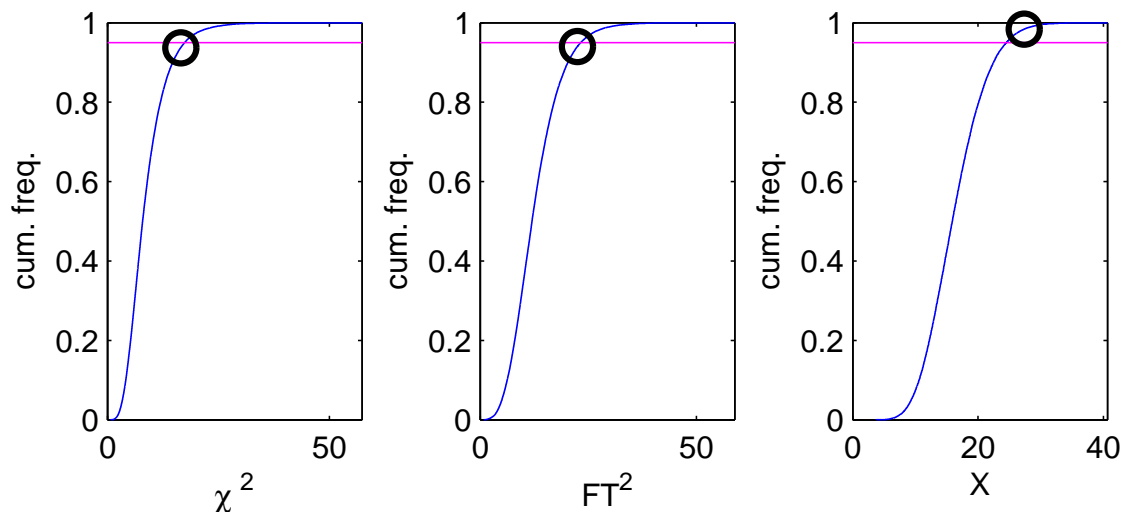


**Figure 3.20:** Goodness-of-fit test for the *Dbp5* kinetics approximation by parametric bootstrapping. The cumulative test statistic distributions (blue line) were estimated by an *m*-out-of-*n* parametric bootstrap. The null hypothesis is accepted if the test statistic of the best fit (black circle) is below the 0.95 quantile (magenta line).  $\chi^2$  = chi-square-,  $FT^2$  = Freeman-Tukey- and  $X$  = the Euclidean-test-statistic.

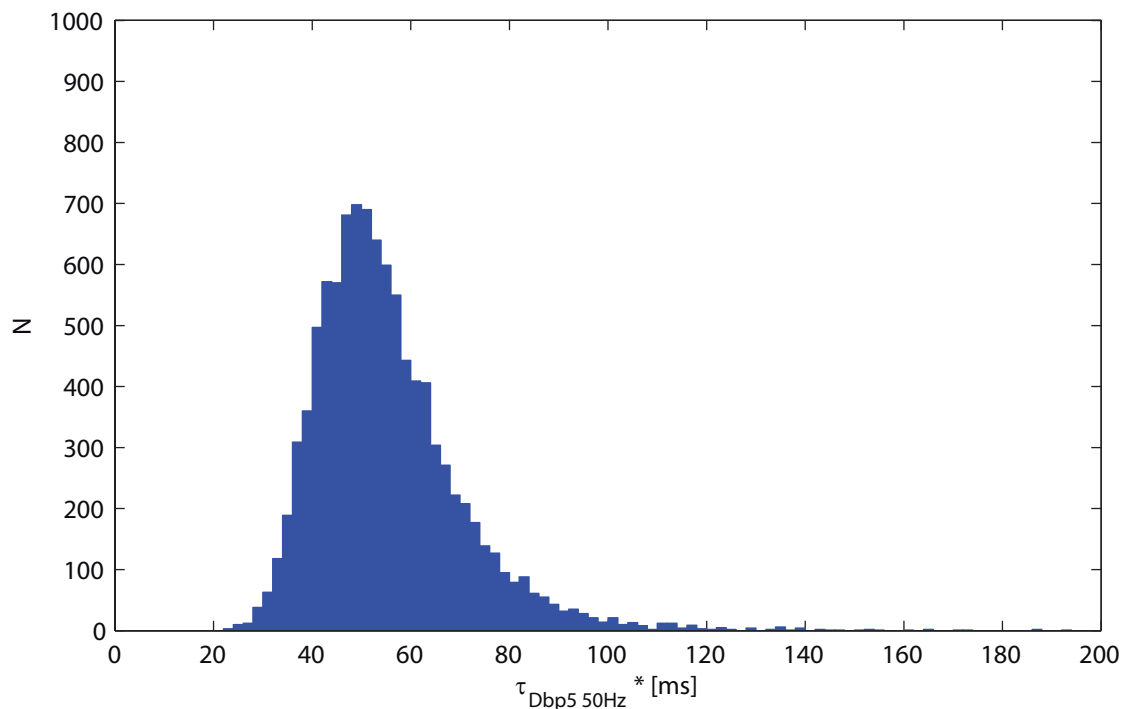


**Figure 3.21:** Variance estimation of  $\tau_{D_{bp5}50Hz^*}$  by non-parametric bootstrapping. An uni-modal gamma-distribution,  $S_{D_{bp5}} = 1$ , was fitted 10,000 times to a bootstrap sample of the experimental *Dbp5* dwell time distribution. The histogram shows the distribution of the fit parameter  $\tau_{D_{bp5}50Hz^*}$ . The bin size is 2 ms.

Several observed complete export events lasted only  $\sim 20$  ms. Thus, Dbp5 NE dwell times are expected to be shorter than a complete export event or 20 ms. Therefore, the Dbp5 NE interaction were imaged in a second series of experiments with a framerate of 5 ms as well. The faster framerate decreased the threshold of the shortest events used for analysis to 15 ms. In total 61 events were analyzed. The cumulative distribution showed two components. The lowest  $AIC_c$  was found for  $S_{1Dbp5_{200Hz}}=2$  and  $S_{2Dbp5_{200Hz}}=1$ . The corresponding time constants are  $\tau_{1Dbp5_{200Hz}} = 12.9$  ms (32.5 ms/48.1 ms) with a fraction of 77% (3%/70%) and  $\tau_{2Dbp5_{200Hz}} = 240$  ms (682 ms/ $8 \times 10^5$  ms) with a fraction of 23% (30%/97%). This results in an average export time for  $\tau_{1Dbp5_{200Hz}}$  of  $t_{1Dbp5_{200Hz}} = \tau_{1Dbp5_{200Hz}} S_{2Dbp5_{200Hz}}^* = 26$  ms (Fig. 3.23). This clearly shows that imaging the Dbp5 NE interaction with a frame rate of 50 Hz is not sufficient. The large estimated variance of the fit parameters are the result of the small number of total observations. The spikey distribution of the faster interaction  $\tau_{1Dbp5_{200Hz}}^*$  shows that single observed dwell times have a strong influence at the obtained fit parameters. Since the empirical CDF contains 61 individual dwell times this result is not surprising. However, the median of  $\tau_{1Dbp5_{200Hz}}^*$  indicates that  $\tau_{1Dbp5_{200Hz}}$  and  $\tau_{2Dbp5_{200Hz}}$  are presumably larger than the here calculated fit value.

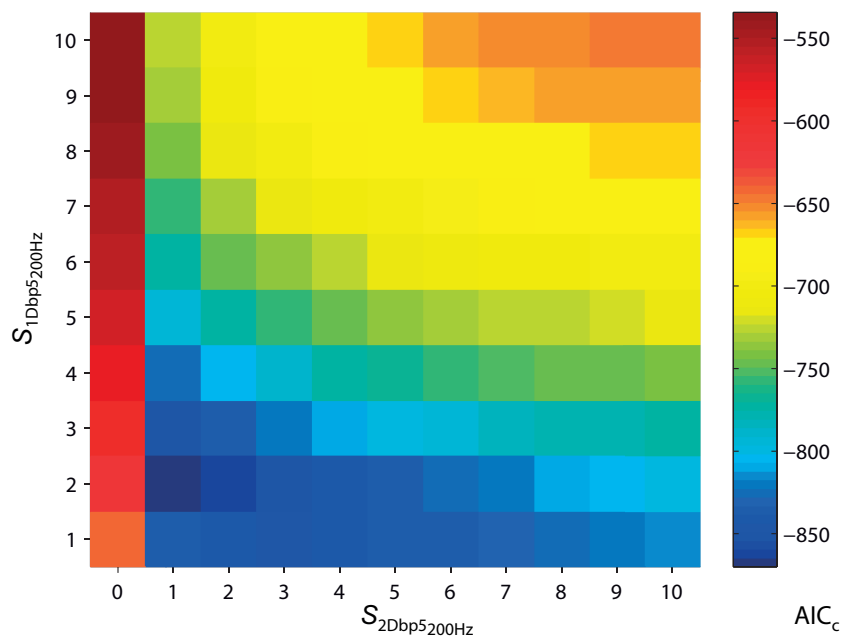


**Figure 3.22: Model selection for Dbp5 NE interaction kinetics imaged with 200Hz.** Color coded  $AIC_c$ -matrix of approximating the Dbp5 binding kinetics to the NPC by a single or the sum of two gamma distributions with varying number of rate limiting steps. The  $AIC_c$  values for the single gamma distributions are located at  $S_{2Dbp5_{200Hz}}=0$ . The model with the lowest  $AIC_c$  was selected.

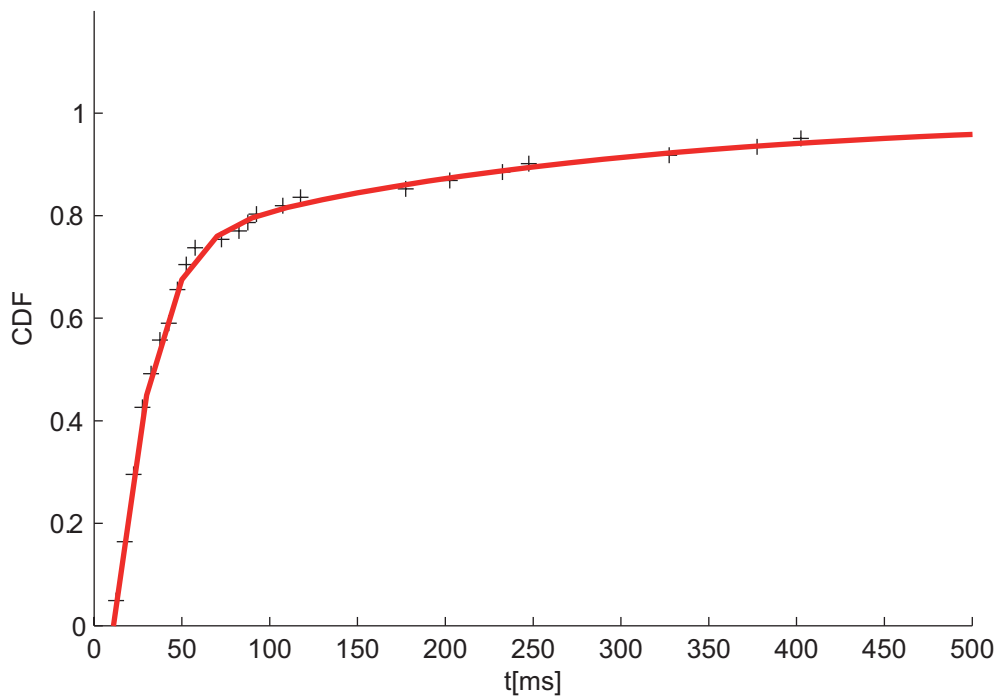


**Figure 3.23:** *Fitting the cumulative NE-interaction kinetics of Dbp5 imaged with 200 Hz. For calculation of the CDF (+) and fitting (red line) only events  $\geq 12.5$  ms were considered.*

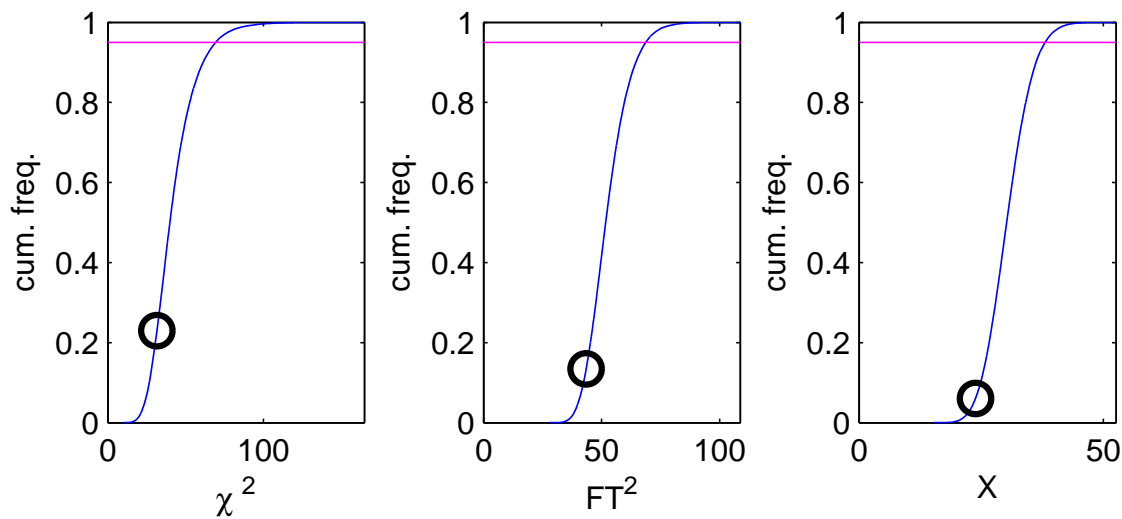


**Figure 3.24:** *Goodness-of-fit test of the Dbp5 NPC binding kinetics approximation by parametric bootstrapping. The cumulative test statistic distributions (blue line) were estimated by an m-out-of-n parametric bootstrap.*

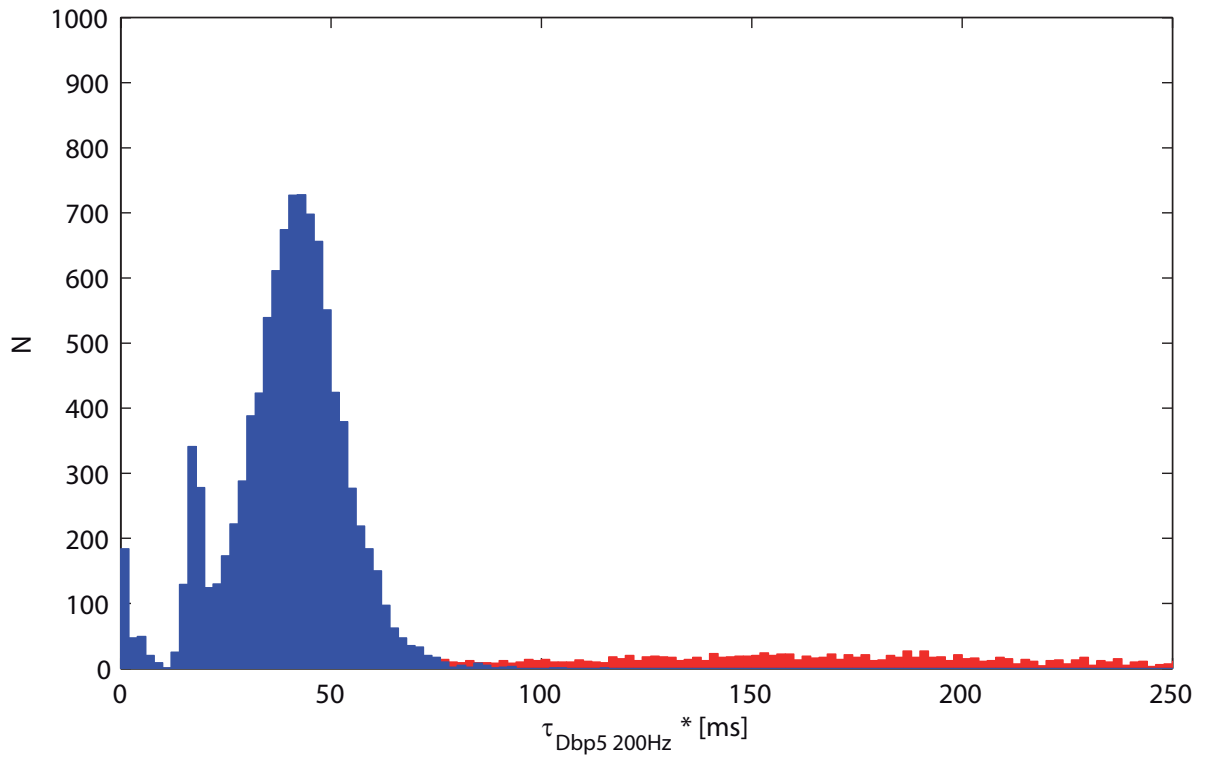


**Figure 3.25:** Estimation of the Variance of  $\tau_{1Dbp5_{200Hz}}$  (blue) and  $\tau_{2Dbp5_{200Hz}}$  (red) by nonparametric bootstrapping. A bimodal gamma-distribution,  $S_{1Dbp5_{200Hz}} = 2$  and  $S_{2Dbp5_{200Hz}} = 1$ , was fitted 10,000 times to a bootstrap sample of the experimental nucleoplasmic probing kinetics. The histogram shows the distribution of the fit parameters  $\tau_{1Dbp5_{200Hz}}$  and  $\tau_{2Dbp5_{200Hz}}$ . The bin size is 2 ms.

## 4 Results II: Transcriptional Regulation of BR-Genes

The starting point to studying the regulation of the BR2-genes transcription under heat-shock was an experiment within the framework of the mRNA-export project. The result was not in agreement with the so far known transcription regulation mechanism. Because of the central importance of transcription regulation this observation was further investigated.

The initial experiment was a control experiment to check if a downregulation of BR-genes transcription could be induced. The necessity to inhibit BR-gene transcription was a result of the used mRNP-particle labeling technique.

Using AF647-tc-Hrp36 as probe to label mRNA, the complete mRNA-pool and not only the large BR2-mRNP-particles as initially intended were labeled. To determine the export kinetics of the large BR2-mRNP-particles, cells with and without BR-gene expression should be examined. It is known that the BR-gene family transcription is down-regulated under heat-shock conditions (see 1.6.2 p. 30).<sup>[75]</sup> Since the BR2-mRNA is of exceptional size and abundance it was assumed that a difference of the mRNP-particle export kinetics between heat- and non-heat-shocked salivary glands should be detectable. The difference would correspond to the BR-mRNP export kinetics. *Lezzi et. al* described that 30 min to 60 min incubation at 37 °C is sufficient to suppress the BR-gene transcription<sup>[72,75]</sup>.

To proof that the transcription of the BR-genes is downregulated during heat-shock and to examine the required heat-shock incubation time until no BR2-mRNA is left in the nucleus salivary glands from heat-shocked larvae were analyzed by FISH (see 2.5 p. 36). The BR2.1 gene expression and mRNA localization were used as a general indicator of BR-gene expression and localization. For heat-shocking larvae were incubated at 37 °C for 1 h in beaker filled with pre-warmed water from the growth dishes.

The FISH analysis shows that after 1 h heat-shock BR2.1-mRNA is still located at the BR2-site (Fig. 4.1). This is surprising because the known transcriptional regulatory mechanisms are located at the promoter region or its proximity. The used BR2.1-mRNA-probe binds to a repetitive sequence motif of the BR2.1-mRNA. The beginning of the repetitive sequence

array is ~1600 bp downstream of the transcription start site. Therefore, the transcription cycle of the detected BR2.1-mRNAs has already entered stable elongation. But the high mRNA concentration at the BR2-site is no proof for transcriptional activity. This result indicated that the downregulation of BR2-transcription under heat-shock does not depend on the so far known transcription regulation mechanisms.

Therefore, the transcription activity was monitored *in vivo* in heat-shocked and control salivary glands. An absence of transcription activity would raise the question why the BR2.1-mRNA stays associated to the BR2-puff. If RNAPII is still present at the BR2-puff it is most likely that the by FiSH detected BR2.1-mRNA is still part of elongation complexes. The presence of elongation complexes provide on the one hand insight into the status and localization of RNAPII at the BR2-puff and on the other hand could confirm the result of RNAPII immunostainings. If non transcribing RNAPII is present at the BR2-puff during heat-shock the phosphorylation status of RNAPII is of interest. Its phosphorylation status can be linked to certain stages of the transcription cycle. Another question would be a possible reactivation of RNAPII after heat-shock release.

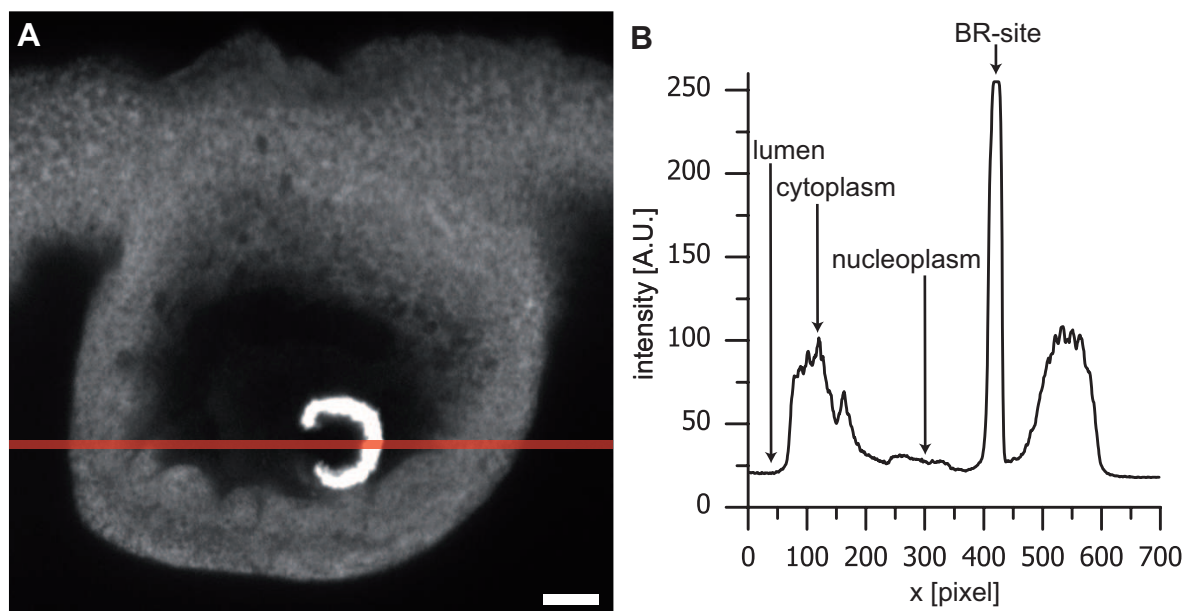


**Figure 4.1:** *BR2.1-mRNA distribution after heat shock.* (A) BR2-site shows a high BR2.1-probe signal after 1 h heat-shock. The nucleoplasm is almost clear of BR2.1-mRNA, while it is abundant in the cytoplasm. (B) The intensity plot along the red line in A shows that the fluorescence signal in the nucleoplasm is only slightly above the background signal. Scale-bar = 10  $\mu$ m.



## 4.1 Transcriptional Block of BR2.1 Genes During Heat-Shock

Hrp36 is only co-transcriptionally incorporated into nascent mRNP-particles. Without transcription Hrp36 is not incorporated into mRNP-particles.<sup>[113]</sup> In explanted salivary glands from control larvae microinjected Hrp36 is incorporated into nascent mRNPs and the BR2-puff becomes rapidly visible (Fig. 4.2 A). Due to the decondensation during transcription the BR2-site is largely extended (Fig. 4.2 D). BR2.1-mRNA and active transcription sites are colocalized at the BR2-puff (Fig. 4.2 D,E). After 60 min heat-shock BR2.1-mRNA can still be detected at the BR2-puff but no transcriptional activity (Figure 4.2 C,F). Various active transcription sites can be detected after heat-shock. Especially IV-2C which is very close to the BR2-puff (Figure 4.2 C asterisk). For IV-2C remaining transcriptional activity during heat-shock is known.<sup>[109]</sup> The size of the BR2-puff seems to be decreased after heat-shock, but the BR2-DNA is still decondensed and forms a puff.

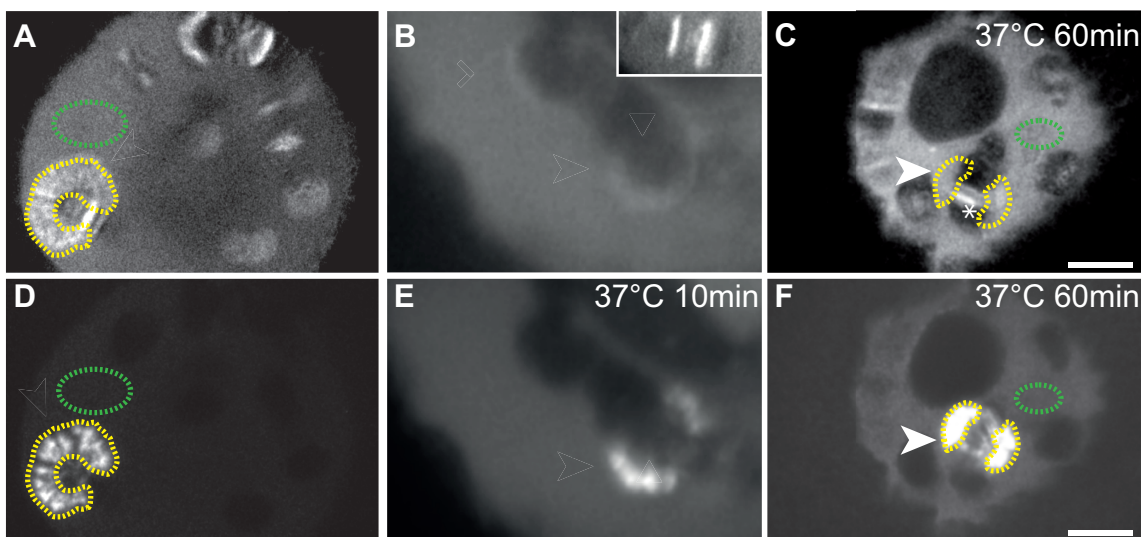


**Figure 4.2: Stable transcription block of BR2.1 induced by 60 min heat-shock.** Without transcriptional activity the BR2.1 transcript remains at the BR site. The images show confocal two-color fluorescence sections of salivary gland cell nuclei, in which (A-C) all active transcription sites and (D-F) the BR2.1 mRNA were labeled. The vertically arranged images show the two different channels of the same nuclei, respectively. Control salivary gland cells show at the BR2 puff (A) active transcription and (D) the presence of high levels of BR2.1-mRNA. (B) A heat-shock for 10 min blocked active transcription at most sites. The inset shows active transcription sites in this nucleus in a different Z-plane. (E) BR2.1-mRNA was still detectable at the BR2-puff. (C) Even after 1 hour of heat-shock no transcriptional activity at the BR2-puff was detectable, while it (F) still contained a high concentration of BR2-mRNA. The BR2-puff are marked by arrow heads and IV-2C by an asterisk. Scale-bar = 10  $\mu$ m.

The reduction of transcriptional activity at the BR2-puff was quantified by measuring the

enrichment of Hrp36 at the BR2-puff after coinjection with a BR2.1-mRNA specific molecular beacon. 10 min after coinjection the BR2-puff was imaged with a Laser Scanning Microscope. A region of interest (ROI) was defined around the BR2-puff labeled by the BR2.1-molecular beacon (Fig. 4.2 dashed yellow lines). A second ROI was placed in the nucleoplasm next to the BR2-puff devoid of any chromosomes or nucleoli (Fig. 4.2 dashed green lines). Pixel intensities were dark count corrected. The corrected pixel values of the BR2-ROI  $I_{ij}$  were divided by the average pixel intensity of the nucleoplasmic ROI  $\bar{I}_{nuc}$ . This was done for Hrp36 and the BR2.1-molecular beacon. The relative pixel intensities of the BR2.1-molecular beacon  $I_{ijBR2}/\bar{I}_{BR2nuc}$  were plotted against the relative Hrp36 pixel intensities  $I_{ijHrp36}/\bar{I}_{Hrp36nuc}$  (Fig. 4.3). The heat-shocked larvae were incubated for 60 min at 37 °C prior salivary gland dissection and microinjection. In total the salivary glands of 11 heat-shocked and 3 control larvae were analyzed.

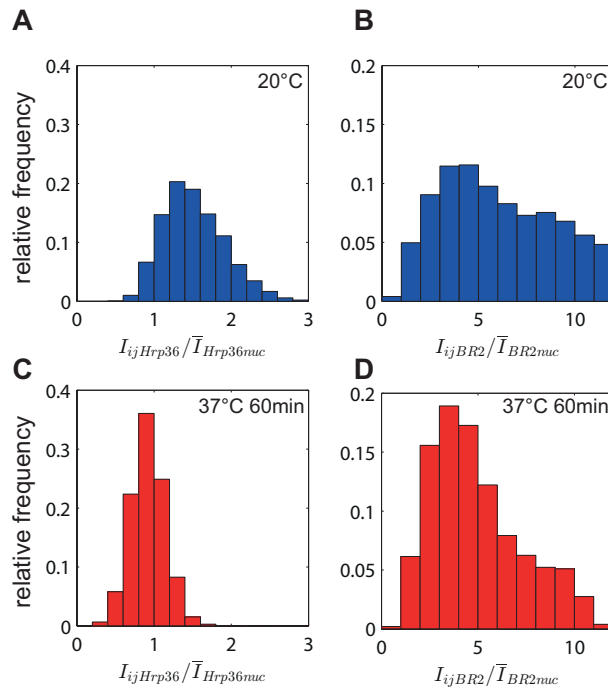


**Figure 4.3: Relative quantification of BR2.1 transcriptional activity of heat-shocked salivary glands and control glands.** (A) Hrp36 fluorescence intensity at BR2-puff of control gland cell nuclei, and (B) BR2.1 oligonucleotide fluorescence intensity. (C) Hrp36 fluorescence intensity at BR2-puff and (D) BR2.1 oligonucleotide fluorescence intensity of salivary gland cells heat-shocked for 60 min. In control cells with normal transcriptional activity hrp36 was clearly enriched at the BR2-puff (mean intensity, 1.44). The amount of Hrp36 at the transcription sites in heat-shocked animals was close to the background (mean value, 0.93). The BR2.1-mRNA concentration at the BR2-puff was only slightly affected by the heat shock. The data in (A) and (C) were based on 11 independently examined glands, and those in (B) and (D) were based on 3 independently analyzed glands. Examples for the ROI selection are given in Fig. 4.2 .

The heat-shocked salivary glands show no significant incorporation of Hrp36 at the BR2-

puff (Fig. 4.3 C). The average Hrp36 fluorescence intensity of the BR2-ROI in heat-shocked salivary glands is slightly below the average nucleoplasmatic intensity. The DNA of the BR2-puff reduces the volume accessible for Hrp36. Without transcriptional activity an average Hrp36 concentration slightly below the nucleoplasmic concentration is therefore expected. In control salivary glands Hrp36 becomes incorporated into the nascent mRNA and is enriched over time. In the nucleoplasmic voxels the expected relative Hrp36 intensity is  $\sim 1$ . In voxels with DNA an enrichment of Hrp36 and therefore relative intensities above 1 are expected as can be seen in Fig. 4.3 A.

During heat-shock BR2.1-mRNA stays localized at the BR2-puff also for extended time periods. After 120 min of heat-shock the characteristic BR2.1-mRNA staining of the BR2-puff was still clearly visible (Fig. 4.4). In the nucleoplasm no significant level of BR2.1-mRNA could be detected, while the cytoplasm still showed a strong staining. This suggests that the BR2.1-mRNA export is continued under heat-shock conditions while the transcription is blocked. Due to the high abundance of BR2.1-mRNA in the cytoplasm translation of BR2.1-mRNA is still possible.

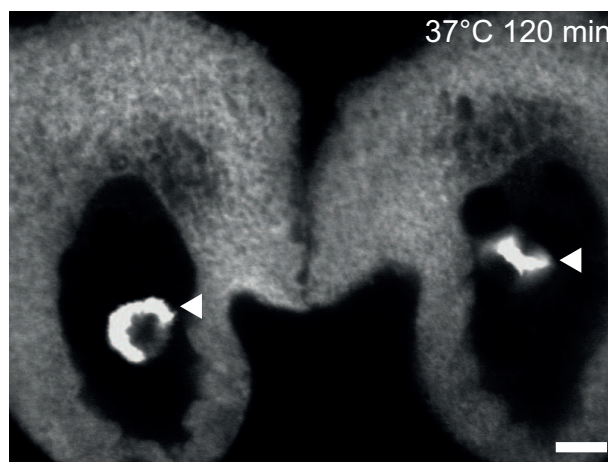


**Figure 4.4:** *Transcription block of the BR2.1 gene is sustained for extended time periods under heat-shock. After 120 min of heat-shock BR2.1-mRNA is still strongly enriched at the BR2 puff while the nucleoplasm contains no BR2.1-mRNA. Scale-bar = 10  $\mu$ m.*

## 4.2 RNA Polymerase II Localization and Transcriptional Status

RNAPII immunostainings show the well known ribbon like pattern of polytene chromosomes. During heat-shock RNAPII is still strongly enriched at the BR2-puff (Fig. 4.5 A). During

heat-shock puffing of well known heat-shock regions like IV-5C was detected (Fig. fig:HS60-RNAPII A wedge). No noticeable differences in RNAPII concentration or pattern at the BR2-puff between heat-shocked and control salivary glands were detected (N=12).

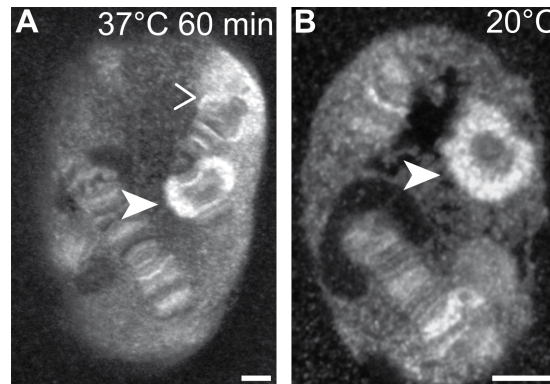


**Figure 4.5:** *RNAPII localization in heat-shocked salivary glands.* Immunostaining of RNAPII in (A) heat-shocked and (B) control salivary glands. The well known heat-shock induced puffing of the chromosomal area IV-5C can be seen in (A) (wedge). The BR2-puffs are labeled by arrowheads. Scale-bar = 10  $\mu$ m.

#### 4.2.1 RNA Polymerase II Footprinting

The localization of RNAPII and BR2-mRNA at the BR2-puff suggests that elongation stops and the transcription complexes stay associated to the DNA. To test if RNAPII still forms transcription bubbles, which are a characteristic feature of elongating RNAPs a potassium permanganate footprinting was performed ( 2.11 p. 42). To yield a high signal from a low number of salivary glands a primer complementary to the repetitive motif of Exon 4 of the *BR2.1* was used for first strand synthesis.

Potassium permanganate footprinting utilizes the different potassium permanganate reactivity of thymidines located in single(ss) and double(ds) stranded DNA. Careful positive and negative controls are needed to ensure the usability of this assay. The incubation time and concentration has to be as long and high to ensure that potassium permanganate reacts sufficiently with thymidines of ssDNA. But it has to be as short that no thymidines in dsDNA are oxidized. Usually extracted, protease digested, naked DNA is used as control to ensure that thymidines of dsDNA are not oxidized. Since *BR2.1* encodes for a saliva protein its expression is limited to the salivary glands. As negative control a potassium permanganate footprinting of *BR2.1* of midgut tissue DNA was used. To ensure that under the chosen reaction conditions thymidines of ssDNA is oxidized, a gene with known transcriptional activity is used as positive control. Here the *glycinamide ribonucleotide synthetase (gars)* gene was used. It is essential for the *de*

*novo* purine biosynthesis.<sup>[107]</sup>

A reaction time of 30 s with  $20 \frac{\text{mmol}}{\text{l}}$  potassium permanganate proved to be suitable. LMM-PCR analysis of RNAP II footprinting at *gars* yielded PCR products ranging from the smallest possible product (45 bp primer1+primer2) up to  $\geq 300$  bp. No PCR products were detectable for the potassium footprinting at the BR2.1-gene of midgut tissue DNA (Fig. 4.6). The used separation length of 20 cm does not allow to distinguish single bands which would be required for a detailed analysis.

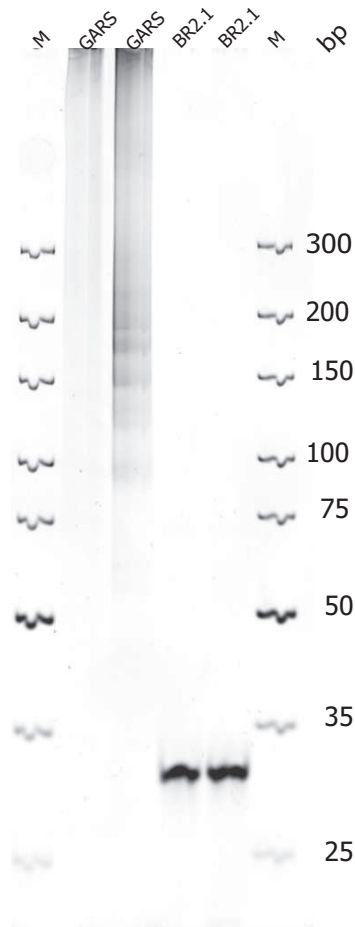


**Figure 4.6:** *Potassium permanganate footprinting of midgut tissue.* PAGE of PCR-fragments yielded by potassium permanganate footprinting of midgut tissue. Each lane shows an independent potassium permanganate footprinting assays. The bands in the BR2.1 lanes correspond to the used genomic primer.

*BR2.1* potassium permanganate footprinting of salivary glands from heat-shocked and control larvae show the same LMM-PCR-product length distribution (Figure 4.7). The different intensities are caused by different sample amounts loaded to the gel. Heat-shocked and control samples show a continuous gradient with some faintly bands present in heat-shocked and

control samples (Figure 4.7).

The maximal separation length of 20 cm was too short to resolve the PCR-products sufficiently. The size ruler shows the dimensions of a band with single base pair width. It clearly shows that a length difference of several base pairs would be needed to resolve single DNA fragments using these separation conditions. Next to the short separation length the maximum voltage was limited to 250 V by the available power supply. Usually voltages of up to 3 kV are used for high resolution nucleotide PAGE. Due to the low voltage the run-time had to be increased to 6 h to 10 h instead of ~1 h at 3 kV. The longer run-time causes additionally a broadening of the bands. To increase the resolution the samples were analyzed by capillary gel electrophoresis (see 2.12 p.45). The peak pattern of heat shocked and control salivary glands measured by capillary gel electrophoresis were equal, too. Just the intensity of some peaks differs slightly. It can be concluded that the heat-shock induced transcription block did not cause a change of RNAPII distribution along Exon 4. Since no transcriptional activity was detected during prolonged heat-shock is blocked RNAPII independent of its position in the BR2.1 gene.

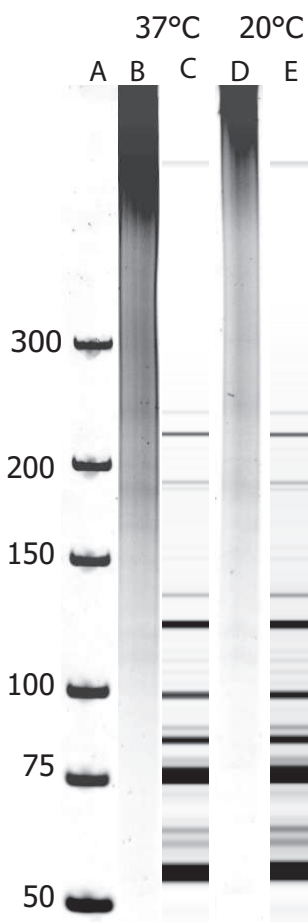


**Figure 4.7: Potassium permanganate footprinting of heat-shocked salivary glands.** Fragments of BR2.1 Exon4 of heat-shocked salivary glands could successfully amplified by LM-PCR after potassium permanganate footprinting(B&C). This shows the presence of transcription bubbles at BR2.1 during heat-shock. A PAGE with 20 cm separation length did not allow the detection of single bands (B&D). Therefore, the LM-PCR products were analyzed by capillary gel electrophoresis. The “Virtual gel view” of the capillary gel electrophoresis shows that peak positions and intensity were remarkably similar between heat-shocked and control glands (C&E). This shows that the RNAPII distribution at BR2.1 not significantly changed upon heat-shock.

### 4.3 RNA Polymerase II CTD Phosphorylation

The phosphorylation of the repetitive heptapeptide sequence  $Y_1S_2P_3T_4S_5P_6S_7$  of the RNAPII-CTD is a key element of transcription regulation. During progression of transcription the CTD phosphorylation pattern changes. Before transcription initiation the CTD is unphosphorylated. At initiation serine-5 becomes phosphorylated. During elongation serine-2 phosphorylation increases while serine-5 phosphorylation decreases until termination. At termination only serine-2 is phosphorylated (see 1.1.1 p. 3).

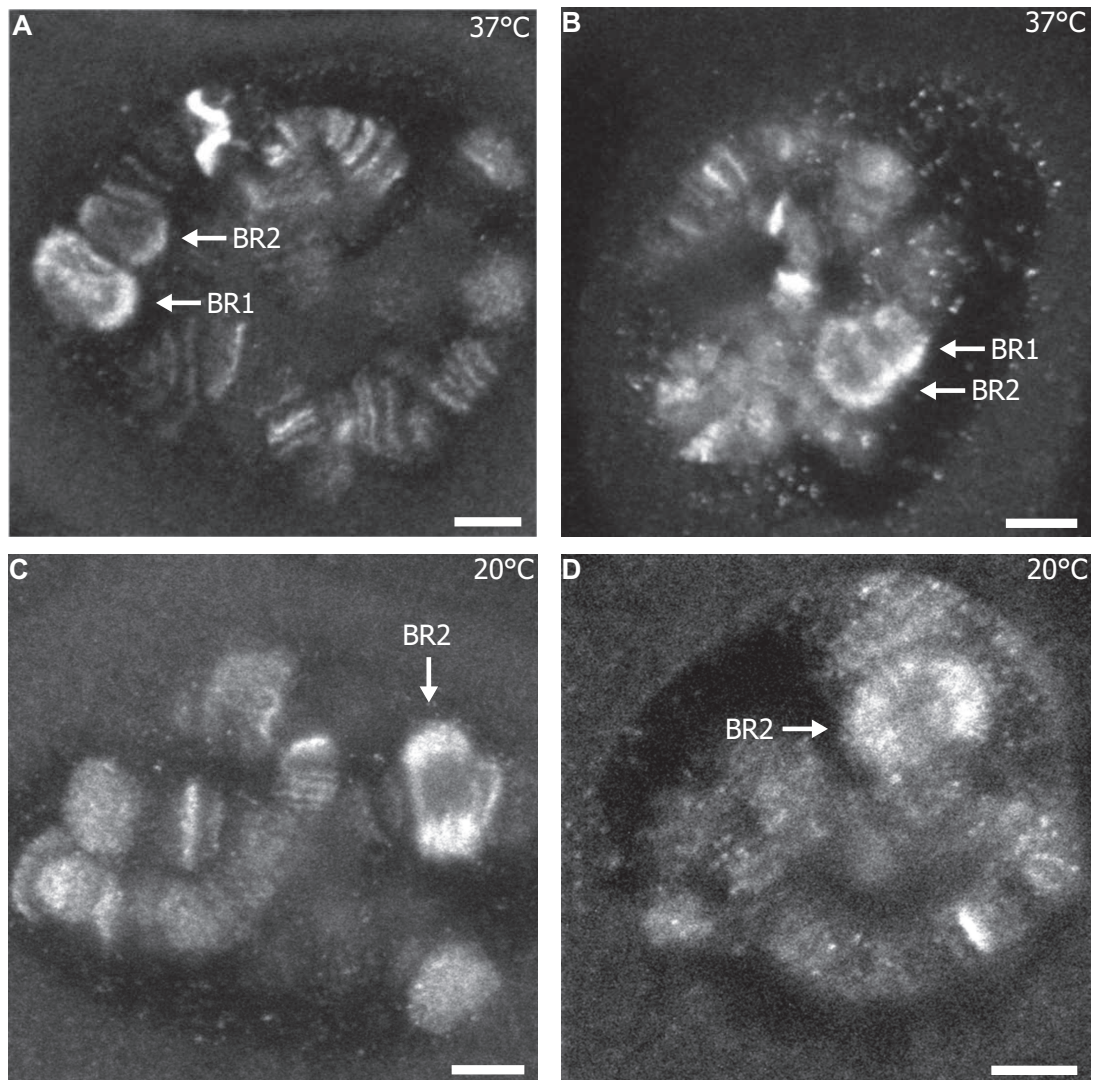


**Figure 4.8:** *Phosphorylation status of RNAPII after heat-shock. (A) Immunostaining of RNAP II phospho S5 CTD of a heat-shocked (1 h) salivary gland. (B) Immunostaining of RNAP II phospho-S2 CTD of heat-shocked (1 h) larvae. (C) Immunostaining of RNAP II phospho S5 CTD of control salivary gland. (D) Immunostaining of RNAP II phospho-S2 CTD of control salivary gland. Scale-bar = 10  $\mu$ m.*



To test the phosphorylation status of RNAPII at the BR2-puff during heat-shock salivary glands were immunostained with CTD-S2P and CTD-S5P sensitive antibodies. The immunostaining does not allow a quantification or the detection of slight changes of the CTD-phosphorylation pattern. By immunostaining no difference in CTD-S5 and CTD-S2 phosphorylation is detectable, but the strong signal of the S2P sensitive antibody indicated that the block of RNAPII activity is not caused by a loss of S2 phosphorylation, which is characteristic for stable elongation (Fig. 4.8 B).

## 4.4 Recovery of BR2 Transcriptional Activity After Heat-Shock Release

An obvious and important question is, whether the blocked RNAPII do regain transcriptional activity after the heat-shock is released. Another possibility would be the proteasomal degradation of blocked transcription complexes after heat-shock release.

Two transcription inhibitors, Flavopiridol and ActinomycinD, were used to answer this question. Flavopiridol is a very potent inhibitor of the transition from initial to stable elongation. RNAPII which already entered productive elongation is not affected by Flavopiridol. ActinomycinD inhibits overall transcription activity by its intercalation in GC-rich DNA sequences.

Salivary glands dissected from heat-shocked animals were incubated for 1 h at 20 °C in hemolymph containing 300  $\frac{\text{nmol}}{\text{l}}$  Flavopiridol. Labeling of the BR2 mRNPs by the BR2.1-specific 2'-O-Methyl-RNA oligonucleotides and imaging of the salivary gland cells revealed that the initial BR2.1-mRNA enrichment at the BR2.1 transcription site (Fig. 4.9 A) vanished after 1 h of Flavopiridol incubation at 20 °C (Fig. 4.9 B).

Next salivary glands were incubated after heat-shock in hemolymph containing 300  $\frac{\text{nmol}}{\text{l}}$  Flavopiridol but in addition also 5  $\frac{\mu\text{g}}{\mu\text{l}}$  ActinomycinD. Compared to the initial BR2.1-mRNA staining no reduction of BR2.1-mRNA at the BR2-puff was observable (Fig. 4.9 C&D). This shows that transcriptional activity is essential for the vanishing of the BR2.1-mRNA observed by only using Flavopiridol. Therefore, it can be concluded that blocked RNAPII remains functional during heat-shock and resumed transcriptional activity after heat-shock release.

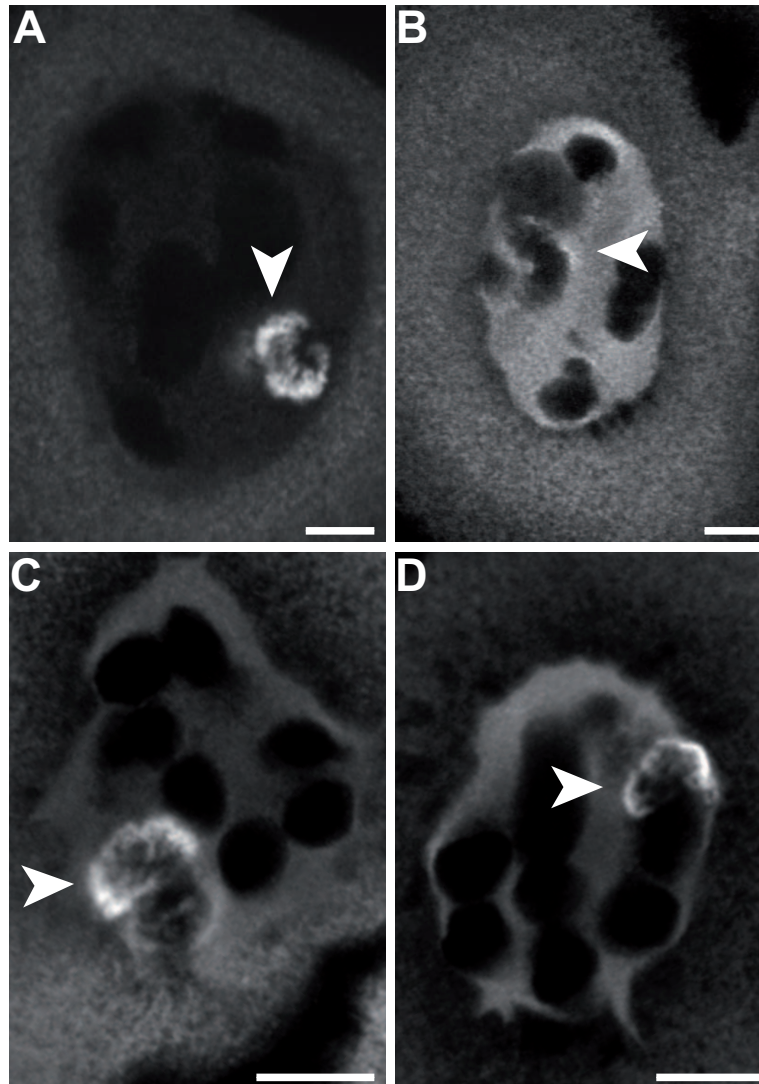


**Figure 4.9:** *Transcriptional activity recovery after heat-shock release.* Confocal sections of salivary gland cell nuclei after labeling by BR2.1-specific oligonucleotides. (A) Directly after heat-shock BR2.1 mRNA was accumulated at the BR2-puff as shown by mRNA-FISH (see arrow head, refer also to 4.2 p. 78). (B) The heat-shocked sister gland was returned to 20 °C, and incubated in hemolymph containing 300 nM Flavopiridol, which inhibited the start of new transcription processes. After 60 min BR2.1 mRNA was not present anymore at the transcription site. Obviously, blocked transcription processes were resumed, completed and the site was emptied. (C) Nucleus of a gland, which was fixed directly after heat-shock showed the presence of BR2.1 mRNA, as did (d) a nucleus of the sister gland, which was incubated after the heat-shock for 60 min at 20 °C in hemolymph containing 300 nM Flavopiridol and 5 μg ml ActinomycinD. The latter inhibited any progress of transcription, and the transcripts remained at the BR. Arrow heads indicate the position of the BR2.1. Scale-bar 10 μm.

# 5 Discussion I: Imaging Export of Single Native mRNP-Particles

Advancement in microscopy allows us to trace the movement of single molecules in cells. Cellular processes, which are shown as static sketch in lectures, with arrows between the different stages to indicate movement and dynamics, become vivid here. Single molecule microscopy allows us to watch molecular biology on a microscopic scale while it happens. Since the human brain is trained in the perception of motion, the static presentation of video sequences never give the same impression as motion pictures. The results of this thesis are partially published<sup>[113]</sup>, thus, a video of an export event is available at:

<http://www.pnas.org/content/suppl/2012/05/21/1201781109.DCSupplemental/SM01.avi>

Exempli gratia single molecule microscopy allows to measure the dwell time distribution of mRNP-particles at the nuclear envelope (NE) instead of measuring its average value as ensemble methods do. The dwell time distribution analysis provides additional insight into the molecular process compared to ensemble methods. One difficulty in single molecule fluorescence microscopy is the limited number of photons which can be collected of the molecule of interest. Since the decisive criterion is the signal-to-noise-ratio, and the number of photons is limited, great attention is paid to noise reduction. Here, a light sheet to confine fluorescence excitation, was able to reduce the background significantly.<sup>[104,105]</sup> To image mRNP-particles in *C. tentans* salivary glands the light sheet microscope built by *J. Ritter* was further optimized.

## 5.1 Imaging the mRNA-Export

To image the mRNP-particles and NE independently, they were labeled with probes linked to different fluorophores. The light sheet microscope that was used is equipped with chromatic cylindrical lenses to form the light sheet. Thereby, a severe chromatic illumination error was

introduced. For optimal sectioning an overlap of the illumination focus and the camera FOV is crucial. The drastic initial chromatic focus shift made optimal sectioning with multiple illumination wavelengths simultaneously in the camera FOV impossible.

In addition, the use of an air immersion illumination objective caused a shift of the light sheet focus if the distance between the illumination objective and the sample chamber was changed. Therefore, a realignment of the light sheet was required every time a new nucleus was imaged. For this alignment the strong signal of the stained NE was used. But optimal sectioning was especially needed to image the single mRNP-particles. A smaller chromatic error of the light sheet made it easier to align the camera FOV with focus of the illumination wavelength used to image single mRNP-particles. Additionally, the localization precision of the NE is improved if the chromatic illumination focus shift is low, when the light sheet position was optimized to image mRNP-particles.

The chromatic shift was reduced from  $\Delta X_{0_{532},640} = 69 \mu\text{m}$  to  $\Delta X_{0_{532},640} = 7 \mu\text{m}$  (Fig. 3.1 p.52) by readjusting the cylindrical lenses positions. The reduced chromatic shift was significantly below the Rayleigh length of the illumination objective, which is  $z_{r_{640}} = 17 \mu\text{m}$  and  $z_{r_{532}} = 41 \mu\text{m}$ .

A co-localization error of less than one pixel was achieved under experimental conditions as shown by double-staining experiments ( $75 \text{ nm} \pm 35 \text{ nm}$  (Fig. 3.2 p.53)). The kymograph were constructed by using the average intensity of the pixels  $\pm 1$  pixel corresponding to the NE position (see 2.17 p. 47). For this pixel extraction the achieved colocalization error was not limiting.

## 5.2 Incubation Media

For decades explanted salivary glands of *C. tentans* are used as model system. Therefore, numerous artificial incubation media for explanted salivary glands are described.<sup>[13,32,140]</sup> Several of these artificial media were tested here. To monitor the viability of the explanted salivary glands the BR2.1-mRNA distribution was monitored. None of the tested artificial media performed satisfactorily (tab 3.1 p. 55).

In the larval body, the salivary glands are embedded in hemolymph. Therefore, it is obvious that hemolymph is the optimal incubation medium. Distribution of BR2.1-mRNA after hemolymph incubation was unchanged. Moreover, hemolymph incubation was able to rescue the BR2.1-mRNA distribution after incubation in artificial media. A severe drawback of this method was the tedious preparation of hemolymph. It had to be manually extracted from single larva. On average, it was possible to extract  $\sim 5 \mu\text{L}$  of hemolymph from a single larvae.

The volume of hemolymph needed to fill the sample chamber is 160  $\mu\text{L}$ . It was possible to reduce this amount significantly to 20  $\mu\text{l}$  by using PTFE-spacers and mineral oil for sealing. Hemolymph was prepared in advance and kept at  $-80\text{ }^{\circ}\text{C}$  for long-term storage. As a result of these improvements, the availability of hemolymph was no limitation to the maximal number of glands imaged per day.

### 5.3 mRNA Labeling

A multitude of mRNA labeling methods has been described.<sup>[129]</sup> For single molecule microscopy, a photostable and bright label is needed. To label native mRNP-particles recombinant tc-Hrp36 was expressed in bacteria and subsequently labeled with AlexaFluor647. AF647-tc-Hrp36 was micro-injected into the cytoplasm of explanted *C. tentans* salivary glands cells.<sup>[54]</sup>

Hrp36 is the *C. tentans* homologue of hnRNPA1, which is one of the most abundant nuclear proteins.<sup>[115]</sup> It is incorporated cotranscriptionally into nascent mRNP-particles. It is involved in mRNA packaging and therefore also termed „RNA histone“.<sup>[52]</sup> The only modification introduced for fluorescence labeling is the amino acid chain of the tc-tag (Cys-Cys-Pro-Gly-Cys-Cys) and up to four AlexaFluor647 maleimide dye molecules attached to it. The photo physical properties of synthetic dyes are far superior to those of fluorescent proteins. By using an accurately adjusted light sheet microscope, it was possible to image single mRNP-particles with a localization precision of 10 nm. This localization precision is even more remarkable when taking into account, that the single molecule imaging was performed  $\sim 70\text{ }\mu\text{m}$  to  $120\text{ }\mu\text{m}$  deep in the sample. The negligible modification introduced to mRNP-particles and use of synthetic dyes are the advantages of this labeling approach. A severe drawback is the non-selective labeling of the complete mRNA pool. Due to the *in vitro* expression and labeling of Hrp36, it has to be delivered by an artificial method to the target cell. Here, microinjection was used. Since a single nucleus was imaged for  $\sim 20$  min and the microinjection of a whole salivary gland took less than 5 min, microinjection was not limiting the throughput. Whether microinjection affects the mRNA-export was not explicitly tested. Microinjection is a well established method which is successfully used for generating transgenic animals or *in vivo* fertilization, so that a severe affection of mRNA-export seems unlikely. Furthermore, it was used by *Guerousov et al.* in an ensemble approach, which revealed no dysfunction of mRNA-export using microinjection.<sup>[44]</sup> To avoid mechanical lesion of the target cell alternatively protein transfection methods could be used for Hrp36 delivery.

The well known MS2-MCP-system allows specific mRNA labeling.<sup>[5]</sup> It uses a fusion-protein as mRNA-probe consisting of an NLS, a fluorescent protein (e.g. YFP) and the coat

protein of the bacteriophage MS2 (MCP), which binds to an artificially introduced RNA-motif (MS2 stem loop). In addition to the specific mRNA-labeling, the targeted mRNA and the label can be genetically encoded in a single cell. The benefit of specific mRNA-targeting comes with the drawback that the resulting mRNP-particle is severely modified.

This approach was previously used to image the mRNA-export.<sup>[40,79,91]</sup> To overcome the unspecific background of unbound mRNA-probes, a high number of fluorescent proteins had to be bound to the target mRNA. Therefore, 24 MS2 stem loops were cloned into the 3'-UTR of the gene of interest.<sup>[40,79]</sup> The 24 MS2 binding motifs allow depositing of up to 48 NLS-MCP-YFP on a single mRNA. This high number of NLS-MCP-YFP fusion-proteins outmatch the mass and volume of most mRNP-particles.<sup>[40]</sup> In addition to the severe steric alteration, this approach severely disturbs the signal peptide composition of the mRNP-particle, by adding a high number of NLS-motifs to the mRNP-particle artificially. It seems probable that after the labeled mRNP-particle reached the cytoplasmic side of the NPC, the NLS signal peptides are immediately bound by Importin  $\alpha$ . Importin  $\alpha$  recruits Importin  $\beta$ , which would give the mRNP-particle an artificial affinity to the FG-repeats.

This raises the question if this modification could alter the mRNA-export kinetics. In the first study investigating mRNA-export, *Grünwald et al.* used immortalized embryonic mouse fibroblasts (MEF) from homozygous mice, which had a cassette of 24 MS2 binding motifs in their  $\beta$ -actin 3'UTR ( $\beta$ -actin-24MBS). Since they detected no difference in growth rate between cell lines with and without MS2-NLS-YFP expression, the authors concluded that mRNA labeling with a high number of NLS-MCP-YFP does not affect the mRNA-export kinetics. Messenger RNA export requires less than a second, whereas the complete protein biosynthesis from transcription to translation takes minutes. Therefore, mRNA export is not rate limiting to protein biosynthesis. Thus, it seems unlikely that an altered mRNA-export kinetics would cause a reduced growth rate. Furthermore, a slower export kinetics can be compensated by a higher expression rate. Taken together the proof that this labeling method is not altering the mRNA-export kinetics is still missing.

Several studies showed that artificial cargoes are efficiently transported across the NPC if fused to NLS-motifs. The  $\beta$ -actin-24MBS mRNP-particle labeled with NLS-MCP-YFP has a diameter of 24 nm.<sup>[40]</sup> *Lu et al.* reported that cargoes of comparable size (18 nm x 14 nm x 9 nm) can be imported efficiently into the nucleus by a single bound transport factor.<sup>[127]</sup> Even more bulky and artificial cargoes as quantum dots decorated with ~40 Importin  $\beta$  - resulting in a complex with a total diameter of 30 nm - are transported across the NPC.<sup>[77]</sup> Therefore, it is likely that mRNP-particles labeled with the MS2-MCP-system do not resemble the native export kinetics.

Another well described method for mRNA-labeling is the use of oligonucleotide hybridization probes. Different hybridization approaches, from short fluorescently labeled complementary oligonucleotides to more advanced probes as e.g. molecular beacons are described.<sup>[129]</sup> All hybridization procedures come with the disadvantage that they cover a certain region of the target mRNA. To study the export of mRNA in *C. tentans*, different oligonucleotides were tested. Using these, it was not possible to detect export events. The tested oligonucleotides were labeled with a single dye molecule and targeted to the especially large BR2.1-mRNAs. In the light of the assumed slow BR2.1 export kinetics, these experiments could also be limited by the bleaching kinetics of the dye.

## 5.4 Export and Probing Kinetics of mRNP-Particles

Three different studies describing mRNA-export at single molecule level were published, to date.<sup>[40,79,113]</sup> This thesis and *Siebrasse et al.* is seen as a single study, here, since they use the same set of data regarding mRNP-particle probing and export events. Only the analysis differs. The studies by *Grünwald et al.* and *Ma et al.* used different labeling strategies and mammal cell lines. In this study the salivary gland cells of the diptera *C. tentans*, which exhibit a special nuclear organization (see 1.6 p. 25), were used as model system.

In total, 7,180 movies from 70 different glands with a total record time of ~40 h were analyzed. The following NE-interaction events were extracted of this video data: 121 export, 313 nucleoplasmic probing and 184 cytoplasmic probing events were extracted. The number of observed export events is comparable to that of *Grünwald et al.* and *Ma et al.* This shows that the observation of mRNA-export is tedious independently of the experimental approach.

### 5.4.1 Dwell Time Analysis

Here, the mRNP-particle export and probing kinetics were described using a mono- or multi-modal gamma distribution. The gamma-distribution allows to extract the number of rate limiting steps which is encoded in the shape of the empirical distribution. The dwell time analysis, here, is based on the assumption that every single rate limiting step is a Poisson process with the same rate constant. Reaction steps, which are much faster than the slowest one, are blurred and covered by the stochastic fluctuation of the slowest reaction step. By fitting the gamma distribution to the interaction kinetics, a rough estimation of the number of rate limiting steps can be obtained.<sup>[33]</sup> The estimation of the number of rate limiting steps becomes worse with increasing numbers of rate limiting steps and decreasing number of observations (see table 7.3

p. 121). Therefore, the number of rate limiting steps obtained by data analysis here should be seen as a rough indicator for the presence of a single or multiple rate limiting reaction steps.

*Grünwald et al.* also took into account that mRNA-export possibly shows a higher complexity.<sup>[40]</sup> They fitted the experimental data with a convolution of two exponential decays with independent time constants. In contrast to the analysis applied in this thesis, this approach takes into account that the time constants of the different rate limiting steps must not necessarily be equal. A strong coupling between the convoluted time constants is expected. Therefore, such a model was not used here.

In this thesis the first step of the dwell time analysis was a model selection based on an objective criteria. In a second step the goodness-of-fit and the confidence of the fit parameters were determined.

In contrast to all previous publications analyzing the export kinetics of mRNP-particles, a model selection procedure based on the objective, well known and easy to use  $AIC_c$  was introduced. The usage of an information criterium eliminates a possible bias introduced by the investigator and allows automation of model selection.

For the analysis of single molecule data, the mathematical model used to describe the data is decisive for its interpretation. That makes it all the more surprising that single molecule studies often provide no goodness-of-fit tests. A frequent problem is that for the selected model the expected sampling frequency of a test-statistic is not known. The expected test-statistic sampling frequency is crucial for a goodness-of-fit test. Parametric bootstrapping allows to estimate the test-statistic sampling frequency as long as the null hypothesis can be numerically described. The hypothesis testing applied here gives a good estimation whether the applied model should be rejected or not. That provides a clear advantage to all previous studies on nuclear mRNA export, since it gives an objective criteria whether the applied model fits the data sufficiently.<sup>[40,79,113]</sup>

The analytical description of the fit parameters confidence intervals, usually relies on the assumption that data follow a known distribution. Unfortunately, this often does not hold true since the measuring procedure itself introduces artifacts or bias. In contrast to classical error estimation, non-parametric bootstrap allows to estimate the confidence intervals of the fit parameters. Instead of giving just a single confidence interval, it allows to estimate the distribution of the confidence interval without making any *a priori* assumptions.

In general, the model selection and the bootstrapping procedures are not limited to a specific distribution. Bootstrapping procedures were implemented as short Matlab scripts. The calculation of the non-parametric bootstrap with 10,000 cycles took ~one hour for a single set of data. The parametric bootstrapping with 50,000 cycles took less than one minute. All calculations



were done on a Intel Core i7 3 GHz CPU using a single core. Therefore, computing power is not limiting.

### 5.4.2 mRNP-Particle Export And Probing Kinetics

The mRNA NE interaction events analyzed in this thesis are the same as previously published by *Siebrasse et al.*<sup>[113]</sup> Due to the advanced analysis here, the obtained time constants differ. Another difference is that for an event to be considered, a fixed threshold of at least three frames was used for all events in this thesis. In *Siebrasse et al.*, this threshold were varied for the different NE-interaction types (export, nuclear- or cytoplasmic probing). The classification of the mRNP-NE-interaction events were done subsequently to its detection and extraction. Therefore, the chance that an event is missed during manual inspection is not affected by the type of interaction. Therefore, the minimal number of frames for an event to be considered was not varied here.

In total, 121 mRNA export events were observed. Here, the complete mRNA-pool was labeled and therefore it is very likely that each export event corresponds to an mRNA of different size. The export kinetics of mRNP-particles are presumably affected by its size, as will be discussed later. Therefore, the low number of observed mRNP-particle exports has to be seen critically. Measuring the export kinetics of the complete mRNA-pool introduces an additional variability.

The durations of the export events were in a range of 20 ms to 5640 ms. For the salivary glands, an abundance of extremely large mRNAs is known. Presumably, the large spread of export time correspond to the large size range of the mRNA-pool.<sup>[28]</sup> *Grünwald et al.* and *Ma et al.* examined the export of mRNA with a length of ~3.3 kb.<sup>[40,79]</sup> Although they reported contradicting export times for mRNAs of the same length (see table 5.1) using the same cell line, they did not observe export events in the range of seconds. This corroborates the assumption of a dependency between mRNA-length and export kinetics.

**mRNP-Particle Export Kinetics** 109 export events from 121 were detected for at least three frames at the NE. The ratio of observed export and nuclear probing events yields a success rate of 28%. This calculation does not take into account that the fraction of events shorter than three frames might not be the same for nucleoplasmic probing and mRNA-export. The success rate is only slightly changed to 26% by extrapolating the respective total number of events based on the dwell time distribution fits. This is in accordance with the success rates described by other studies (see table 5.1).

cell type	mRNA	size[kb]	label	dwelt time[ms]	success rate [%]	cycle time[ms]
MEF <sup>[79]</sup>	$\beta$ -actin	3.3	NLS-YFP-MCP	21	32	20
MEF <sup>[79]</sup>	$\beta$ -actin	3.3	NLS-YFP-MCP	12	36	2
HeLa <sup>[79]</sup>	Firefly luciferase	3.3	NLS-mCherry-MCP	16	31	20
HeLa <sup>[79]</sup>	Firefly luciferase	3.3	NLS-mCherry-MCP	11	31	2
MEF <sup>[40]</sup>	$\beta$ -actin	3.3	NLS-YFP-MCP	180	15	20
<i>C. t. s.g.</i>	un.	un.	AF647-tc-Hrp36	$t_{exp1}=76$ $t_{exp2}=158$	26	20

**Table 5.1:** Comparison of the export kinetics of all single molecule studies including this. *C. t. s.g.* = *C. tentans* salivary gland and un. = unknown.

The lowest  $AIC_c$  value was achieved by fitting the cumulative mRNA-export kinetics with a bimodal cumulative gamma distributions (Fig. 3.7 p.62). The best fit suggests a fast export process consisting of multiple rate limiting steps ( $S_{exp1} = 21$ ,  $\sigma_{S_{exp1}} = 144$ ) with a time constant of  $\tau_{exp1} = 3.6$  ms and a total average export time of  $t_{exp1} = 76$  ms. The slower export process was dominated by a single rate limiting step ( $S_{exp2} = 1$ ,  $\sigma_{S_{exp2}} = 0.4$ ) and a time constant of  $\tau_{exp2} = 158$  ms.

Several extremely long lasting export events with durations of up to several seconds were observed. These export events are not sufficiently describable with the fitted bimodal gamma distribution (Fig. 3.8). The  $AIC_c$  for a trimodal gamma distribution was worse than for a bimodal model. To model this extremely long lasting export events a higher number of observations is needed. Compared to the bimodal exponential decay applied in *Siebrasse et al.*, the applied bimodal gamma distribution here describes the data more accurately. The p-value of the euclidean test-statistic was increased from 0.34 (bimodal exponential fit) to 0.83 (bimodal gamma distribution).

The number of rate limiting steps estimated for the faster export process shows a high uncertainty. To reduce the uncertainty for a process with 21 rate limiting steps to  $\sigma_S = 1$ , nearly seven million export events have to be observed. This is clearly not realizable with the experimental design used in thesis. Nearly 1000 days of observation time would be needed to provide such a high number of export events. In contrast, only 11 export events are needed to determine the number of rate limiting steps for a process with  $S = 1$  with an uncertainty of  $\sigma_{(S=1)}=1$ . This shows that the faster mRNA-export is governed by more than one rate limiting steps. However, to determine the number of rate limiting steps more precisely the number of observations has to be increased tremendously.

The uncertainty of the estimated slower export time constant suggests that its value should be seen with care and rather as a trend indicator than as an absolute number. The kinetics of the

slower export events show only a single rate limiting step. Assuming that all export processes have the same “reaction scheme”, this indicates that a single step of the mRNA-export process is significantly prolonged for slower export events. To analyze the biologic meaning of the number of rate limiting steps the trajectory data will be discussed first.

The experimentally achieved co-localization precision did not allow to directly overlay the positions of the export trajectory with the NPC structure. For the overlay, the best superposition of the export trajectories and the NPC shape were found by iterative testing. The nuclear basket area offers the largest area and especially the largest extension along the NE plane. Therefore, it seems very probable that the best superposition for the center of gravity of the trajectories is located in the nuclear basket. But the superposition of the trajectories also resembles accurately the dimensions of the NPC shape along the nucleo-cytoplasmic axis (Fig. 3.18 p. 70). Therefore, this result does not seem to be an artifact created by the large area of the nuclear basket.

As shown by the trajectory overlay of export events  $\geq 300$  ms with the shape of the *C. tentans* NPC structure, mRNP-particles are ‘waiting at the gate’ before they enter the central channel of the NPC. Therefore, the slow rate limiting step seems to be localized at the nucleoplasmic side of the NPC. *Daneholt et al.* were able to show by EM that large BR-particles change their geometry dramatically during passage through the central channel of the NPC.<sup>[26,84]</sup> The reshaping takes place at the nuclear basket. Therefore, the single rate limiting step of the slower mRNA-export process could represent the reshaping of large mRNPs or mRNP-quality control processes, which also take place at the nuclear basket.

*C. tentans* is well known for its especially large mRNP-particles mainly the BR mRNP-particles. The BR-mRNAs have a length ranging from 26000 to 40000 nucleotides. But mRNAs of this size are not a unique feature of *C. tentans*. For example the human genome harbors 19 genes whose transcripts are  $\geq 26000$  nucleotides. Therefore, the reshaping of mRNPs before translocation through the NPC should be a common phenomenon.

The highest localization precision in a study subjected to mRNA-export was achieved by *Ma et al.* Their co-localization precision enabled a direct 2D-overlay of the export trajectories and the NPC structure with subsequent 3D deconvolution. They observed a peak of the mRNA distribution at the cytoplasmic side of the NPC.<sup>[79]</sup> *Grünwald et al.* described for the same mRNA in the same cell line an enrichment at the nucleo- and the cytoplasmic side of the NPC. Due to the far superior precision, only the data of *Ma et al.* will be discussed.

Here, the superposition of the trajectories of successful nuclear exports was calculated only for exports events longer than 300 ms. These events presumably correspond to large BR-mRNP-particles. The mRNA examined by *Ma et al.* was at least ten times smaller than

BR-mRNAs. It is known for BR-mRNA that a rearrangement of the mRNP-particle starts at the nuclear basket. No such observation was made for mRNP-particles of smaller mRNAs. Therefore, the results are not contradicting each other.

Another reason for the cytoplasmic enrichment of exported mRNA reported by *Ma et al.* at NPC cytoplasmic face could be the mRNA labeling technique that was used. They used the MS2 system to label mRNP-particles. This introduces artificial NLS sequences to the mRNP-particle. After reaching the cytoplasmic side of the NPC, these NLS recruit importins to the NPC, which give the labeled mRNP-particle an affinity to the FG-repeats and potentially hinder the release of the mRNP-particle from the NPC.

Taking together, the single rate limiting steps of the slower mRNA-export process could represent the reshaping of large mRNP-particles or mRNP-particle quality control processes which also take place at the nuclear basket. The multiple rate limiting steps could correspond to the mRNP-particle quality control step, which is located at the nuclear basket, too, a possible reshaping before entering the NPC and the dissociation from the NPC. The nucleoplasmic probing kinetics are in the same order of magnitude as the mRNA-export kinetics. Taken this and the low success rate into account, the translocation of mRNP-particles through the NPC seems not to be rate limiting to mRNA-export.

Overall, mRNA-export seems not to be rate limiting to protein-biosynthesis as reported by *Hoyle and Ish-Horowicz*.<sup>[49]</sup> An average human gene has 10 kbp to 15 kbp and encodes 500 to 600 amino acids.<sup>[118]</sup> Its transcription requires at least 140 s and its translation 100 s. Therefore, the time range of milliseconds to a few seconds, which mRNA-export requires, is rather neglectable.

**mRNP-Particle Nucleoplasmic Probing Kinetics** The majority of nuclear mRNP-particles returned into the nucleoplasm after NE interaction (74%). These so-called nuclear probing events ( $N_{nprobing} = 313$ ) had two time constants  $t_{nprobing1} = 67$  ms (93%) and  $t_{nprobing2} = 320$  ms (7%). The estimated number of rate limiting steps are  $S_{1nprobing} = 3$  and  $S_{2nprobing} = 1$ . The different kinetics of the nuclear probing might represent different types of interactions between mRNP-particles and the NE and/or the NPC. Presumably, the short interactions are collisions without specific NPC interaction. The slower probing kinetics could correspond to mRNPs which fail to take a suitable position or conformation to be successfully exported or are retained from export.

It is known that not fully processed mRNAs are retained in the nucleus. Essential for this retardation is MLP1, which is localized at the filaments of the nuclear basket.<sup>[36]</sup> Based on current knowledge, it is not possible to correlate the measured nuclear probing kinetics with

the retardation of not fully processed mRNAs.  $t_{nprobing1}$  is close to the event length threshold of 50 ms. Due to the rapid nuclear probing kinetics many events were presumably missed. Therefore, imaging the nuclear probing with higher frame-rates would be desirable to gain accuracy.

The high uncertainty of the slower nuclear probing kinetics results from the low number of observations and the inherently noisy nature of stochastic processes.

**mRNP-Particle Cytoplasmic Probing Kinetics** Messenger-RNP-particles showed probing, too. The cytoplasmic probing kinetics could be described by a single rate limiting step reaction with a time constant of 79 ms. Noteworthy the cytoplasmic probing time constant is higher than the fast nucleoplasmic probing and as the fast average time constant. Since the lack of any hints of the type of this interaction, the cytoplasmic probing can not be linked to any cellular process.

## 5.5 Dbp5 Turnover Kinetics at the NPC

Imaging the Dbp5 NE interaction with a framerate of 50 Hz suggests a mean time constant  $\tau_{Dbp5_{50Hz}} = 52$  ms.

Since the time constant is close to the lower threshold for events to be included in the analysis, the experiments were repeated with a framerate of 200 Hz. To calculate the CDF only events lasting three or more frames were used, but due to the higher framerate this threshold equals 15 ms. Surprisingly this high temporal resolution data revealed that the dwell time kinetics of Dbp5 consists of two processes. Fitting a bimodal gamma distribution shows that the fast kinetics is governed by two rate-limiting steps and the slower by only a single rate limiting step. The time constants were  $t_{1Dbp5_{200Hz}} = 26$  ms with a ratio of 77% and  $\tau_{2Dbp5_{200Hz}} = 240$  ms with a ratio of 23%. Since it is described that the mRNA interaction is needed for the release of Dbp5 from Gle1 it is unlikely that the fast kinetics correspond to an unspecific binding of Dbp5 to the NPC.<sup>[95]</sup> *Noble et al.* reported that the rate limiting step of the Dbp5 cycle is the Dbp5-Gle1 interaction.<sup>[95]</sup> The other rate limiting step could correspond to the waiting of Dbp5 to bind an mRNA at the cytoplasmic interface. However based on the current knowledge it is not possible to give a clear answer which steps in the Dbp5 cycle are the two rate limiting steps observed here.

The slower Dbp5 interaction kinetics show only a single rate limiting step. The TEM micrographs of *Daneholt et al.* shows that the complete central framework of the NPC is filled by the exported large BR-mRNPs.<sup>[65]</sup> The slower Dbp5 kinetics could be the consequence of Dbp5

waiting for an mRNA as binding partner while the NPC is blocked by a large mRNP-particle which is being prepared for export at the nuclear basket or clogs the central channel during mRNP-particle export.

## 6 Discussion II: Heat-Shock-Induced Transcription Block

In the second part of this thesis a so far unknown transcriptional regulation mechanism could be described. It is shown that the processivity of RNAPII can be reversibly blocked after it has entered stable elongation. This block is triggered by a heat-shock. The to-date known mechanisms, which control transcription are located at or the proximity of the promoter. After entering stable elongation RNAPII was thought to proceed through the remainder of the gene.<sup>[110]</sup>

The suppression of BR-genes transcription during heat-shock is well known.<sup>[72,73,75,109]</sup> Therefore, it was surprising to observe BR2.1-mRNA was still accumulated at the BR2-puff after heat-shock. The BR-gene transcription following a heat-shock was examined by several studies.<sup>[72,73,75,109]</sup> Therefore, the question arises why the BR2.1-mRNA at the BR-puff during heat-shock remained undiscovered. In all previous studies, the incorporation of radioactive labeled nucleotides were used to monitor transcription activity. The absence of transcription activity was seen as an indicator for mRNA absence. In difference to that, here the BR2.1-mRNA was detected directly RNA-FISH. Furthermore, transcription activity and RNA-localization could be observed independently and even simultaneously by combining the *in vivo* transcription surveillance assay and usage of micro-injected fluorescent oligonucleotides.

The localization of BR2.1-mRNA during heat-shock was reproducible in independent experiments (N=19) and also *in vivo* by BR2.1-mRNA labeling with molecular beacons (Fig 4.2 p.78) (Fig. 4.1 p. 77).

No transcription activity at the BR2-puff was detected during heat-shock by the *in vivo* transcription surveillance assay, whereas the BR2.1-mRNA accumulation at the BR2-puff showed no difference to control salivary glands (Fig. 4.2 p.78). This experiment confirms the results of previous studies, which describe the absence of transcriptional activity after heat-shock.<sup>[72,73,75,109]</sup> It confirms the presence of BR2.1-mRNA during heat-shock, too (Fig. 4.1 p. 77).

Immunostaining of RNAPII shows that RNAPII is localized at the BR2-puff during heat-

shock, too (Fig. 4.5 p.81). The transition from early to stable elongation is accompanied by serine 2 phosphorylation of RNAPII-CTD. The phosphorylation status of the CTD was analyzed by immunostaining. The immunostaining showed, that RNAPII covering the complete BR2-puff of heat-shocked salivary glands are phosphorylated at serine 5 and serine 2. Although immunostainings does not allow a detailed analysis of the CTD phosphorylation pattern the positive serine-2 staining suggests that RNAP II entered the productive elongation at the BR2 site before transcriptional arrest. Furthermore, no difference of serine 2 and serine 5 phosphorylation was detected between control and heat-shocked cells. Therefore, the transcription block during stable elongation seems not to be linked to a change in the phosphorylation pattern of the RNAPII-CTD.

The FISH-probe used here is complementary to the repetitive sequence of the BR2.1-mRNA. The beginning of this motif is located at exon 4, ~1600 bp downstream of the promoter.<sup>[120]</sup> Therefore, the transcription of the detected mRNAs has already entered productive elongation. The presence of transcription bubbles was tested by a potassium permanganate footprinting. To exclude possible interference with the mRNA, a genomic primer complementary to the non-coding-strand of a repetitive sequence motif of Exon 4, was chosen for potassium permanganate footprinting. This additionally ensures that the detected complexes are at least ~1600 bp downstream of the promoter and 2000 bp upstream of the termination site (Fig. 1.16 p.30). Therefore, detected open complexes are not linked to regulatory mechanisms during transcription initiation, early elongation and termination. Due to the fact that the genomic primer has numerous binding spots in the gene, a strong signal is expected even from a single gland. The drawback of multiple binding sites is the inability to measure the absolute position of detected RNAPII. Since the focus of this experiment was to test if RNAPII forms open complexes, this restriction was of no concern.

DNA-fragments yielded from the LMM-PCR were first analyzed by conventional PA-gel-electrophoresis. This analysis was sufficient to evaluate the assay in general and test the specificity of the primer. For a detailed analysis of the control and heat-shock samples the resolution was not sufficient. Therefore, the samples were analyzed by high resolution capillary gel electrophoresis. To label the PCR-products, fluorescent ATTO488-UTP was added to the PCR-reaction following the first strand synthesis. By using capillary gel electrophoresis, distinct peaks with several base pairs distance could be detected. The resolution was still lacking behind expectations. The PCR-product length could not be resolved with single base-pair resolution. The random labeling positions and variable degree of labeling presumably decreased the resolution. Fluorescently labeled primers might be used to introduce a single dye molecule at a defined position to further improve the resolution.



A central question is, by what mechanism RNAPII is transiently blocked during heat-shock. Since the distribution of RNAP II differed only slightly between control and heat-shock glands, the block is probably not linked to particular sequence motifs (Fig. 2.1 p. 42). This makes it improbable that the stable arrest is induced by proteins binding to the specific DNA motifs. Since transcription continues at other genes, it is unlikely that the reversible block during stable elongation is caused by proteins binding sequence unspecifically to the DNA. Thus, the stable block might be induced by factors binding to or dissociating from RNAPII and thereby inducing the transcription block. It is also possible that, RNAPII is primed during transcription initiation to be down-regulated at *BR2.1* upon heat shock. Such a priming is known to happen, in case the promoter structure is involved in downstream events like splice site selection.<sup>[25]</sup> The long term stability (Fig. 4.4 p. 80) and reversibility (Fig. 4.9 p. 87) of the transcriptional block suggests that it is achieved by a mechanism, which protects the blocked RNAPII from ubiquitin-mediated degradation.

In this work, the focus was laid on the transcriptional regulation of *BR2.1* during heat-shock. Heat-shocking led to a suppressed transcription of most genes in *C. tentans* salivary glands while other genes were activated.<sup>[109]</sup> It is likely that other genes are suppressed in a similar fashion. RNAPII is highly conserved throughout eukaryotes. Therefore, it is very probable that RNAPII could be blocked during productive elongation in other organisms, too.

The transient transcription block reported here is an efficient mechanism which presumably increases the temporal dynamics of transcription regulation dramatically. As outlined before *BR2.1*-mRNA is an especially long transcript. Like other salivary proteins, and especially the *BR*-genes, it is expressed in very high numbers, because it encodes a protein which is needed to build the larval housing tube. An abort of transcription and subsequent re-initiation would waste an enormous amount of cellular resources. Therefore, a transient freezing of RNAPII activity during the elongation process would be biologically rational because it avoids wasting energy for decomposing the nascent mRNAs. Also, it significantly decreases the temporal delay of transcription regulation. For promoter proximal pausing this gain of temporal dynamic is known since it reduces the number of reaction steps which are needed for activation and shut-down of transcription.<sup>[8]</sup>



# 7 Outlook

## 7.1 How to Proceed in Imaging mRNP-Particle Export?

The results obtained in this work, give a first insight into the mRNA-export kinetics and a first hint to a dependence of mRNA-size and export kinetics. Therefore, it is obviously necessary to analyze the export kinetics of mRNAs with different size. An mRNA-specific labeling is needed to image the export of mRNA of a certain size. Unfortunately, the mRNA labeling technique used here does not allow specific mRNA-labeling. The already discussed classical MS2-system can be used for specific mRNA-labeling, but introduces severe changes to the mRNP-particle. A combination of both approaches could combine the advantages of both methods. A MS2-MCP fusion protein labeled with synthetic dyes would improve the photo-physical properties of the MS2 based mRNA probe. The improved photo-physical properties would overcome the need of multiple MS2-MCP probes bound to the target mRNA. The mass added by a single MS2-MCP would be neglectable in comparison to the total mass of the mRNP-particle. *In vitro* labeled MS2-MCP could be easily delivered by microinjection directly into the nucleus of *C. tentans* salivary glands. Such an MS2 does not have to be fused to an NLS sequence, which is suspected to artificially affect the mRNA-export kinetics.

The MS2-MCP binds to MS2 stem loops, which are integrated into the UTR of the target gene by genetic engineering. Usually, cell lines which stably express the modified target mRNA are used. Until now no techniques are published to create transgenic *C. tentans*. Vectors featuring the homologous region 5 (hr5) enhancer and the immediate early 1 (ie1) promoter from *Autographa californica nuclear polyhedrosis virus* (AcNPV), allows to recruit the endogenous transcription machinery in insect cells.<sup>[42]</sup> Arbitrary mRNAs could be expressed in *C. tentans* salivary glands by microinjecting such vectors into the nucleus.

Next to the mRNA-size, interactions with the mRNP-quality control mechanisms are especially assumed to have a significant impact on mRNA-export kinetics. Incompletely processed mRNAs are thought to be bound by specific proteins localized at the nuclear basket and are rejected until the processing is finished. Therefore, it would also be of great interest to test mRNAs with or without splice sites. Since the number of binding sites for incompletely pro-

cessed mRNP-particles at the NPCs is limited, these binding sites could be saturated. Application of splicing inhibitors like SplicostatinA or Isoginkgetin could be used to test the assumed saturation of the quality control mechanisms. Changes of the mRNA-export success rate and kinetics would allow to correlate the here observed diverse kinetics to specific stages of mRNA export.

Targeted splice site mutations can cause splicosome stalling.<sup>[70]</sup> Such engineered mRNAs could be used to study the interactions of incompletely processed mRNAs and the NPC. The NE-interaction kinetics of such mRNA could provide a deeper understanding of the rate limiting reaction steps of mRNA-export.

Inspecting the video data manually, was one of the most time consuming processes in this thesis. A fully automatic video data analysis would increase the experimental throughput dramatically and be a prerequisite to the latter described experiments.

## 7.2 Further Investigation of the Reversible Transcription Block During Stable Elongation

Two questions emerged by the description of a new transcriptional regulation mechanism.

1. What is the molecular mechanism of the transcription block during stable elongation?
2. How frequent is a transcription block during stable elongation in *C. tentans* and other organisms?

As already mentioned, it is very likely that the block of RNAPII during stable elongation is linked to factors associating and/or dissociating from the transcription complex. Proteomics of isolated chromatin segments (PiCh) allow to extract specific DNA target sequences and the proteins bound to it.<sup>[30]</sup> Combining this technique with sophisticated mass spectrometry methods, proteins bound to single DNA regions can be identified.<sup>[88]</sup> Extracting the repetitive sequences of *BR2.1* with PiCh, a high amount of transcription complexes could be collected straightforward. Comparing the protein composition of *BR2.1* transcription complexes of control and heat-shocked salivary glands cells could reveal the factors involved in the transcription block. Candidates found by PiCH could be used in a ChIP-on-chip experiment to identify more genes, whose expression is regulated by a transcription block during stable elongation.

Additionally, a global run-on sequencing approach could be used to identify more genes, which show a comparable block of RNAPII as observed here for *BR2.1*.<sup>[22]</sup>

# Works cited

- [1] H. Akaike. “A new look at the statistical model identification”. In: *Automatic Control, IEEE Transactions on* 19.6 (1974), pp. 716–723. ISSN: 0018-9286.
- [2] E.G. Balbiani. “Sur la structure du noyau des cellules salivaires chez les larves de Chironomus”. In: *Zool. Anz.* 4 (1881), pp. 637–641.
- [3] W. Beermann. “Directed changes in the pattern of Balbiani ring puffing in Chironomus: effects of a sugar treatment.” In: *Chromosoma* 41.3 (1973), pp. 297–326.
- [4] W. Beermann. “Chromomere constancy and specific modifications of the chromosome structure in development and organ differentiation of Chironomus tentans.” In: *Chromosoma* 5.2 (1952), Unknown.
- [5] E. Bertrand, P. Chartrand, M. Schaefer, S. M. Shenoy, R. H. Singer, and R. M. Long. “Localization of ASH1 mRNA particles in living yeast.” In: *Mol Cell* 2.4 (Oct. 1998), pp. 437–445.
- [6] A. L. Beyer, M. E. Christensen, B. W. Walker, and W. M. LeSturgeon. “Identification and characterization of the packaging proteins of core 40S hnRNP particles.” In: *Cell* 11.1 (May 1977), pp. 127–138.
- [7] P.J. Bickel, F. Götze, and W.R. Zwet. “Resampling Fewer Than n Observations: Gains, Losses, and Remedies for Losses”. In: *Selected Works of Willem van Zwet*. Ed. by Sara van de Geer and Marten Wegkamp. Selected Works in Probability and Statistics. Springer New York, 2012, pp. 267–297. ISBN: 978-1-4614-1313-4.
- [8] Alistair N. Boettiger, Peter L. Ralph, and Steven N. Evans. “Transcriptional regulation: effects of promoter proximal pausing on speed, synchrony and reliability.” In: *PLoS Comput Biol* 7.5 (May 2011), e1001136.
- [9] Timothy A Bolger, Andrew W Folkmann, Elizabeth J Tran, and Susan R Wenthe. “The mRNA export factor Gle1 and inositol hexakisphosphate regulate distinct stages of translation.” In: *Cell* 134.4 (Aug. 2008), pp. 624–633.
- [10] Fulvia Bono and Niels H. Gehring. “Assembly, disassembly and recycling: the dynamics of exon junction complexes.” In: *RNA Biol* 8.1 (2011), pp. 24–29.
- [11] Kenneth P Burnham and David R Anderson. *Model selection and multi-model inference: a practical information-theoretic approach*. Springer, 2002.
- [12] Kenneth P Burnham, David R Anderson, and Kathryn P Huyvaert. “AIC model selection and multimodel inference in behavioral ecology: some background, observations, and comparisons”. In: *Behavioral Ecology and Sociobiology* 65.1 (2011), pp. 23–35.
- [13] Grace B Cannon. “Culture of Insect Salivary Glands in a Chemically Defined Medium”. In: *Science (New York, NY)* 146.3647 (1964), p. 1063.

- [14] Sean R Carmody and Susan R Wentz. "mRNA nuclear export at a glance." In: *J Cell Sci* 122.Pt 12 (June 2009), pp. 1933–1937.
- [15] S. T. Case and B. Daneholt. "The size of the transcription unit in Balbiani ring 2 of *Chironomus tentans* as derived from analysis of the primary transcript and 75 S RNA." In: *J Mol Biol* 124.1 (Sept. 1978), pp. 223–241.
- [16] Xuefeng Chen, Baojin Ding, Danielle LeJeune, Christine Ruggiero, and Shisheng Li. "Rpb1 sumoylation in response to UV radiation or transcriptional impairment in yeast." In: *PLoS One* 4.4 (2009), e5267.
- [17] Hong Cheng, Kobina Dufu, Chung-Sheng Lee, Jeanne L Hsu, Anusha Dias, and Robin Reed. "Human mRNA export machinery recruited to the 5' end of mRNA." In: *Cell* 127.7 (Dec. 2006), pp. 1389–1400.
- [18] Alan C M. Cheung and Patrick Cramer. "Structural basis of RNA polymerase II backtracking, arrest and reactivation." In: *Nature* 471.7337 (Mar. 2011), pp. 249–253.
- [19] Kunitoshi Chiba, Junichi Yamamoto, Yuki Yamaguchi, and Hiroshi Handa. "Promoter-proximal pausing and its release: molecular mechanisms and physiological functions." In: *Exp Cell Res* 316.17 (Oct. 2010), pp. 2723–2730.
- [20] Jonathan R. Chubb, Tatjana Trcek, Shailesh M. Shenoy, and Robert H. Singer. "Transcriptional pulsing of a developmental gene." In: *Curr Biol* 16.10 (May 2006), pp. 1018–1025.
- [21] Cedric R. Clapier and Bradley R. Cairns. "The biology of chromatin remodeling complexes." In: *Annu Rev Biochem* 78 (2009), pp. 273–304.
- [22] Leighton J. Core, Joshua J. Waterfall, and John T. Lis. "Nascent RNA sequencing reveals widespread pausing and divergent initiation at human promoters." In: *Science* 322.5909 (Dec. 2008), pp. 1845–1848.
- [23] P. Cramer et al. "Structure of eukaryotic RNA polymerases." In: *Annu Rev Biophys* 37 (2008), pp. 337–352.
- [24] P. Cramer, J. F. Cáceres, D. Cazalla, S. Kadener, A. F. Muro, F. E. Baralle, and A. R. Kornblihtt. "Coupling of transcription with alternative splicing: RNA pol II promoters modulate SF2/ASF and 9G8 effects on an exonic splicing enhancer." In: *Mol Cell* 4.2 (Aug. 1999), pp. 251–258.
- [25] P. Cramer, C. G. Pesce, F. E. Baralle, and A. R. Kornblihtt. "Functional association between promoter structure and transcript alternative splicing." In: *Proc Natl Acad Sci U S A* 94.21 (Oct. 1997), pp. 11456–11460.
- [26] B. Daneholt. "Packing and delivery of a genetic message." In: *Zool. Anz.* 110.3 (July 2001), pp. 173–185.
- [27] B. Daneholt, S. T. Case, J. Hyde, L. Nelson, and L. Wieslander. "Production and fate of Balbiani ring products." In: *Prog Nucleic Acid Res Mol Biol* 19 (1976), pp. 319–334.
- [28] B. Daneholt, J. E. Edström, E. Egyházi, B. Lambert, and U. Ringborg. "RNA synthesis in a Balbiani ring in *Chironomus tentans* salivary gland cells." In: *Chromosoma* 28.4 (1969), pp. 418–429.
- [29] Xavier Darzacq, Yaron Shav-Tal, Valeria de Turris, Yehuda Brody, Shailesh M. Shenoy, Robert D. Phair, and Robert H. Singer. "In vivo dynamics of RNA polymerase II transcription." In: *Nat Struct Mol Biol* 14.9 (Sept. 2007), pp. 796–806.
- [30] Jérôme Déjardin and Robert E. Kingston. "Purification of proteins associated with specific genomic Loci." In: *Cell* 136.1 (Jan. 2009), pp. 175–186.

- [31] B Efron. "Bootstrap Methods: Another Look at the Jackknife". In: *Annals of Statistics* 7.1 (1979), pp. 1–26. ISSN: 0090-5364.
- [32] Conrad E. Firling and Brian K. Kobilka. "A medium for the maintenance of *Chironomus tentans* salivary glands in vitro". In: *Journal of Insect Physiology* 25.1 (1979), pp. 93–103.
- [33] Daniel L Floyd, Stephen C Harrison, and Antoine M Van Oijen. "Analysis of kinetic intermediates in single-particle dwell-time distributions". In: *Biophysical journal* 99.2 (2010), pp. 360–366.
- [34] Steffen Frey and Dirk Görlich. "A saturated FG-repeat hydrogel can reproduce the permeability properties of nuclear pore complexes." In: *Cell* 130.3 (Aug. 2007), pp. 512–523.
- [35] J. Galli and L. Wieslander. "A new member of the balbiani ring multigene family in the dipteran *Chironomus tentans* consists of a single-copy version of a unit repeated in other gene family members." In: *J Mol Evol* 37.5 (Nov. 1993), pp. 457–463.
- [36] Vincent Galy, Olivier Gadad, Micheline Fromont-Racine, Alper Romano, Alain Jacquier, and Ulf Nehrass. "Nuclear retention of unspliced mRNAs in yeast is mediated by perinuclear Mlp1." In: *Cell* 116.1 (Jan. 2004), pp. 63–73.
- [37] E. P. Geiduschek and R. Haselkorn. "Messenger RNA." In: *Annu Rev Biochem* 38 (1969), pp. 647–676.
- [38] Fernando Gómez-Herreros, Lola de Miguel-Jiménez, Gonzalo Millán-Zambrano, Xenia Peñate, Lidia Delgado-Ramos, Mari Cruz Muñoz-Centeno, and Sebastián Chávez. "One step back before moving forward: regulation of transcription elongation by arrest and backtracking." In: *FEBS Lett* 586.18 (Aug. 2012), pp. 2820–2825.
- [39] Einat Grossman, Ohad Medalia, and Monika Zwerger. "Functional architecture of the nuclear pore complex." In: *Annu Rev Biophys* 41 (June 2012), pp. 557–584.
- [40] David Grünwald and Robert H Singer. "In vivo imaging of labelled endogenous  $\beta$ -actin mRNA during nucleocytoplasmic transport." In: *Nature* 467.7315 (Sept. 2010), pp. 604–607.
- [41] P. Grüter, C. Taberner, C. von Kobbe, C. Schmitt, C. Saavedra, A. Bachi, M. Wilm, B. K. Felber, and E. Izaurralde. "TAP, the human homolog of Mex67p, mediates CTE-dependent RNA export from the nucleus." In: *Mol Cell* 1.5 (Apr. 1998), pp. 649–659.
- [42] LINDA A Guarino and W Dong. "Expression of an enhancer-binding protein in insect cells transfected with the *Autographa californica* nuclear polyhedrosis virus IE1 gene." In: *Journal of virology* 65.7 (1991), pp. 3676–3680.
- [43] Matthew G. Guenther, Stuart S. Levine, Laurie A. Boyer, Rudolf Jaenisch, and Richard A. Young. "A chromatin landmark and transcription initiation at most promoters in human cells." In: *Cell* 130.1 (July 2007), pp. 77–88.
- [44] Serge Gueroussov, Stefan P Tarnawsky, Xianying A Cui, Kohila Mahadevan, and Alexander F Palazzo. "Analysis of mRNA nuclear export kinetics in mammalian cells by microinjection". In: *Journal of visualized experiments: JoVE* 46 (2010).
- [45] Jeremy R. Haag and Craig S. Pikaard. "Multisubunit RNA polymerases IV and V: purveyors of non-coding RNA for plant gene silencing." In: *Nat Rev Mol Cell Biol* 12.8 (Aug. 2011), pp. 483–492.

- [46] Thomas Hertner, Barbara Meyer, HansM. Eppenberger, and Rodolfo Mähr. “The secretion proteins in *Chironomus tentans* salivary glands: Electrophoretic characterization and molecular weight estimation”. In: *Wilhelm Roux’s archives of developmental biology* 189.1 (1980), pp. 69–72. ISSN: 0340-0794.
- [47] Christine A Hodge, Elizabeth J Tran, Kristen N Noble, Abel R Alcazar-Roman, Rakefet Ben-Yishay, John J Scarcelli, Andrew W Folkmann, Yaron Shav-Tal, Susan R Wentz, and Charles N Cole. “The Dbp5 cycle at the nuclear pore complex during mRNA export I: dbp5 mutants with defects in RNA binding and ATP hydrolysis define key steps for Nup159 and Gle1.” In: *Genes Dev* 25.10 (May 2011), pp. 1052–1064.
- [48] André Hoelz, Erik W. Debler, and Günter Blobel. “The structure of the nuclear pore complex.” In: *Annu Rev Biochem* 80 (2011), pp. 613–643.
- [49] Nathaniel P Hoyle and David Ish-Horowicz. “Transcript processing and export kinetics are rate-limiting steps in expressing vertebrate segmentation clock genes”. In: *Proceedings of the National Academy of Sciences* 110.46 (2013), E4316–E4324.
- [50] Timothy A. Isgro and Klaus Schulten. “Association of nuclear pore FG-repeat domains to NTF2 import and export complexes.” In: *J Mol Biol* 366.1 (Feb. 2007), pp. 330–345.
- [51] Elisa Izaurrealde, Artur Jarmolowski, Christina Beisel, Iain W Mattaj, Gideon Dreyfuss, and Utz Fischer. “A role for the M9 transport signal of hnRNP A1 in mRNA nuclear export”. In: *The Journal of cell biology* 137.1 (1997), pp. 27–35.
- [52] Jacques Jean-Philippe, Sean Paz, and Massimo Caputi. “hnRNP A1: the Swiss army knife of gene expression.” In: *Int J Mol Sci* 14.9 (2013), pp. 18999–19024.
- [53] Jason M. Johnson, John Castle, Philip Garrett-Engle, Zhengyan Kan, Patrick M. Loerch, Christopher D. Armour, Ralph Santos, Eric E. Schadt, Roland Stoughton, and Daniel D. Shoemaker. “Genome-wide survey of human alternative pre-mRNA splicing with exon junction microarrays.” In: *Science* 302.5653 (Dec. 2003), pp. 2141–2144.
- [54] Tim P. Kaminski, Jan-Hendrik Spille, Claudio Nietzel, Jan Peter Siebrasse, and Ulrich Kubitscheck. “Nuclear Trafficking and Export of Single, Native mRNPs in *Chironomus tentans* Salivary Gland Cells.” In: *Methods Mol Biol* 1042 (2013), pp. 73–85.
- [55] Tae Hoon Kim, Leah O. Barrera, Ming Zheng, Chunxu Qu, Michael A. Singer, Todd A. Richmond, Yingnian Wu, Roland D. Green, and Bing Ren. “A high-resolution map of active promoters in the human genome.” In: *Nature* 436.7052 (Aug. 2005), pp. 876–880.
- [56] E. Kiseleva, M. W. Goldberg, T. D. Allen, and C. W. Akey. “Active nuclear pore complexes in *Chironomus*: visualization of transporter configurations related to mRNP export.” In: *J Cell Sci* 111 ( Pt 2) (Jan. 1998), pp. 223–236.
- [57] Ronen Benjamin Kopito and Michael Elbaum. “Nucleocytoplasmic transport: a thermodynamic mechanism.” In: *HFSP J* 3.2 (Apr. 2009), pp. 130–141.
- [58] Ronen Benjamin Kopito and Michael Elbaum. “Reversibility in nucleocytoplasmic transport.” In: *Proc Natl Acad Sci U S A* 104.31 (July 2007), pp. 12743–12748.
- [59] Alberto R. Kornblihtt. “Chromatin, transcript elongation and alternative splicing.” In: *Nat Struct Mol Biol* 13.1 (Jan. 2006), pp. 5–7.



- [60] Alberto R. Kornblihtt, Manuel de la Mata, Juan Pablo Fededa, Manuel J. Munoz, and Guadalupe Nogues. "Multiple links between transcription and splicing." In: *RNA* 10.10 (Oct. 2004), pp. 1489–1498.
- [61] Jennifer A. Kruk, Arnob Dutta, Jianhua Fu, David S. Gilmour, and Joseph C. Reese. "The multifunctional Ccr4-Not complex directly promotes transcription elongation." In: *Genes Dev* 25.6 (Mar. 2011), pp. 581–593.
- [62] Jason N. Kuehner, Erika L. Pearson, and Claire Moore. "Unravelling the means to an end: RNA polymerase II transcription termination." In: *Nat Rev Mol Cell Biol* 12.5 (May 2011), pp. 283–294.
- [63] Saikat Kumar, B Ghosh, Anamika Missra, and David S Gilmour. "Negative elongation factor accelerates the rate at which heat shock genes are shut off by facilitating dissociation of heat shock factor." In: *Mol Cell Biol* 31.20 (Oct. 2011), pp. 4232–4243.
- [64] Karin Kylberg, Petra Björk, Nathalie Fomproix, Birgitta Ivarsson, Lars Wieslander, and Bertil Daneholt. "Exclusion of mRNPs and ribosomal particles from a thin zone beneath the nuclear envelope revealed upon inhibition of transport." In: *Exp Cell Res* (Oct. 2009).
- [65] Karin Kylberg, Birgitta Björkroth, Birgitta Ivarsson, Nathalie Fomproix, and Bertil Daneholt. "Close coupling between transcription and exit of mRNP from the cell nucleus." In: *Exp Cell Res* 314.8 (May 2008), pp. 1708–1720.
- [66] López, Casimiro C and Edström, Jan-Erik. "Interspersed centromeric element with a CENP-B box-like motif in *Chironomus pallidivittatus*". In: *Nucleic acids research* 26.18 (1998), pp. 4168–4172.
- [67] M. M. Lamb and B. Daneholt. "Characterization of active transcription units in Balbiani rings of *Chironomus tentans*." In: *Cell* 17.4 (Aug. 1979), pp. 835–848.
- [68] H. Le Hir, E. Izaurralde, L. E. Maquat, and M. J. Moore. "The spliceosome deposits multiple proteins 20–24 nucleotides upstream of mRNA exon-exon junctions." In: *EMBO J* 19.24 (Dec. 2000), pp. 6860–6869.
- [69] Sarah Ledoux and Christine Guthrie. "Regulation of the Dbp5 ATPase cycle in mRNP remodeling at the nuclear pore: a lively new paradigm for DEAD-box proteins." In: *Genes Dev* 25.11 (June 2011), pp. 1109–1114.
- [70] P. Legrain and M. Rosbash. "Some cis- and trans-acting mutants for splicing target pre-mRNA to the cytoplasm." In: *Cell* 57.4 (May 1989), pp. 573–583.
- [71] Remi Lemoine et al. "Source to sink transport and regulation by environmental factors". In: *Frontiers in Plant Science* 4.272 (2013). ISSN: 1664-462X.
- [72] Markus Lezzi. "Heat-shock phenomena in *Chironomus tentans* II. In vitro effects of heat and overheat on puffing and their reversal". In: *Chromosoma* 90 (3 1984), pp. 198–203. ISSN: 0009-5915.
- [73] Markus Lezzi, Friederike Gatzka, and Barbara Meyer. "Heat-shock phenomena in *Chironomus tentans* III. Quantitative autoradiographic studies on 3H-uridine incorporation into Balbiani ring 2 and heat-shock puff IV-5C". In: *Chromosoma* 90 (3 1984), pp. 204–210. ISSN: 0009-5915.
- [74] M. Lezzi and L. I. Gilbert. "Control of gene activities in the polytene chromosomes of *Chironomus tentans* by ecdysone and juvenile hormone." In: *Proc Natl Acad Sci U S A* 64.2 (Oct. 1969), pp. 498–503.

- [75] M. Lezzi, B. Meyer, and R. Mähr. “Heat shock phenomena in *Chironomus tentans* I. In vivo effects of heat, overheat, and quenching on salivary chromosome puffing.” In: *Chromosoma* 83.3 (1981), pp. 327–339.
- [76] Chor-Wai Lo, Daisuke Kaida, Shinichi Nishimura, Akihisa Matsuyama, Yoko Yashiroda, Hiroshi Taoka, Ken Ishigami, Hidenori Watanabe, Hidenori Nakajima, Tokio Tani, Sueharu Horinouchi, and Minoru Yoshida. “Inhibition of splicing and nuclear retention of pre-mRNA by spliceostatin A in fission yeast.” In: *Biochem Biophys Res Commun* 364.3 (Dec. 2007), pp. 573–577.
- [77] Alan R Lowe, Jake J Siegel, Petr Kalab, Merek Siu, Karsten Weis, and Jan T Liphardt. “Selectivity mechanism of the nuclear pore complex characterized by single cargo tracking.” In: *Nature* 467.7315 (Sept. 2010), pp. 600–603.
- [78] Robert Duncan Luce. *Response Times: Their Role in Inferring Elementary Mental Organization* 3. Vol. 8. Oxford University Press, 1986.
- [79] Jiong Ma, Zhen Liu, Nicole Michelotti, Sethuramasundaram Pitchaiya, Ram Veerapaneni, John R. Androsavich, Nils G. Walter, and Weidong Yang. “High-resolution three-dimensional mapping of mRNA export through the nuclear pore.” In: *Nat Commun* 4 (2013), p. 2414.
- [80] R. Mähr, B. Meyer, B. Daneholt, and H. M. Eppenberger. “Activation of Balbiani ring genes in *Chironomus tentans* after a pilocarpine-induced depletion of the secretory products from the salivary gland lumen.” In: *Dev Biol* 80.2 (Dec. 1980), pp. 409–418.
- [81] Shivani Malik, Shruti Bagla, Priyasri Chaurasia, Zhen Duan, and Sukesh R. Bhaumik. “Elongating RNA polymerase II is disassembled through specific degradation of its largest but not other subunits in response to DNA damage in vivo.” In: *J Biol Chem* 283.11 (Mar. 2008), pp. 6897–6905.
- [82] Manuel de la Mata, Claudio R. Alonso, Sebastián Kadener, Juan P. Fededa, Matías Blaustein, Federico Pelisch, Paula Cramer, David Bentley, and Alberto R. Kornblihtt. “A slow RNA polymerase II affects alternative splicing in vivo.” In: *Mol Cell* 12.2 (Aug. 2003), pp. 525–532.
- [83] Gwenn Le Mee, Nader Ezzeddine, Michele Capri, and Ounissa Ait-Ahmed. “Repeat length and RNA expression level are not primary determinants in CUG expansion toxicity in *Drosophila* models.” In: *PLoS One* 3.1 (2008), e1466.
- [84] H. Mehlin, B. Daneholt, and U. Skoglund. “Translocation of a specific premessenger ribonucleoprotein particle through the nuclear pore studied with electron microscope tomography.” In: *Cell* 69.4 (May 1992), pp. 605–613.
- [85] H. Mehlin, U. Skoglund, and B. Daneholt. “Transport of Balbiani ring granules through nuclear pores in *Chironomus tentans*.” In: *Exp Cell Res* 193.1 (Mar. 1991), pp. 72–77.
- [86] B. Meyer, R. Mähr, H. M. Eppenberger, and M. Lezzi. “The activity of Balbiani rings 1 and 2 in salivary glands of *Chironomus tentans* larvae under different modes of development and after pilocarpine treatment.” In: *Dev Biol* 98.2 (Aug. 1983), pp. 265–277.
- [87] Sigrid Milles and Edward A Lemke. “Single Molecule Study of the Intrinsically Disordered FG-Repeat Nucleoporin 153.” In: *Biophys J* 101.7 (Oct. 2011), pp. 1710–1719.

- [88] Gerhard Mittler, Falk Butter, and Matthias Mann. “A SILAC-based DNA protein interaction screen that identifies candidate binding proteins to functional DNA elements.” In: *Genome Res* 19.2 (Feb. 2009), pp. 284–293.
- [89] Dagmar Mohr, Steffen Frey, Torsten Fischer, Thomas Güttler, and Dirk Görlich. “Characterisation of the passive permeability barrier of nuclear pore complexes.” In: *EMBO J* 28.17 (Sept. 2009), pp. 2541–2553.
- [90] Ben Montpetit, Nathan D Thomsen, Kara J Helmke, Markus A Seeliger, James M Berger, and Karsten Weis. “A conserved mechanism of DEAD-box ATPase activation by nucleoporins and InsP6 in mRNA export.” In: *Nature* 472.7342 (Apr. 2011), pp. 238–242.
- [91] Amir Mor, Shimrit Suliman, Rakefet Ben-Yishay, Sharon Yunger, Yehuda Brody, and Yaron Shav-Tal. “Dynamics of single mRNP nucleocytoplasmic transport and export through the nuclear pore in living cells.” In: *Nat Cell Biol* 12.6 (June 2010), pp. 543–552.
- [92] James L. Nation. *Insect Physiology and Biochemistry*. CRC Press, 2008.
- [93] Sergei Nechaev and Karen Adelman. “Pol II waiting in the starting gates: Regulating the transition from transcription initiation into productive elongation.” In: *Biochim Biophys Acta* 1809.1 (Jan. 2011), pp. 34–45.
- [94] Sergei Nechaev and Karen Adelman. “Promoter-proximal Pol II: when stalling speeds things up.” In: *Cell Cycle* 7.11 (June 2008), pp. 1539–1544.
- [95] Kristen N Noble, Elizabeth J Tran, Abel R Alcázar-Román, Christine A Hodge, Charles N Cole, and Susan R Wenthe. “The Dbp5 cycle at the nuclear pore complex during mRNA export II: nucleotide cycling and mRNP remodeling by Dbp5 are controlled by Nup159 and Gle1.” In: *Genes Dev* 25.10 (May 2011), pp. 1065–1077.
- [96] M. Palangat and R. Landick. “Roles of RNA:DNA hybrid stability, RNA structure, and active site conformation in pausing by human RNA polymerase II.” In: *J Mol Biol* 311.2 (Aug. 2001), pp. 265–282.
- [97] G. Paulsson, K. Bernholm, and L. Wieslander. “Conserved and variable repeat structures in the Balbiani ring gene family in *Chironomus tentans*.” In: *J Mol Evol* 35.3 (Sept. 1992), pp. 205–216.
- [98] William Perkins, Gary Simon, and Mark Tygert. “Computing the asymptotic power of a Euclidean-distance test for goodness-of-fit”. In: *arXiv 12066378* (2012).
- [99] William Perkins, Mark Tygert, and Rachel Ward. “ $\chi^2$  and classical exact tests often wildly misreport significance; the remedy lies in computers”. In: *Uploaded to ArXiv* (2011).
- [100] Hemali P Phatnani and Arno L Greenleaf. “Phosphorylation and functions of the RNA polymerase II CTD.” In: *Genes Dev* 20.21 (Nov. 2006), pp. 2922–2936.
- [101] J. Pustell, F. C. Kafatos, U. Wobus, and H. Bäumlein. “Balbiani ring DNA: sequence comparisons and evolutionary history of a family of hierarchically repetitive protein-coding genes.” In: *J Mol Evol* 20.3-4 (1984), pp. 281–295.
- [102] Arjun Raj, Charles S. Peskin, Daniel Tranchina, Diana Y. Vargas, and Sanjay Tyagi. “Stochastic mRNA synthesis in mammalian cells.” In: *PLoS Biol* 4.10 (Oct. 2006), e309.
- [103] Patricia Richard and James L Manley. “Transcription termination by nuclear RNA polymerases.” In: *Genes Dev* 23.11 (June 2009), pp. 1247–1269.

- [104] Jörg G. Ritter, Roman Veith, Jan-Peter Siebrasse, and Ulrich Kubitscheck. “High-contrast single-particle tracking by selective focal plane illumination microscopy.” In: *Opt Express* 16.10 (May 2008), pp. 7142–7152.
- [105] Jörg Gerhard Ritter, Roman Veith, Andreas Veenendaal, Jan Peter Siebrasse, and Ulrich Kubitscheck. “Light sheet microscopy for single molecule tracking in living tissue.” In: *PLoS One* 5.7 (2010), e11639.
- [106] Sheldon M Ross. *Introduction to probability and statistics for engineers and scientists*. Academic Press, 2009.
- [107] J Rudolph and J Stubbe. “Investigation of the mechanism of phosphoribosylamine transfer from glutamine phosphoribosylpyrophosphate amidotransferase to glycinamide ribonucleotide synthetase”. In: *Biochemistry* 34.7 (1995), pp. 2241–2250.
- [108] Hideaki Saeki and Jesper Q. Svejstrup. “Stability, flexibility, and dynamic interactions of colliding RNA polymerase II elongation complexes.” In: *Mol Cell* 35.2 (July 2009), pp. 191–205.
- [109] H. Sass. “Transcription of heat shock gene loci versus non-heat shock loci in Chironomus polytene chromosomes: evidence for heat-induced formation of novel putative ribonucleoprotein particles (hsRNPs) in the major heat shock puffs.” In: *Chromosoma* 103.8 (Feb. 1995), pp. 528–538.
- [110] Abbie Saunders, Leighton J Core, and John T Lis. “Breaking barriers to transcription elongation.” In: *Nat Rev Mol Cell Biol* 7.8 (Aug. 2006), pp. 557–567.
- [111] Knut Schmidt-Nielsen. *Animal Physiology: Adaption and Environment*. Cambridge University Press, 1997.
- [112] A. J. Shatkin and J. L. Manley. “The ends of the affair: capping and polyadenylation.” In: *Nat Struct Biol* 7.10 (Oct. 2000), pp. 838–842.
- [113] Jan Peter Siebrasse, Tim Kaminski, and Ulrich Kubitscheck. “Nuclear export of single native mRNA molecules observed by light sheet fluorescence microscopy.” In: *Proc Natl Acad Sci U S A* (May 2012).
- [114] Jan Peter Siebrasse, Roman Veith, Akos Dobay, Heinrich Leonhardt, Bertil Daneholt, and Ulrich Kubitscheck. “Discontinuous movement of mRNP particles in nucleoplasmic regions devoid of chromatin.” In: *Proc Natl Acad Sci U S A* 105.51 (Dec. 2008), pp. 20291–20296.
- [115] H. Siomi and G. Dreyfuss. “A nuclear localization domain in the hnRNP A1 protein.” In: *J Cell Biol* 129.3 (May 1995), pp. 551–560.
- [116] U. Skoglund, K. Andersson, B. Strandberg, and B. Daneholt. “Three-dimensional structure of a specific pre-messenger RNP particle established by electron microscope tomography.” In: *Nature* 319.6054 (1986), pp. 560–564.
- [117] Baggavalli P. Somesh, Stefan Sigurdsson, Hideaki Saeki, Hediye Erdjument-Bromage, Paul Tempst, and Jesper Q. Svejstrup. “Communication between distant sites in RNA polymerase II through ubiquitylation factors and the polymerase CTD.” In: *Cell* 129.1 (Apr. 2007), pp. 57–68.
- [118] T. Strachan and A.P. Read. *Human Molecular Genetics 4*. Garland Science/Taylor & Francis Group, 2011. ISBN: 9780815341499.
- [119] Lisa A. Strawn, Tianxiang Shen, Nataliya Shulga, David S. Goldfarb, and Susan R. Wentz. “Minimal nuclear pore complexes define FG repeat domains essential for transport.” In: *Nat Cell Biol* 6.3 (Mar. 2004), pp. 197–206.

- [120] J. Sümegi, L. Wieslander, and B. Daneholt. "A hierarchic arrangement of the repetitive sequences in the Balbiani ring 2 gene of *Chironomus tentans*." In: *Cell* 30.2 (Sept. 1982), pp. 579–587.
- [121] Jesper Q Svejstrup. "Contending with transcriptional arrest during RNAPII transcript elongation." In: *Trends Biochem Sci* 32.4 (Apr. 2007), pp. 165–171.
- [122] C. N. Tennyson, H. J. Klamut, and R. G. Worton. "The human dystrophin gene requires 16 hours to be transcribed and is cotranscriptionally spliced." In: *Nat Genet* 9.2 (Feb. 1995), pp. 184–190.
- [123] Laura J Terry, Eric B Shows, and Susan R Wenthe. "Crossing the nuclear envelope: hierarchical regulation of nucleocytoplasmic transport." In: *Science* 318.5855 (Nov. 2007), pp. 1412–1416.
- [124] Mary C Thomas and Cheng-Ming Chiang. "The general transcription machinery and general cofactors." In: *Crit Rev Biochem Mol Biol* 41.3 (2006), pp. 105–178.
- [125] Elizabeth J Tran, Yingna Zhou, Anita H Corbett, and Susan R Wenthe. "The DEAD-box protein Dbp5 controls mRNA export by triggering specific RNA:protein remodeling events." In: *Mol Cell* 28.5 (Dec. 2007), pp. 850–859.
- [126] Jean-François Trempe. "Reading the ubiquitin postal code." In: *Curr Opin Struct Biol* 21.6 (Dec. 2011), pp. 792–801.
- [127] Li-Chun Tu, Guo Fu, Anton Zilman, and Siegfried M. Musser. "Large cargo transport by nuclear pores: implications for the spatial organization of FG-nucleoporins." In: *EMBO J* (Nov. 2013).
- [128] Li-Chun Tu and Siegfried M. Musser. "Single molecule studies of nucleocytoplasmic transport." In: *Biochim Biophys Acta* 1813.9 (Sept. 2011), pp. 1607–1618.
- [129] Sanjay Tyagi. "Imaging intracellular RNA distribution and dynamics in living cells." In: *Nat Methods* 6.5 (May 2009), pp. 331–338.
- [130] Roman Veith, Thomas Sorkalla, Eugen Baumgart, Johannes Anzt, Hanns Häberlein, Sanjay Tyagi, Jan Peter Siebrasse, and Ulrich Kubitscheck. "Balbiani ring mRNPs diffuse through and bind to clusters of large intranuclear molecular structures." In: *Biophys J* 99.8 (Oct. 2010), pp. 2676–2685.
- [131] N. Visa, A. T. Alzhanova-Ericsson, X. Sun, E. Kiseleva, B. Björkroth, T. Wurtz, and B. Daneholt. "A pre-mRNA-binding protein accompanies the RNA from the gene through the nuclear pores and into polysomes." In: *Cell* 84.2 (Jan. 1996), pp. 253–264.
- [132] Yaolai Wang, Feng Liu, and Wei Wang. "Dynamic mechanism for the transcription apparatus orchestrating reliable responses to activators." In: *Sci Rep* 2 (2012), p. 422.
- [133] James D Watson, Francis HC Crick, et al. "Molecular structure of nucleic acids". In: *Nature* 171.4356 (1953), pp. 737–738.
- [134] Vikki M. Weake and Jerry L. Workman. "Inducible gene expression: diverse regulatory mechanisms." In: *Nat Rev Genet* 11.6 (June 2010), pp. 426–437.
- [135] Christine S Weirich, Jan P Erzberger, Jeffrey S Flick, James M Berger, Jeremy Thorner, and Karsten Weis. "Activation of the DExD/H-box protein Dbp5 by the nuclear-pore protein Gle1 and its coactivator InsP6 is required for mRNA export." In: *Nat Cell Biol* 8.7 (July 2006), pp. 668–676.

- [136] Steven West, Natalia Gromak, and Nick J. Proudfoot. "Human 5' → 3' exonuclease Xrn2 promotes transcription termination at co-transcriptional cleavage sites." In: *Nature* 432.7016 (Nov. 2004), pp. 522–525.
- [137] Kenneth D. Westover, David A. Bushnell, and Roger D. Kornberg. "Structural basis of transcription: nucleotide selection by rotation in the RNA polymerase II active center." In: *Cell* 119.4 (Nov. 2004), pp. 481–489.
- [138] L. Wieslander. "The Balbiani ring multigene family: coding repetitive sequences and evolution of a tissue-specific cell function." In: *Prog Nucleic Acid Res Mol Biol* 48 (1994), pp. 275–313.
- [139] Marcus D. Wilson, Michelle Harreman, and Jesper Q. Svejstrup. "Ubiquitylation and degradation of elongating RNA polymerase II: the last resort." In: *Biochim Biophys Acta* 1829.1 (Jan. 2013), pp. 151–157.
- [140] C. Wyss. "Chironomus tentans epithelial cell lines sensitive to ecdysteroids, juvenile hormone, insulin and heat shock." In: *Exp Cell Res* 139.2 (June 1982), pp. 309–319.
- [141] Ping Xu, Duc M. Duong, Nicholas T. Seyfried, Dongmei Cheng, Yang Xie, Jessica Robert, John Rush, Mark Hochstrasser, Daniel Finley, and Junmin Peng. "Quantitative proteomics reveals the function of unconventional ubiquitin chains in proteasomal degradation." In: *Cell* 137.1 (Apr. 2009), pp. 133–145.
- [142] H. Yamamoto. "Heat-shock induced puffing changes in Balbiani rings." In: *Chromosoma* 32.2 (1970), pp. 171–190.
- [143] Weidong Yang. "'Natively unfolded' nucleoporins in nucleocytoplasmic transport: clustered or evenly distributed?" In: *Nucleus* 2.1 (2011), pp. 10–16.
- [144] Julia Zeitlinger, Alexander Stark, Manolis Kellis, Joung-Woo Hong, Sergei Nechaev, Karen Adelman, Michael Levine, and Richard A. Young. "RNA polymerase stalling at developmental control genes in the *Drosophila melanogaster* embryo." In: *Nat Genet* 39.12 (Dec. 2007), pp. 1512–1516.
- [145] Jing Zhou, Volker Schweikhard, and Steven M. Block. "Single-molecule studies of RNAPII elongation." In: *Biochim Biophys Acta* 1829.1 (Jan. 2013), pp. 29–38.
- [146] Abdelhak M. Zoubir and D. Robert Iskander. *Bootstrap Techniques for Signal Processing*. Cambridge University Press, 2004.
- [147] K Zu, MARTHA L Sikes, and AL Beyer. "Separable roles in vivo for the two RNA binding domains of *Drosophila* A1-hnRNP homolog." In: *Rna* 4.12 (1998), pp. 1585–1598.

# Works not-cited

- [148] Karen M Arndt and Caroline M Kane. “Running with RNA polymerase: eukaryotic transcript elongation.” In: *Trends Genet* 19.10 (Oct. 2003), pp. 543–550.
- [149] G. Jogesh Babu and C. R. Rao. “Goodness-of-Fit Tests When Parameters Are Estimated”. In: *Sankhy?: The Indian Journal of Statistics (2003-2007)* 66.1 (2004), pages. ISSN: 09727671.
- [150] Peter J. Bickel and Anat Sakov. *On the Choice of m in the m Out of n Bootstrap and Confidence Bounds for Extrema*.
- [151] J. Bickel Peter and Jian-Jian Ren. *The bootstrap in hypothesis testing*. Ed. by Mathisca de Gunst, Chris Klaassen, and Aad van der Vaart. Vol. 36. Institute of Mathematical Statistics, 2000.
- [152] Silvija Bilokapic and Thomas U Schwartz. “3D ultrastructure of the nuclear pore complex.” In: *Curr Opin Cell Biol* 24.1 (Feb. 2012), pp. 86–91.
- [153] Stephen Buratowski. “Progression through the RNA polymerase II CTD cycle.” In: *Mol Cell* 36.4 (Nov. 2009), pp. 541–546.
- [154] Michael F. Carey, Craig L. Peterson, and Stephen T. Smale. *Transcriptional Regulation in Eukaryotes: Concepts, Strategies and Techniques*. 2nd ed. Cold Spring Harbor Laboratory Press, 2009.
- [155] S. T. Case. “Correlated changes in steady-state levels of Balbiani ring mRNAs and secretory polypeptides in salivary glands of *Chironomus tentans*.” In: *Chromosoma* 94.6 (1986), pp. 483–491.
- [156] S. Chávez, T. Beilharz, A. G. Rondón, H. Erdjument-Bromage, P. Tempst, J. Q. Svejstrup, T. Lithgow, and A. Aguilera. “A protein complex containing Tho2, Hpr1, Mft1 and a novel protein, Thp2, connects transcription elongation with mitotic recombination in *Saccharomyces cerevisiae*.” In: *EMBO J* 19.21 (Nov. 2000), pp. 5824–5834.
- [157] Denise V Clark and Steven Henikoff. “Unusual organizational features of the *Drosophila* Gart locus are not conserved within diptera”. In: *Journal of molecular evolution* 35.1 (1992), pp. 51–59.
- [158] Pierre Druilhet and Denys Pommeret. “Invariant conjugate analysis for exponential families”. In: *Bayesian Analysis* 7.4 (2012), pp. 903–916.
- [159] J. E. Edström, L. Rydlander, and C. Francke. “Concomitant induction of a Balbiani ring and a giant secretory protein in *Chironomus* salivary glands.” In: *Chromosoma* 81.1 (1980), pp. 115–124.
- [160] Nico B. Eisele, Aksana A. Labokha, Steffen Frey, Dirk Görlich, and Ralf P. Richter. “Cohesiveness tunes assembly and morphology of FG nucleoporin domain meshworks - Implications for nuclear pore permeability.” In: *Biophys J* 105.8 (Oct. 2013), pp. 1860–1870.
- [161] Steffen Frey and Dirk Görlich. “FG/FxFG as well as GLFG repeats form a selective permeability barrier with self-healing properties.” In: *EMBO J* 28.17 (Sept. 2009), pp. 2554–2567.

- [162] D. Gatfield, H. Le Hir, C. Schmitt, I. C. Braun, T. Köcher, M. Wilm, and E. Izaurralde. “The DExH/D box protein HEL/UAP56 is essential for mRNA nuclear export in *Drosophila*.” In: *Curr Biol* 11.21 (Oct. 2001), pp. 1716–1721.
- [163] Christian Genest and Bruno Rémillard. “Validity of the parametric bootstrap for goodness-of-fit testing in semiparametric models”. In: *Annales de l’institut Henri Poincaré (B) Probabilités et Statistiques* 44.6 (2008), pp. 1096–1127.
- [164] Saikat Kumar B. Ghosh, Anamika Missra, and David S. Gilmour. “Negative elongation factor accelerates the rate at which heat shock genes are shut off by facilitating dissociation of heat shock factor.” In: *Mol Cell Biol* 31.20 (Oct. 2011), pp. 4232–4243.
- [165] Daniel A. Gilchrist, George Fromm, Gilberto dos Santos, Linh N. Pham, Ivy E. McDaniel, Adam Burkholder, David C. Fargo, and Karen Adelman. “Regulating the regulators: the pervasive effects of Pol II pausing on stimulus-responsive gene networks.” In: *Genes Dev* 26.9 (May 2012), pp. 933–944.
- [166] David Grünwald, Robert H Singer, and Michael Rout. “Nuclear export dynamics of RNA-protein complexes.” In: *Nature* 475.7356 (July 2011), pp. 333–341.
- [167] Bastian B. Hülsmann, Aksana A. Labokha, and Dirk Görlich. “The permeability of reconstituted nuclear pores provides direct evidence for the selective phase model.” In: *Cell* 150.4 (Aug. 2012), pp. 738–751.
- [168] Joseph B Kadane and Nicole A Lazar. “Methods and Criteria for Model Selection”. In: *Journal of the American Statistical Association* 99.465 (2004), pp. 279–290. eprint: <http://www.tandfonline.com/doi/pdf/10.1198/016214504000000269>.
- [169] Sachin Kadloor, Raviraj S Adve, and Andrew W Eckford. “Molecular communication using brownian motion with drift”. In: *NanoBioscience, IEEE Transactions on* 11.2 (2012), pp. 89–99.
- [170] Alberto R. Kornblihtt. “Shortcuts to the end.” In: *Nat Struct Mol Biol* 11.12 (Dec. 2004), pp. 1156–1157.
- [171] Thanasis Margaritis and Frank C P. Holstege. “Poised RNA polymerase II gives pause for thought.” In: *Cell* 133.4 (May 2008), pp. 581–584.
- [172] H. Mehlín, B. Daneholt, and U. Skoglund. “Structural interaction between the nuclear pore complex and a specific translocating RNP particle.” In: *J Cell Biol* 129.5 (June 1995), pp. 1205–1216.
- [173] Irene M. Min, Joshua J. Waterfall, Leighton J. Core, Robert J. Munroe, John Schimenti, and John T. Lis. “Regulating RNA polymerase pausing and transcription elongation in embryonic stem cells.” In: *Genes Dev* 25.7 (Apr. 2011), pp. 742–754.
- [174] Helen Neil, Christophe Malabat, Yves d’Aubenton-Carafa, Zhenyu Xu, Lars M. Steinmetz, and Alain Jacquier. “Widespread bidirectional promoters are the major source of cryptic transcripts in yeast.” In: *Nature* 457.7232 (Feb. 2009), pp. 1038–1042.
- [175] J. I. Piruat and A. Aguilera. “A novel yeast gene, THO2, is involved in RNA pol II transcription and provides new evidence for transcriptional elongation-associated recombination.” In: *EMBO J* 17.16 (Aug. 1998), pp. 4859–4872.
- [176] A. E. Rougvie and J. T. Lis. “The RNA polymerase II molecule at the 5’ end of the uninduced hsp70 gene of *D. melanogaster* is transcriptionally engaged.” In: *Cell* 54.6 (Sept. 1988), pp. 795–804.



- 
- [177] Roland T Rust, Duncan Simester, Roderick J Brodie, and V Nilikant. “Model selection criteria: An investigation of relative accuracy, posterior probabilities, and combinations of criteria”. In: *Management Science* 41.2 (1995), pp. 322–333.
- [178] Murray Stewart. “Nuclear export of mRNA.” In: *Trends Biochem Sci* 35.11 (Nov. 2010), pp. 609–617.
- [179] K. Strässer and E. Hurt. “Splicing factor Sub2p is required for nuclear mRNA export through its interaction with Yra1p.” In: *Nature* 413.6856 (Oct. 2001), pp. 648–652.
- [180] Katja Strässer, Seiji Masuda, Paul Mason, Jens Pfannstiel, Marisa Oppizzi, Susana Rodriguez-Navarro, Ana G. Rondón, Andres Aguilera, Kevin Struhl, Robin Reed, and Ed Hurt. “TREX is a conserved complex coupling transcription with messenger RNA export.” In: *Nature* 417.6886 (May 2002), pp. 304–308.
- [181] Jesper Q. Svejstrup. “Mechanisms of transcription-coupled DNA repair.” In: *Nat Rev Mol Cell Biol* 3.1 (Jan. 2002), pp. 21–29.
- [182] Robert Szoszkiewicz, Sri Rama Koti Ainavarapu, Arun P. Wiita, Raul Perez-Jimenez, Jose M. Sanchez-Ruiz, and Julio M. Fernandez. “Dwell time analysis of a single-molecule mechanochemical reaction.” In: *Langmuir* 24.4 (Feb. 2008), pp. 1356–1364.
- [183] H. Tang, Y. Liu, L. Madabusi, and D. S. Gilmour. “Promoter-proximal pausing on the hsp70 promoter in *Drosophila melanogaster* depends on the upstream regulator.” In: *Mol Cell Biol* 20.7 (Apr. 2000), pp. 2569–2580.
- [184] Ichiro Taniguchi and Mutsuhito Ohno. “ATP-dependent recruitment of export factor Aly/REF onto intronless mRNAs by RNA helicase UAP56.” In: *Mol Cell Biol* 28.2 (Jan. 2008), pp. 601–608.
- [185] Laura J. Terry and Susan R. Wentz. “Flexible gates: dynamic topologies and functions for FG nucleoporins in nucleocytoplasmic transport.” In: *Eukaryot Cell* 8.12 (Dec. 2009), pp. 1814–1827.
- [186] Andreas Wagner. “Energy constraints on the evolution of gene expression.” In: *Mol Biol Evol* 22.6 (June 2005), pp. 1365–1374.



# List of Abbreviations and Notations

AF	AlexaFluor
AIC	Akaike Information Criterion
ATP	adenosine triphosphate
$B$	number of bootstrap cycles
$bp$	base pair(s)
$\beta$ -MeOH	$\beta$ -mercaptoethanol
BR	Balbani ring
Cdc	cell division cycle related protein
CTD	carboxy-terminal domain
cdf	cumulative distribution function
Da	Dalton
Dbp	dead box protein
DNA	deoxyribonucleic acid
DRB	5,6-Dichloro-1- $\beta$ -D-ribofuranosylbenzimidazole
DSIF	DRB sensitivity inducing factor
EDTA	ethylenediaminetetraacetic acid
Elc	elongin C
$F(x)$	cumulative function of $f(x)$
FG-repeat	phenylalanine-glycine repeats
FOV	field of view
$\Gamma(t)$	gamma function evaluated at $t$
hnRNP	heterogeneous nuclear ribonucleoproteins
$k$	rate constant
PDF	propability density function
PiCh	Proteomics of isolated chromatin segments
FisH	fluorescence <i>in situ</i> hybridization
mRNA	messenger ribonucleic acid
MS2-MCP	MS2 coat protein
NE	nuclear envelope
NELF	negative elongation factor
NLS	nuclear localization sequence
NPC	nuclear pore complex
Ntf	nuclear transport factor
Nxf	nuclear RNA export factor
Nxt1	Ntf2-related export protein 1

---

Nup	nucleoporin
PAGE	polyacrylamide gel electrophoresis
PDF	propability density function
PIC	transcription pre-initiation complex
P-TEFb	positive transcription elongation factor b
Rpb	RNA polymerase b subunit
RNA	ribonucleic acid
RNAP	RNA-polymerase
RNP	ribonucleoprotein
$S$	number of rate limiting reaction steps
SDS	sodium dodecyl sulfate
$t$	total time constant $t = \tau S$
TF	transcription factor
$\tau$	single step time constant
THO	transcriptional defects of <i>hpr1</i> $\Delta$ by overexpression
Tris	tris(hydroxymethyl)aminomethane)
Ubc	ubiquitin C
$x_i$	random sample
$x_i^*$	bootstrap resample of $x_i$
YFP	yellow fluorescent protein

# Appendix

parameter	fitvalue	p-values			avg-bootstrap	quantiles				
		$\chi^2$	$FT^2$	$X$		0.025	0.25	0.5	0.75	0.975
$\tau_{exp1}$	3.6				3.6	3.0	3.4	3.6	3.8	4.1
$A_{\tau_{exp1}}$	0.3	0.61	0.92	0.83	0.3	0.11	0.23	0.29	0.36	0.5
$\tau_{exp2}$	158				165	107	137	157	184	268
$A_{\tau_{exp2}}$	0.7				0.7	0.5	0.64	0.71	0.77	0.89
$\tau_{nprobing1}$	22.3				21.7	17.5	20.5	21.8	23.0	25.2
$A_{\tau_{nprobing1}}$	0.9	0.15	0.13	0.57	0.76	0.1	0.75	0.8	0.83	0.88
$\tau_{nprobing2}$	320				2.2e4	112	208	267	333	5e4
$A_{\tau_{nprobing2}}$	0.1				0.24	0.12	0.17	0.2	0.25	0.9
$\tau_{cprobing}$	86				88.3	71	81.6	87.7	94.5	108.4
$\tau_{Dbp5_{50Hz}}$	52	0.06	0.06	0.02	85.4	34.4	45.1	52.6	62.3	92.2
$\tau_{1Dbp5_{200Hz}}$	12.9	0.77	0.87	0.94	39.6	4.5	32.5	40.9	48.1	64.1
$A_{\tau_{1Dbp5_{200Hz}}}$	0.77				0.4	0	0.03	0.42	0.7	1.0
$\tau_{2Dbp5_{200Hz}}$	240				1.16e3	65.7	682	1.2e5	8e5	5e6
$A_{\tau_{2Dbp5_{200Hz}}}$	0.23				0.6	0	0.3	0.58	0.97	1.0

**Table 7.2:** Fitted time constants and ratios for nuclear export, nucleoplasmic probing, cytoplasmic probing and the Dbp5 NE interaction.

$S \backslash n$	20	40	60	80	100	120	140	160	180	200	220	240	260	280	300
1	0.763	0.54	0.441	0.382	0.341	0.312	0.289	0.27	0.254	0.241	0.23	0.22	0.212	0.204	0.197
2	2.53	1.79	1.46	1.26	1.13	1.03	0.956	0.894	0.843	0.8	0.763	0.73	0.702	0.676	0.653
3	5.17	3.66	2.98	2.58	2.31	2.11	1.95	1.83	1.72	1.63	1.56	1.49	1.43	1.38	1.33
4	8.64	6.11	4.99	4.32	3.86	3.53	3.26	3.05	2.88	2.73	2.6	2.49	2.4	2.31	2.23
5	12.9	9.13	7.45	6.45	5.77	5.27	4.88	4.56	4.3	4.08	3.89	3.73	3.58	3.45	3.33
6	18	12.7	10.4	8.98	8.03	7.33	6.79	6.35	5.99	5.68	5.41	5.18	4.98	4.8	4.64
7	23.8	16.8	13.7	11.9	10.6	9.71	8.99	8.41	7.93	7.52	7.17	6.86	6.59	6.35	6.14
8	30.4	21.5	17.5	15.2	13.6	12.4	11.5	10.7	10.1	9.6	9.15	8.76	8.42	8.11	7.84
9	37.7	26.7	21.8	18.8	16.9	15.4	14.2	13.3	12.6	11.9	11.4	10.9	10.5	10.1	9.73
10	45.8	32.4	26.4	22.9	20.5	18.7	17.3	16.2	15.3	14.5	13.8	13.2	12.7	12.2	11.8
11	54.6	38.6	31.5	27.3	24.4	22.3	20.6	19.3	18.2	17.3	16.5	15.8	15.1	14.6	14.1
12	64.1	45.3	37	32.1	28.7	26.2	24.2	22.7	21.4	20.3	19.3	18.5	17.8	17.1	16.6
13	74.4	52.6	43	37.2	33.3	30.4	28.1	26.3	24.8	23.5	22.4	21.5	20.6	19.9	19.2
14	85.4	60.4	49.3	42.7	38.2	34.9	32.3	30.2	28.5	27	25.8	24.7	23.7	22.8	22.1
15	97.1	68.7	56.1	48.6	43.4	39.7	36.7	34.3	32.4	30.7	29.3	28	26.9	26	25.1
16	110	77.5	63.3	54.8	49	44.7	41.4	38.7	36.5	34.7	33	31.6	30.4	29.3	28.3
17	123	86.8	70.9	61.4	54.9	50.1	46.4	43.4	40.9	38.8	37	35.4	34	32.8	31.7
18	137	96.6	78.9	68.3	61.1	55.8	51.6	48.3	45.5	43.2	41.2	39.4	37.9	36.5	35.3
19	151	107	87.3	75.6	67.6	61.7	57.1	53.5	50.4	47.8	45.6	43.6	41.9	40.4	39
20	166	118	96.1	83.2	74.5	68	62.9	58.9	55.5	52.6	50.2	48.1	46.2	44.5	43
21	182	129	105	91.2	81.6	74.5	69	64.5	60.8	57.7	55	52.7	50.6	48.8	47.1
22	199	141	115	99.6	89.1	81.3	75.3	70.4	66.4	63	60.1	57.5	55.2	53.2	51.4
23	217	153	125	108	96.9	88.4	81.9	76.6	72.2	68.5	65.3	62.5	60.1	57.9	55.9
24	235	166	136	117	105	95.8	88.7	83	78.2	74.2	70.8	67.8	65.1	62.7	60.6
25	254	179	146	127	113	104	95.8	89.6	84.5	80.2	76.4	73.2	70.3	67.8	65.5

**Table 7.3:** Theoretical  $\sigma_S$  for given number of observations  $n$  and number of rate limiting steps  $S$ .

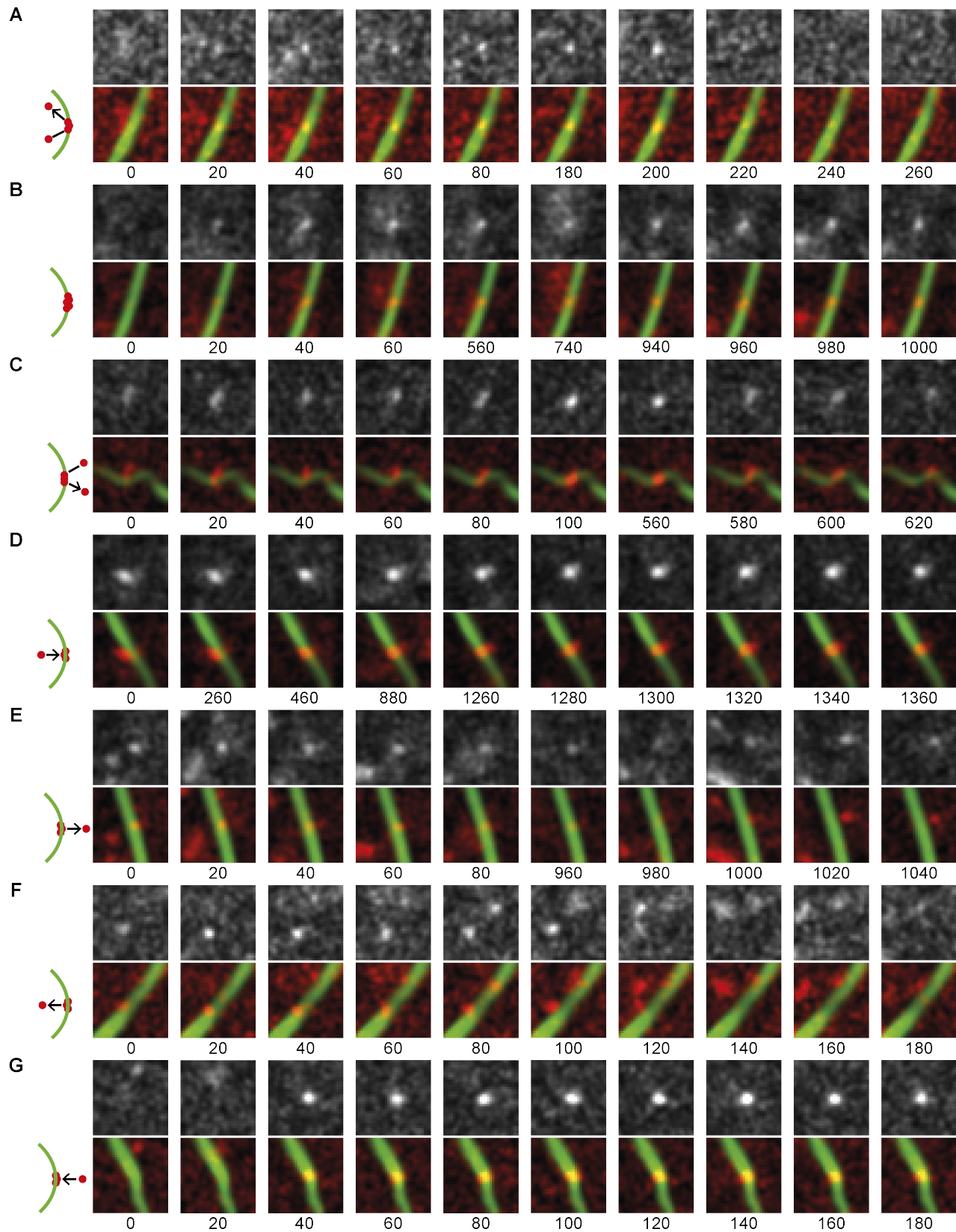


**Figure 7.1:** *Interaction types of mRNP-particles with the NE. (A) Nuclear probing ; (B) only nuclear envelope; (C) cytosolic probing, cp; (D) nucleus to envelope; (E) envelope to cytosol; (F) envelope to nucleosol; (G) cytosol to envelope. Modified from Siebrasse et al.<sup>[113]</sup>*

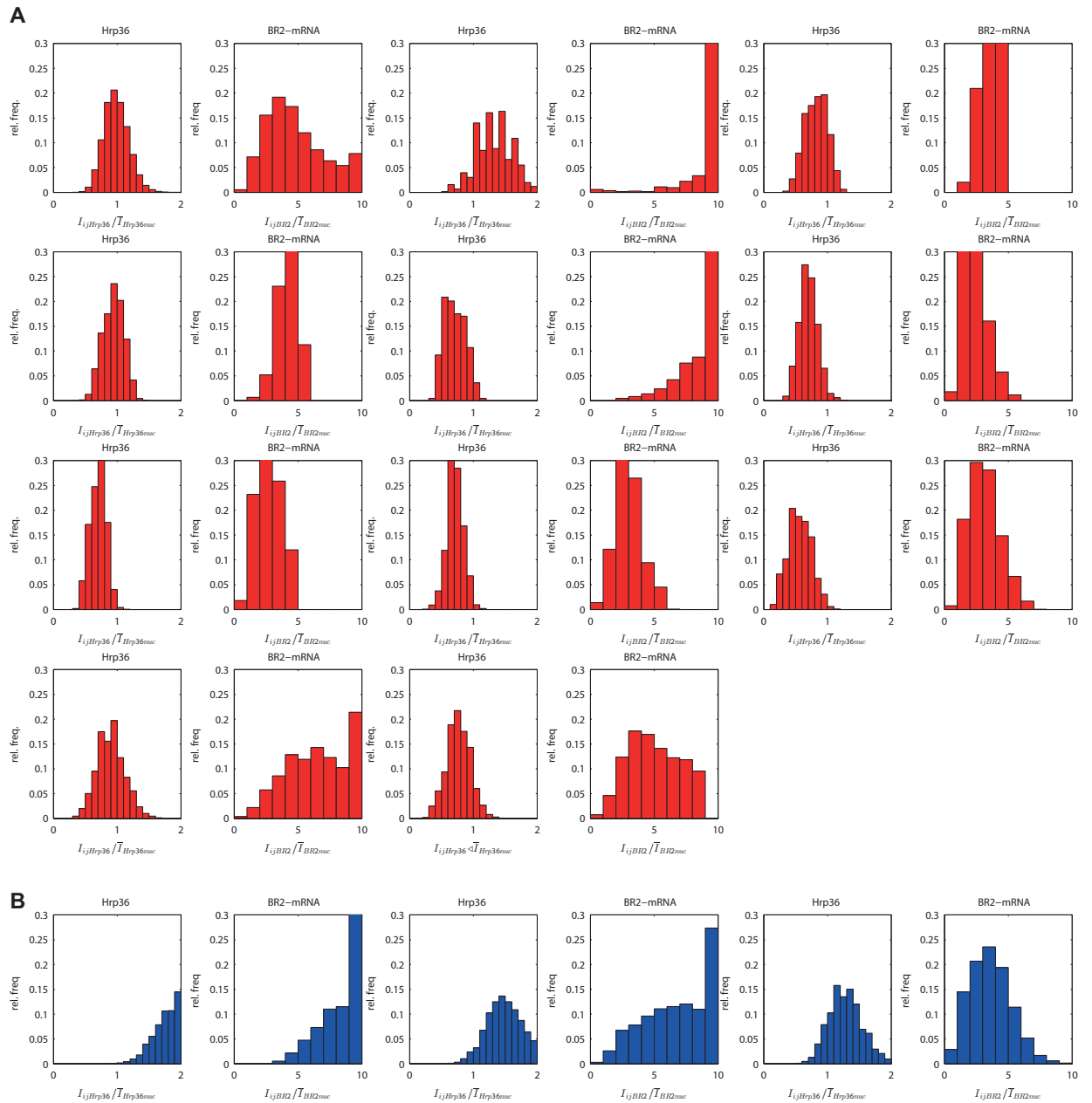


**Figure 7.2:** *Quantification of the transcriptional activity and transcript concentration at the BR2-puff before and after heat shock. Here, the data of Fig. 4.3 (p. 79) are shown cell by cell. (A) Hrp36 and BR2.1 oligonucleotide fluorescence intensity at BR2-puff of 60 min heat-shocked salivary gland cells, and (B) at BR sites of control gland cell nuclei. The respective Hrp36 and BR2.1 oligonucleotide data of the single larvae were displayed side by side. Only in a single nucleus a partially remaining transcription activity after a heat shock of 60 min at 37 °C (first row, third item). The BR2.1 mRNA accumulation varied between the single larvae but no trend was observable*



# Summary

Eucaryotes store most of their genetic information in the nucleus. Parts of this information encode the amino acid sequence of proteins. To synthesize a protein according to the nucleotide sequence, first the corresponding DNA-sequence is transcribed by RNA-Polymerase II to mRNA. Subsequently ribosomes translate the mRNA into the correct amino acid sequence.

In eucaryotes the ribosomes are localized in the cytoplasm and are separated from the nucleus by the nuclear envelope. On the one hand separation of transcription and translation enables eucaryotes to process the transcript post-transcriptionally, on the other it requires a transport of the mRNA from the nucleoplasm into the cytoplasm. The nucleoplasm is interconnected with the cytoplasm by nuclear pore complexes. Most of the nucleo-cytoplasmic trafficking is facilitated through the nuclear pore complexes. Messenger RNA is exported into the cytoplasm through the nuclear pore complexes, too. During transcription the nascent mRNA is bound by several proteins which are essential e.g. for mRNA processing and export. The complex of the mRNA and its associated proteins is called an mRNP-particle. Fully processed mRNP-particles are able to cross the permeability barrier of nuclear pore complexes. In this thesis the kinetics of the mRNA-export were measured in salivary gland cells of *C. tentans* at the single molecule level.

Therefore, mRNA was labeled by Hrp36, which was bacterially expressed and subsequently covalently linked to a fluorescent dye. Hrp36 associates cotranscriptionally with the nascent mRNA and is part of the mRNP-particle. After microinjection, labeled Hrp36 is transported into the nucleus, via its endogenous M9-shuttle domain. As all mRNP-particles, also the labeled ones, diffuse through the nucleus after transcription is finished and can be imaged by advanced fluorescence microscopy.

In this thesis it is shown that the kinetics of the mRNA-export across the nuclear pore complexes follow a broad distribution in the range of 20 ms to seconds. Furthermore, only 30% of all mRNP-particles are exported after they engaged an NPC. Fitting the mRNA-export kinetics with a bimodal gamma distribution revealed average export times of  $t_{1exp} = 76$  ms, which is governed by multiple rate limiting steps and  $t_{2exp} = 158$  ms, which is governed by just a single rate limiting step. Therefore, the translocation of the mRNA across the nuclear pore complex is not rate limiting for protein-biosynthesis which takes on average several minutes.

Trajectory analysis of export events  $\geq 300$  ms, showed that the mRNA were localized mainly in the nuclear basket during the export process. Here proteins are localized which are crucial for the mRNP-particle quality control. These proteins bind mRNP-particles, which are only partially processed, and thereby inhibit their translocation through the nuclear pore complex until their processing is completed. Assuming that the general reaction scheme is the same for all mRNP-particles and considering the fact that these slow export events show only a single rate limiting reactions step, this export events presumably correspond to mRNP-particles, whose processing were not finished.

In addition to the mRNP-particle export kinetics, the Dbp5 interaction kinetics with the nuclear pore complexes were measured. Dbp5 is a RNA-helicase, which is essential for mRNP-particle export. It is assumed that Dbp5 removes the transport receptors from the mRNA via its helicase activity and thereby inhibit the translocation of mRNA back into the nucleus. The interaction kinetics of Dbp5 showed two interaction times ( $t_{1Dbp5_{200Hz}} = 26$  ms &  $t_{2Dbp5_{200Hz}} = 240$  ms). Due to the low number of observations, the interaction times gained by fitting the data with a bimodal gamma distribution showed a high uncertainty This makes a comparison of this results with the observed mRNA-export kinetics not advisable.

In the second part of the thesis a so far unknown regulation mechanism of transcription was studied. First hints to this mechanism were observed by a control experiment during the examination of the mRNA-export kinetics. Transcription can be subdivided into the four stages of initiation, early elongation, stable elongation and termination. It was previously believed that after transition into stable elongation the transcription process is either completed or terminated prematurely. The results of this thesis give evidence that the transcription process in salivary gland cells of *C. tentans* can be halted temporally at the stage of stable elongation by applying a heat-shock to the larvae. The halted transcription processes can be resumed after heat-shock is released.

Since RNA-polymerase II is highly conserved throughout eucaryotes, it seems very likely that this regulatory mechanism is not limited to *C. tentans* . The transcription halt during stable elongation described here, shows that eucaryotes have a more direct and far-ranging access to transcription as believed. This direct control of transcription significantly increases the temporal dynamic of transcriptional regulation.

# Zusammenfassung

Der größte Teil der genetischen Information ist bei Eukaryoten im Zellkern lokalisiert. Ein Teil dieser Information dient der Speicherung der Aminosäuresequenz von Proteinen. Die Aminosäuresequenz wird durch die Abfolge der vier verschiedenen Nukleotide codiert. Um ein, der Nukleotidfolge entsprechendes Polypeptid zu synthetisieren, wird der entsprechende DNA-Abschnitt zunächst in die sogenannte mRNA mittels der RNA-Polymerase II transkribiert. Ribosomen translatieren die mRNA in die korrespondierende Polypeptidsequenz.

In Eukaryoten sind die Ribosomen im Cytoplasma lokalisiert und vom Zellkern durch die Zellkernmembran getrennt. Die räumliche Trennung von Transkription und Translation ermöglicht einerseits eine post-transkriptionelle Prozessierung der mRNAs, macht allerdings einen Transport der mRNA vom Zellkern in das Cytoplasma notwendig. Der Stoffaustausch zwischen Zellkern und Cytoplasma erfolgt hauptsächlich durch die sogenannten Kernporenkomplexe. Durch diese wird auch die mRNA in das Cytoplasma exportiert. Die Kinetik des mRNA-Exports wurde im Rahmen dieser Arbeit in Speicheldrüsenzellen von *C. tentans* gemessen.

Dazu wurde die mRNA mittels bakteriell exprimierten und anschließend fluoreszenzmarkiertem Hrp36 markiert. Hrp36 bindet cotranskriptionell an mRNA und ist Bestandteil des aus Proteinen und mRNA bestehenden mRNP-Partikels. Das fluoreszenzmarkierte Hrp36 wurde mittels Mikroinjektion in das Cytoplasma von *C. tentans* Speicheldrüsenzellen injiziert. Aufgrund seiner endogenen M9-Shuttledomäne wird das fluoreszenzmarkierte Hrp36, analog zum Wildtyp-Hrp36, in den Zellkern transportiert und in entstehende mRNP-Partikel inkorporiert. Die so markierten mRNP-Partikel diffundieren nach Abschluss der Transkription im Zellkern. Treffen mRNP-Partikel dabei auf einen Kernporenkomplex und ist ihre post-transkriptionelle Prozessierung abgeschlossen, können sie durch die Permeabilitätsbarriere der Kernporen diffundieren.

Im Rahmen dieser Arbeit konnte gezeigt werden, dass der mRNA-Export von 20 ms bis zu wenigen Sekunden dauern kann. Weiterhin konnte gezeigt werden, dass nur ~jeder dritte Kontakt zwischen einem mRNP-Partikel und einer Kernpore in einem Export resultiert. Die Approximation der ermittelten mRNA-Exportkinetik zeigte einen schnelleren mRNA-Export  $t_{1exp} = 76$  ms, der von mehreren ratenlimitierenden Schritten beherrscht wird und einen langsameren mRNA-Exportprozess  $t_{2exp} = 158$  ms, der nur einen ratenlimitierenden Schritt aufweist. Da-

her ist für die Proteinbiosynthese, die insgesamt mehrere Minuten benötigt, der mRNA-Export nicht limitierend.

Besonders langsame Exportprozesse hielten sich hauptsächlich im sogenannten nukleären Korb der Kernporenkomplexe auf, wo Qualitätskontrollmechanismen lokalisiert sind, die noch nicht vollständig prozessierte mRNAs am Übertritt in das Cytoplasma hindern. Davon ausgehend, dass alle Exportprozesse die gleichen Schritte durchlaufen und für die langsamen Exportprozesse ein einzelner Schritt die Kinetik beherrscht, lässt sich vermuten, dass diese Exportprozesse mRNP-Partikel entsprechen, die aufgrund unvollständiger Prozessierung am Übertritt in das Cytoplasma gehindert werden. Eine andere Erklärung für die Reduzierung der ratenlimitierenden Schritte könnte eine Konformationsänderung des mRNP-Partikels sein, wie sie für besonders große mRNP-Partikel beschrieben ist.

Neben der Kinetik des mRNA-Exports wurde die Interaktionskinetik von Dbp5 mit Kernporen gemessen. Dbp5 ist eine RNA-Helikase die essentiell für den mRNA-Export ist. Es wird vermutet, dass durch die Helikaseaktivität von Dbp5, auf der cytoplasmatischen Seite der Kernporen, die Transportrezeptoren von der mRNA abgespalten werden und so eine erneute Translokation durch die Kernpore verhindert wird. Die Interaktionskinetik von Dbp5 mit der Kernpore hatte zwei deutlich unterschiedliche Komponenten. Einerseits konnte eine sehr schnelle, als auch eine deutlich langsamere Komponente detektiert werden ( $t_{1Dbp5_{200Hz}} = 26$  ms &  $t_{2Dbp5_{200Hz}} = 240$  ms). Allerdings sind die Fitparameter aufgrund der geringen Zahl an Beobachtungen vermutlich mit einem großen Fehler behaftet, so dass ein Vergleich mit den für den Export bestimmten Parametern nicht sinnvoll erscheint.

Im zweiten Teil dieser Arbeit wurde dem Verdacht nachgegangen, dass während eines Kontroll-experiments ein bislang nicht bekannter Transkriptionregulationsmechanismus beobachtet wurde. Die Transkription kann in die vier Phasen Initiation, frühe Elongation, stabile Elongation und Termination eingeteilt werden. Bislang ging man davon aus, dass nach dem Übergang zur stabilen Elongation es nur die Möglichkeit der frühzeitigen Termination oder der Fertigstellung des Transkripts gibt. Im Rahmen dieser Arbeit konnte gezeigt werden, dass durch einen Hitzeschock in Speicheldrüsenzellen von *C. tentans* die Transkription, für die Dauer des Hitzeschocks, auch während der stabilen Elongation angehalten werden kann. Nach Ende des Hitzeschocks können die so angehaltenen Transkriptionsprozesse fortgesetzt werden.

Da RNA-Polymerase II innerhalb der Eukaryoten stark konserviert ist, ist anzunehmen, dass dieser Mechanismus nicht auf *C. tentans* beschränkt ist. Der hier gezeigte Transkriptionregulationsmechanismus zeigt, dass Eukaryoten einen deutlich direkteren Zugriff auf die RNA-Polymerase II besitzen als bislang gedacht. Ein solch direkter Zugriff auf die Transkription erhöht die Dynamik der Transkriptionsregulation signifikant.

# Danksagung

Auf den letzten Seiten meiner Dissertation möchte ich den Menschen danken, die mich, jeder auf seine Art und Weise, unterstützt haben.

Großer Dank gilt meinem Doktorvater Prof. Dr. Ulrich Kubitscheck. Als mein Promotionsvorhaben am Institut für Biochemie und Molekularbiologie, aufgrund gesundheitlicher Probleme des Betreuers, nicht fortgesetzt werden konnte, hat er mir spontan die Möglichkeit zur Promotion in seiner Arbeitsgruppe eröffnet, so dass der Schock, des nach einem Jahr zwangsweise beendeten Promotionsvorhabens, gar nicht zur Entfaltung kam. Er hat mir ermöglicht sehr frei und selbstbestimmt zu Arbeiten. Auch für seine stete Bereitschaft zum Gedankenaustausch und kritischen Diskussion danke ich.

Prof. Dr. Rudolf Merkel danke ich für die bereitwillige Übernahme des Zweitgutachtens. Weiterhin hat er mir mit seiner bemerkenswert ausgeprägten Fähigkeit des kritischen Hinterfragens von Ergebnissen und Hinweisen zum Bootstrapping sehr geholfen.

Prof. Dr. Arne Lützen danke ich für die unkomplizierte Bereitschaft als fachnahes Mitglied der Promotionskommission anzugehören.

Prof. Dr. Hanns Häberlein danke ich für die Bereitschaft als fachfremdes Mitglied für die Promotionskommission zur Verfügung zu stehen. Für sein immer entgegengebrachtes Vertrauen, seine gewährte Unterstützung und allzeitige Gesprächsbereitschaft danke ich.

Jörg Ritter danke ich für die Einweisung in die Light Sheet Mikroskopie. Mit ihm konnte man auch wunderbar auf den Straßen Bulgariens oder dem Mittelmeer, während einer scheinbar endlosen Fährfahrt, den ein oder anderen, nicht immer so ernst gemeinten, Gedanken diskutieren.

Rücken an Rücken haben Jan-Hendrik Spille und ich die Promotion gestartet. Mittlerweile nebeneinandersitzend, war unser Gedankenaustausch für mich eine stete Quelle der Reflexion und Prüfung meiner Gedanken. Dafür danke ich.

Claudio Nietzel danke ich für die unermüdliche Unterstützung bei der Proteinproduktion und guter musikalischer Unterhaltung im Labor. Marc Mimberg danke ich insbesondere für die Unterstützung bei der Hämolymphegewinnung.

Allen weiteren Kollegen, die mich unterstützt und ihren Anteil dazu beigetragen haben, dass ich stets gerne in dieser Gruppe gearbeitet habe, möchte ich danken.

Für das Korrekturlesen danke ich meinem Bruder Kai Kaminski, Jan-Hendrik Spille, Prof. Dr. Ulrich Kubitscheck und insbesondere und allen voran Katharina Klein. Für ihre Geduld und Mühe mit meinem Werk, von ganzem Herzen, Dankeschön!

Ein großer Dank gilt meiner Oberstufenbiologielehrerin Frau Winkler, die mit ihrem erstklassigen Unterricht den Grundstein für eine wissenschaftliche Denkweise gelegt hat. Diese bildete ein solides Fundament auf das ich während meiner bisherigen akademischen Laufbahn immer aufbauen konnte.

Meinem Bruder und meinen Eltern gehört mein besonderer Dank für ihre Unterstützung während und neben der Promotion.

Meiner Ehefrau möchte ich dafür danken, dass sie stets Verständnis dafür hatte, dass mal wieder eine Messung so dringend erschien, dass die Nacht durchgemessen wurde. Auch wurde sie nie müde meinen Ausführungen über neue Ideen und den hin und wieder auftauchenden Hindernissen und war es auch das "trockenste" Statistikproblem, zuzuhören. Da auch die teilweise Aufzählung der tagtäglichen Unterstützung durch sie die Seitenzahl stark erhöhen und ich mit Sicherheit trotzdem irgendetwas Wichtiges vergessen würde, möchte ich mit einem innigen Danke an sie schließen!

**Eidesstattliche Erklärung** Hiermit erkläre ich, dass ich die vorliegende Arbeit ohne unzulässige Hilfe Dritter und ohne Benutzung anderer als der angegebenen Hilfsmittel angefertigt habe. Die aus anderen Quellen direkt oder indirekt übernommenen Daten und Konzepte sind unter Angabe der Quelle gekennzeichnet. Die Arbeit wurde bisher weder im In- noch im Ausland in gleicher oder ähnlicher Form einer anderen Prüfungsbehörde vorgelegt.

Bonn, Mai 2014

# Tim P. Kaminski | Curriculum Vitae

## Education

---

**since 10/09 Ph.D. in Biophysical Chemistry**

*University of Bonn*

Thesis title: "Nuclear export of single native mRNA molecules observed via light sheet fluorescence microscopy and transcriptional regulation of BR2.1 during heat-shock".

**10/03-09/08 Diploma Study of Biology**

*University of Bonn*

Thesis title: "Characterizing the Interaction of Hyaluronan with MDA-MB-231-cells at the single molecule level".

**1993-2002 Abitur**

*Städt. Gymnasium Vohwinkel*

General qualification for university entrance.

## Awards

---

**2011: Poster Presentation Award of the German Society for Cell Biology**

The best 10 of 300 posters presented at the annual meeting were awarded.

**2010: Ph.D. Scholarship of the German National Academic Foundation**

Awarded to excellent and highly motivated Ph.D. students whose thesis contribute to questions of scientific importance.

**2007: Diploma Study Scholarship of the German National Academic Foundation**

Awarded to students with an outstanding performance at the subject of study.

## conference contributions

---

**2012:** Poster presentation at the EMBL Symposium: Complex Life of mRNA

**2011:** Poster presentation at the Embo Workshop on Mechanisms of Nucleocytoplasmic Trafficking

**2011:** Poster & selected talk at the Annual Meeting of the German Society for Cell Biology

**2010:** Poster presentation at the Annual Meeting of the German Society for Cell Biology

**2010:** Poster presentation at the Annual Meeting of the German Biophysical Society

## international peer-reviewed articles

---

- [1] Tim P. Kaminski, Jan Peter Siebrasse, and Ulrich Kubitscheck. "A single molecule view on Dbp5 and mRNA at the nuclear pore." eng. In: *Nucleus* 4.1 (2013), pp. 8–13.
- [2] Tim P. Kaminski, J. H. Spille, C. Nietzel, J. P. Siebrasse, and U. Kubitscheck. "Nuclear trafficking and export of single, native mRNPs in *Chironomus tentans* salivary gland cells". In: *Meth. Mol. Biol* 1042 (2013).
- [3] Jennifer S. Rinne, Tim P. Kaminski, Ulrich Kubitscheck, and Alexander Heckel. "Light-inducible molecular beacons for spatio-temporally highly defined activation." eng. In: *Chem Commun (Camb)* (May 2013).

- [4] Jan Peter Siebrasse, Tim P. Kaminski, and Ulrich Kubitscheck. "Nuclear export of single native mRNA molecules observed by light sheet fluorescence microscopy." eng. In: *Proc Natl Acad Sci U S A* 109.24 (June 2012), pp. 9426–9431.
- [5] Jan-Hendrik Spille, Tim P. Kaminski, Heinz-Peter Koenigshoven, and Ulrich Kubitscheck. "Dynamic three-dimensional tracking of single fluorescent nanoparticles deep inside living tissue." eng. In: *Opt Express* 20.18 (Aug. 2012), pp. 19697–19707.
- [6] Anne Sieben, Tim P. Kaminski, Ulrich Kubitscheck, and Hanns Haerberlein. "Terbutaline causes immobilization of single beta2-adrenergic receptor-ligand complexes in the plasma membrane of living A549 cells as revealed by single-molecule microscopy." eng. In: *J Biomed Opt* 16.2 (Feb. 2011), p. 026013.
- [7] Debora Gerlach, Tim P. Kaminski, Fabian Perez-Willard, Gregor Kirfel, Volkmar Gieselmann, and Joachim Kappler. "Nanofibers in a hyaluronan-based pericellular matrix." eng. In: *Matrix Biol* 29.8 (Oct. 2010), pp. 664–667.
- [8] Joachim Kappler, Tim P. Kaminski, Volkmar Gieselmann, Ulrich Kubitscheck, and Joerg Jerosch. "Single-molecule imaging of hyaluronan in human synovial fluid." eng. In: *J Biomed Opt* 15.6 (2010), p. 060504.
- [9] Annette Pusch, Annika Boeckenhoff, Tamara Glaser, Tim P. Kaminski, Gregor Kirfel, Michael Hans, Barbara Steinfarz, Dieter Swandulla, Ulrich Kubitscheck, Volkmar Gieselmann, Oliver Bruestle, and Joachim Kappler. "CD44 and hyaluronan promote invasive growth of B35 neuroblastoma cells into the brain." eng. In: *Biochim Biophys Acta* 1803.2 (Feb. 2010), pp. 261–274.
- [10] Joerg G. Ritter, Jan-Hendrik Spille, Tim P. Kaminski, and Ulrich Kubitscheck. "A cylindrical zoom lens unit for adjustable optical sectioning in light sheet microscopy." eng. In: *Biomed Opt Express* 2.1 (2010), pp. 185–193.
- [11] Tim P. Kaminski, Jan-Peter Siebrasse, Volkmar Gieselmann, Ulrich Kubitscheck, and Joachim Kappler. "Imaging and tracking of single hyaluronan molecules diffusing in solution." eng. In: *Glycoconj J* 25.6 (Aug. 2008), pp. 555–560.

## international peer-reviewed conferences/proceedings

---

- [1] Jan-Hendrik Spille, Tim P. Kaminski, and Ulrich Kubitscheck. "Astigmatic Light Sheet Microscopy Allows 3D Localization Deep Inside Living Cells". In:
- [2] Jan-Hendrik Spille, Tim P. Kaminski, Katharina Scherer, Florian Kotzur, and Ulrich Kubitscheck. "Fast 3D Single Molecule Tracking With High Sensitivity". In:
- [3] Jan Peter Siebrasse, Tim P. Kaminski, Katharina Scherer, and Ulrich Kubitscheck. "Nuclear Export of Single Native mRNA". In: vol. 102. 3. Cell Press, 2012, 525a.
- [4] Tim P. Kaminski, J-P Siebrasse, R Veith, and U Kubitscheck. "Imaging the export of single native mRNP particles in living cells". In: *European Journal of Cell Biology*. Vol. 89. Elsevier. 2010, pp. 47–47.

## non-peer-reviewed journal articles

---

- [1] E Baumgart, Tim P. Kaminski, and U. Kubitscheck. "Scanned fluorescence light sheet microscopy with confocal detection". In: *G.I.T. Imaging & Microscopy* 15 (Mar. 2013).
- [2] J.-H. Spille, J. P. Siebrasse, Tim P. Kaminski, and U. Kubitscheck. "Single molecule light sheet microscopy". In: *G.I.T. Imaging & Microscopy* (2012), pp. 30–32.
- [3] J Kappler, Tim P. Kaminski, Gieselmann V., U Kubitscheck, and J. Jerosch. "Molekulare Mechanismen von Hyaluronan in gesunden Gelenken und bei Arthrose". In: *Orthopaedische Praxis* 46.9 (2010), p. 452.